COMPUTATIONAL AERODYNAMICS (R22A2112)

COURSEFILE

III B. Tech I Semester

(2024-25)

Prepared By

Mr E. Dinesh Guptha

Asst.Prof

Departmentof AeronauticalEngineering

MALLA REDDY COLLEGE OF ENGINEERING&TECHNOLOGY

(AutonomousInstitution–UGC, Govt.ofIndia)

AffiliatedtoJNTU, Hyderabad, Approved by AICTE -AccreditedbyNBA&NAAC –_A‘Grade-ISO 9001:2015 Certified)

Maisammaguda, Dhulapally (PostVia.Kompally),Secunderabad–500100,TelanganaState,India.

MRCET VISION

- To become a model institution in the fields of Engineering, Technology and Management.
- To have a perfect synchronization of the ideologies of MRCET with challenging demands of International Pioneering Organizations.

MRCET MISSION

To establish a pedestal for the integral innovation, team spirit, originality and competence in the students, expose them to face the global challenges and become pioneers of Indian vision of modern society.

MRCET QUALITY POLICY.

- To pursue continual improvement of teaching learning process of Undergraduate and Post Graduate programs in Engineering & Management vigorously.
- To provide state of art infrastructure and expertise to impart the quality education.

PROGRAM OUTCOMES
(PO's)

Engineering Graduates will be able to:

1. **Engineering knowledge**: Apply the knowledge of mathematics, science, engineering fundamentals, and an engineering specialization to the solution of complex engineering problems.
2. **Problem analysis**: Identify, formulate, review research literature, and analyze complex engineering problems reaching substantiated conclusions using first principles of mathematics, natural sciences, and engineering sciences.
3. **Design / development of solutions** : Design solutions for complex engineering problems and design system components or processes that meet the specified needs with appropriate consideration for the public health and safety, and the cultural, societal, and environmental considerations.
4. **Conduct investigations of complex problems**: Use research-based knowledge and research methods including design of experiments, analysis and interpretation of data, and synthesis of the information to provide valid conclusions.
5. **Modern tool usage**: Create, select, and apply appropriate techniques, resources, and modern engineering and IT tools including prediction and modeling to complex engineering activities with an understanding of the limitations.
6. **The engineer and society**: Apply reasoning informed by the contextual knowledge to assess societal, health, safety, legal and cultural issues and the consequent responsibilities relevant to the professional engineering practice.
7. **Environment and sustainability**: Understand the impact of the professional engineering solutions in societal and environmental contexts, and demonstrate the knowledge of, and need for sustainable development.
8. **Ethics**: Apply ethical principles and commit to professional ethics and responsibilities and norms of the engineering practice.
9. **Individual and team work**: Function effectively as an individual, and as a member or leader in diverse teams, and in multidisciplinary settings.
10. **Communication**: Communicate effectively on complex engineering activities with the engineering community and with society at large, such as, being able to comprehend and write effective reports and design documentation, make effective presentations, and give and receive clear instructions.
11. **Project management and finance**: Demonstrate knowledge and understanding of the engineering and management principles and apply these to one̛s own work, as a member and leader in a team, to manage projects and in multi disciplinary environments.
12. **Life- long learning**: Recognize the need for, and have the preparation and ability to engage in independent and life-long learning in the broadest context of technological change.

DEPARTMENT OF AERONAUTICAL ENGINEERING

VISION

Department of Aeronautical Engineering aims to be indispensable source in Aeronautical Engineering which has a zeal to provide the value driven platform for the students to acquire knowledge and empower themselves to shoulder higher responsibility in buildinga strong nation.

MISSION

The primary mission of the department is to promote engineering education and research. To strive consistently to provide quality education, keeping in pace with time and technology. Department passions to integrate the intellectual, spiritual, ethical and social development of the students for shaping them into dynamic engineers.

QUALITY POLICY STATEMENT

Impart up-to-date knowledge to the students in Aeronautical area to make them quality engineers. Make the students experience the applications on quality equipment and tools. Provide systems, resources and training opportunities to achieve continuous improvement. Maintain global standards in education, training and services.

PROGRAM EDUCATIONAL OBJECTIVES – Aeronautical Engineering

1. **PEO1 (PROFESSIONALISM & CITIZENSHIP):** To create and sustain a community of learning in which students acquire knowledge and learn to apply it professionally with due consideration for ethical, ecological and economic issues.
2. **PEO2 (TECHNICAL ACCOMPLISHMENTS):** To provide knowledge based services to satisfy the needs of society and the industry by providing hands on experience in various technologies in core field.
3. **PEO3 (INVENTION, INNOVATION AND CREATIVITY):** To make the students to design, experiment, analyze, and interpret in the core field with the help of other multi disciplinary concepts wherever applicable.
4. **PEO4 (PROFESSIONAL DEVELOPMENT):** To educate the students to disseminate research findings with good soft skills and become a successful entrepreneur.
5. **PEO5 (HUMAN RESOURCE DEVELOPMENT):** To graduate the students in building national capabilities in technology, education and research

PROGRAM SPECIFIC OUTCOMES – Aeronautical Engineering

1. To mould students to become a professional with all necessary skills, personality and sound knowledge in basic and advance technological areas.
2. To promote understanding of concepts and develop ability in design manufacture and maintenance of aircraft, aerospace vehicles and associated equipment and develop application capability of the concepts sciences to engineering design and processes.
3. Understanding the current scenario in the field of aeronautics and acquire ability to apply knowledge of engineering, science and mathematics to design and conduct experiments in the field of Aeronautical Engineering.
4. To develop leadership skills in ourstudents necessary to shape the social, intellectual, business and technical worlds.

MALLA REDDY COLLEGEOF ENGINEERING AND TECHNOLOGY

IVYEARB.Tech.AE–I SEM

L	T/P/D	C
4	1/-/-	4

(R22A2112)COMPUTATIONALAERODYNAMICS

Objectives:

The course should enable the students to:

- Application of CFD to various engineering problems.
- Understand the physics of mathematical equations governing aerodynamic flows.
- Numerical methods to solve fluid flow problems

UNIT-I-INTRODUCTIONTOCOMPUTATIONALFLUIDDYNAMICS

CFD and its importance, Application of CFD to various Engineering problems. Models of fluid flow- Finite Control Volume, Infinitesimal Fluid Element. Substantial derivatives, divergence of Velocity.

UNIT-II-GOVERNINGEQUATIONSOFFLUIDDYNAMICS

Continuity equation, Momentum equation, Energy equation, physical boundary conditions. Form of Governing equation suited for CFD-Conservation form-shock fitting and shock capturing. Impact of partial differential equations on CFD. Classification of Quasi-Linear Partial differential equation, The Eigen value method, General behavior of different classes of Partial differential equation – elliptic, parabolic and hyperbolic with examples.

UNIT-IV–DISCRETIZATIONTECHNIQUES

Introduction, Finite differences and formulas for first and second derivatives, difference equations, Explicit and implicit approaches. Basis of finite volume method- conditions on the finite volume selections-approaches - Cell-centered and cell-vertex. Definition of finite volume discretization general formulation ofa numerical scheme.

UNIT-IV-GRIDGENERATION

Need for grid generation. Structured grids- Cartesian grids, body fitted structured grids, Multi-block grids - overset grids with applications. Unstructured grids- triangular/ tetrahedral cells, hybrid grids, quadrilateral/hexahedracells.GridGenerationtechniques-Delaunaytriangulation,Advancefontmethod.Grid quality parameters.

UNIT-V–CFDTECHNIQUES

Lax-Wendroff technique, Mac Cormack's technique, Relaxation technique, Alternating-Direction-Implicit (ADI) Technique. Pressure correction technique, Numerical procedure- SIMPLE algorithm, Boundary conditions for the pressure correction method.

TEXTBOOKS

1. John.D.Anderson "Computational Fluid Dynamics", Mc Graw Hill
2. CharlesHirsch"Numericalcomputationofinternalandexternalflows"SecondEditionButterworth-Heinemann is an imprint of Elsevier

REFERENCES

1. Hoffmann, K.A: Computational Fluid Dynamics for Engineers, Engineering Education System, Austin, Tex., 1989
2. JBlazek"ComputationalFluidDynamics:PrinciplesandApplications"Elsevier.
3. IntroductiontoComputationalFluidDynamics,ChowCY,JohnWiley,1979

Outcomes:

The student should be able to

- Solve differentialequationsgoverning fluid flow problems.
- The student will demonstrate an ability to recognize the type of fluid flow that is occurring in a particular physical system and to use the appropriate model equations to investigatethe flow.
- Generation of grid according to geometry of flow.
- The student can able to select appropriate discretization methodto solve given problem.
- Application of CFD techniques foraerospaceproblems.

UNIT I
Introduction to Computational Fluid Dynamics

1. 1 COMPUTATIONAL FLUID DYNAMICS

Computational fluid dynamics constitutes a new "third approach" in the philosophical study and development of the whole discipline of fluid dynamics. Computational fluid dynamics has certainly evolved, integrating not only the disciplines of fluid mechanics with mathematics but also computer science, as illustrated in Figure 1.1.

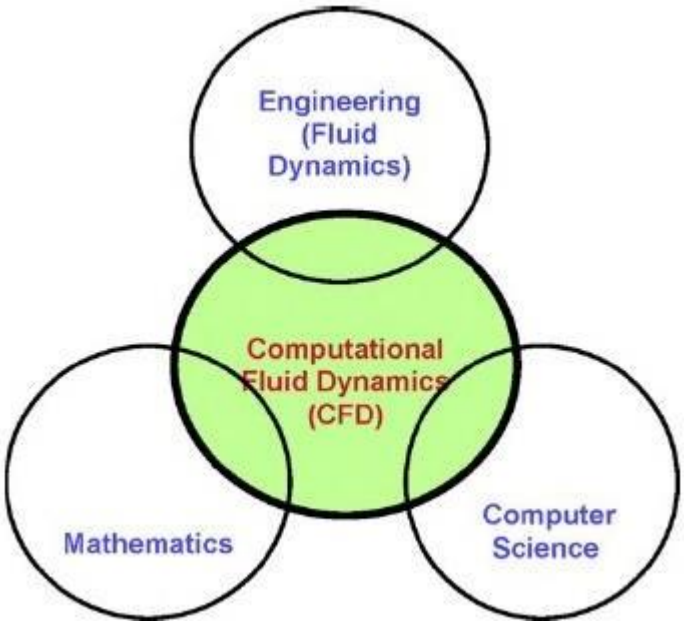

Figure 1.1 The different disciplines involved in computational fluid dynamics

The physical characteristics of the fluid motion can usually be described through fundamental mathematical equations, usually in partial differential form, which govern a process of interest and are often called governing equations in CFD. In order to solve these mathematical equations, computer scientists using high- level computer programming languages convert the equations into computer programs or software packages.

The “computational” part simply means the study of the fluid flow using numerical simulations, which involves employing computer programs or software packages performed on high-speed digital computers to attain the numerical solutions. CFD has also become one of the three basic methods or approaches that can be employed to solve problems in fluid dynamics and heat transfer. As demonstrated in Figure 1.2, the approaches that are strongly interlinked do not work in isolation.

Traditionally, both experimental and analytical methods have been used to study the various aspects of fluid dynamics and to assist engineers in the design of equipment and industrial processes involving fluid flow and heat transfer. With the advent of digital computers, the computational (numerical) aspect has emerged as another viable approach. Although the analytical method is still practiced by many, and experiments will continue to be significantly performed, the trend is clearly toward greater reliance on the computational approach for industrial designs, particularly when the fluid flows are very complex.

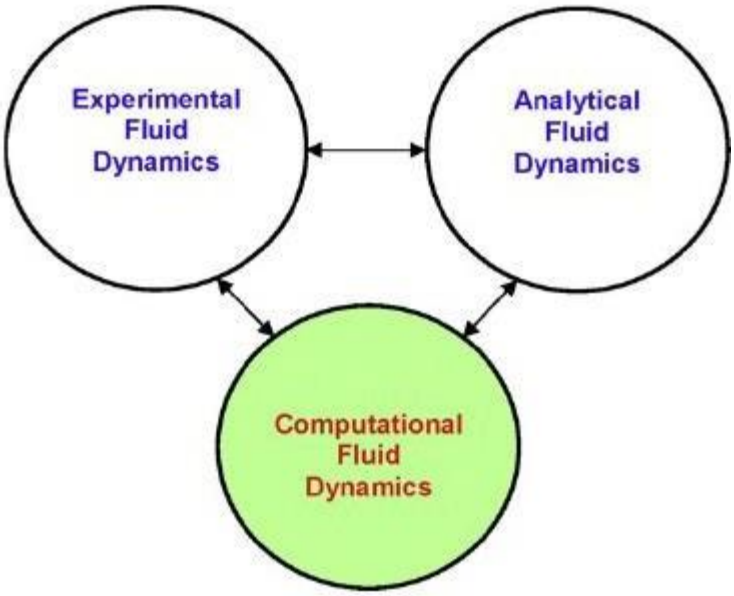

Figure 1.2 The three basic approaches to solve problems in fluid dynamics and heat transfer.

1.2 ADVANTAGES OF COMPUTATIONAL FLUID DYNAMICS (CFD)

With the rapid advancement of digital computers, CFD is poised to remain at the forefront of cutting- edge research in the sciences of fluid dynamics and heat transfer. Also, the emergence of CFD as a practical tool in modern engineering practice is steadily attracting much interest.

i. CFD complements experimental and analytical approaches by providing an alternative cost effective means of simulating real fluid flows.

ii. CFD substantially reduces lead times and costs in design and production compared with experimentally based approaches and offers the ability to solve a range of complicated flow problems where the analytical approach is lacking.

iii. CFD has the capacity to simulate flow conditions that are not reproducible in experimental tests found in geophysical and biological fluid dynamics, such as nuclear accident scenarios or scenarios that are too huge or too remote to be simulated experimentally (e.g., the Indonesian Tsunami of 2004).

iv. CFD can provide detailed visualization and comprehensive information when compared to analytical and experimental fluid dynamics.

v. CFD permits alternative designs to be evaluated over a range of dimensionless parameters that may include the Reynolds number, Mach number, Rayleigh number, and flow orientation. The utilization of such an approach is usually very effective in the early stages of development for fluid-system designs.

vi. CFD can provide detailed information and understanding of the flow processes to be obtained, such as the occurrence of flow separation or whether the wall temperature exceeds some maximum limit.

1.2.1 DISADVANTAGES OF COMPUTATIONAL FLUID DYNAMICS (CFD)

- In spite of CFD's advantages, the reader must also be fully aware of some inherent limitations of applying CFD. Numerical errors exist in computations; therefore, there will be differences between computed results and reality.

- Visualization of numerical solutions using vectors, contours, or animated movies of unsteady flows is by far the most effective way of interpreting the huge amount of data generated from the numerical calculation. However, there is a danger that an erroneous solution, which may look good, will not correspond to the expected flow behavior.

- Any numerical results obtained must always be thoroughly examined before they are believed. Hence, a CFD user needs to learn how to properly analyze and make critical judgments about the computed results.

1.3 COMPUTATIONAL FLUID DYNAMICS AND ITS IMPORTANCE AS RESEARCH TOOL

CFD can be employed to better understand the physical events or processes that occur in the flow of fluids around and within the designated objects. These events are closely related to the action and interaction of phenomena associated with dissipation, diffusion, convection, boundary layers, and turbulence. Whether the flows are incompressible or compressible, many of the most important aspectsof these types of flows are non-linear and, as a consequence, often do not have
any analytic solution. This motivates the search for numerical solutions for the partial differential equations using CFD.

CFD, analogous to wind-tunnel tests, can be employed as a research tool to perform numerical experiments. CFD can be utilized to better understand the observed flow structures and some important physical aspects of a flow field, similar to a real laboratory experiment.

CFD simulations can work harmoniously with experiments, providing not only qualitative comparison but also a means to interpret some basic phenomenological aspects of the experimental condition. More important, numerical experiments can provide more comprehensive information and details of the flow visualized in three dimensions, , when compared to laboratory experiments.

1.4 COMPUTATIONAL FLUID DYNAMICS AND ITS IMPORTANCE AS DESIGN TOOL

CFD is becoming an integral part of the engineering design and analysis environment in prominent industries. Companies are progressively seeking industrial solutions through the extensive use of CFD for the optimization of product development and processes and/or to predict the performance of new designs before they are manufactured or implemented.

Software applications can now provide numerical analyses and solutions to pertinent flow problems through the employment of common desktop computers. As a viable design tool, CFD has assisted by providing significant and substantial insights into the flow characteristics within the equipment and processes required to increase production, improve longevity, and decrease waste. Increasing computer processing power is certainly revolutionizing the use of CFD in new and existing industries.

1.5 APPLICATION OF CFD TO VARIOUS ENGINEERING PROBLEMS

1.5.1 Aerospace

Computational fluid dynamics has certainly enjoyed a long and illustrious history of development and

application in the aerospace and defense industries. To maintain an edge in a very competitive environment, CFD is playing a crucial role in overcoming many challenges faced by these industries in improving flight and in solving a diverse array of designs. Indeed, many engineers associate CFD withits well-known application to aerodynamics in the calculation of the lift force on an aircraft wingspan.

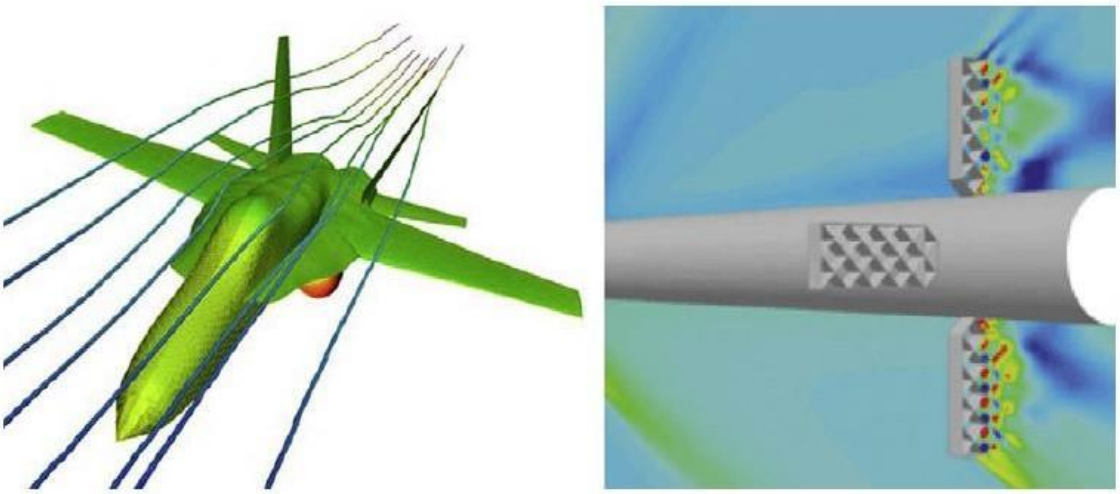

Figure 1.3 Example of CFD results for applications in the aerospace and defense industries

Figure 1.3 illustrates the simulation of fluid path lines in the vicinity of an F18 jet (left) and prediction of pressure coefficient contours at a 10o angle of attack around a supersonic missile system with grid fins (right). These are just a small sample of the numerous applications of CFD in aerodynamic design and military applications. CFD has also been employed in resolving a number of complex operational problems in aircraft design, such as studying the impact of trailing vortices on the safe operation of successive aircraft taking off and landing on a runway, as well as in enhancing passenger and crew comfort by improving cabin ventilation, heating, and cooling.

1.5.2 Automobile Engineering

Automobile engineers are increasingly relying on more simulation techniques to bring new vehicle design concepts to fruition. Computer-aided engineering has been at the forefront of creating innovative internal systems that will enhance the overall driving experience, impro ve driver and passenger comfort and safety, and advance fuel economy. CFD has long been an essential element in automotive design and manufacture.

CFD in automotive engineering has many advantages. The technology has delivered the ability to shorten cycles, to optimize existing engineering components and systems to improve energy efficiency and to meet strict standards and specifications, to improve the in-car environment, and to study importantexternal aerodynamics, as illustrated in Figure 1.4.

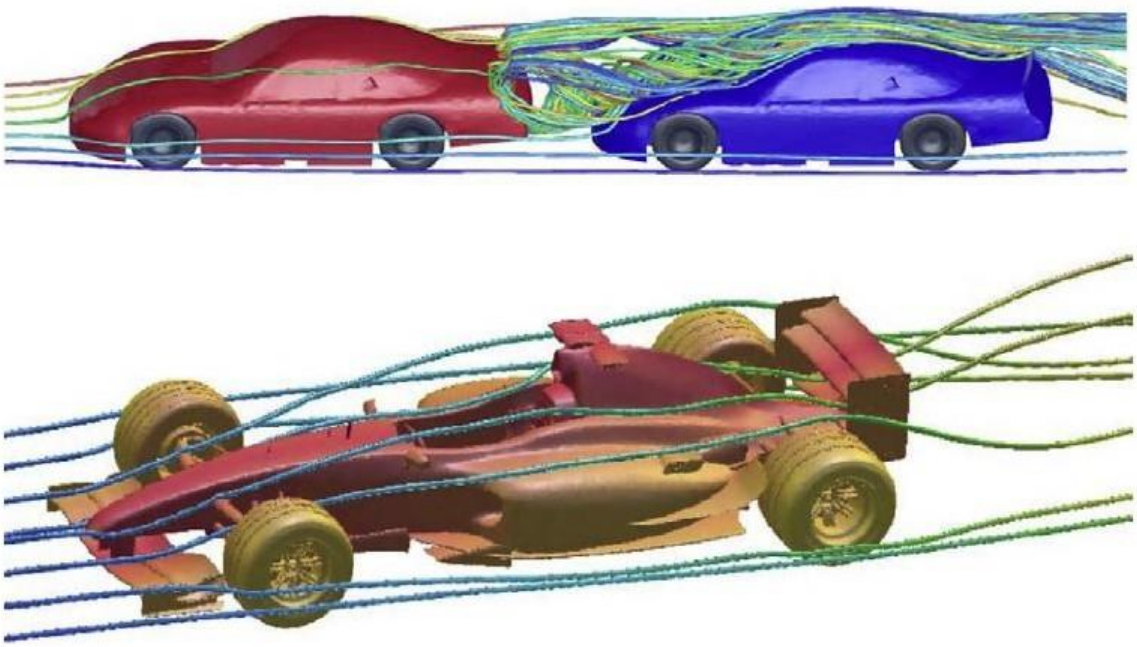

Figure 1.4 Examples of automotive aerodynamics

1.5.3 Biomedical Science and Engineering

Nowadays,medical researchers rely on simulation tools to assist in predicting the behavior of blood flow inside the human body. Computational simulations can provide invaluable information that is extremely difficult to obtain experimentally, and they allow many variations of fluid-dynamics problems to be parametrically studied. Figures 1.5 and 1.6 illustrate just one of the many sample applications of CFD in the biomedical area, in this case where blood flows through originally stenosed and virtually stented arteries are predicted. With the breadth of physical models and advances in areas of fluid–structure interaction, particle tracking, turbulence modeling, and better meshing facilities, rigorous CFD analysis is increasingly performed to study the fluid phenomena inside the human vascular system.

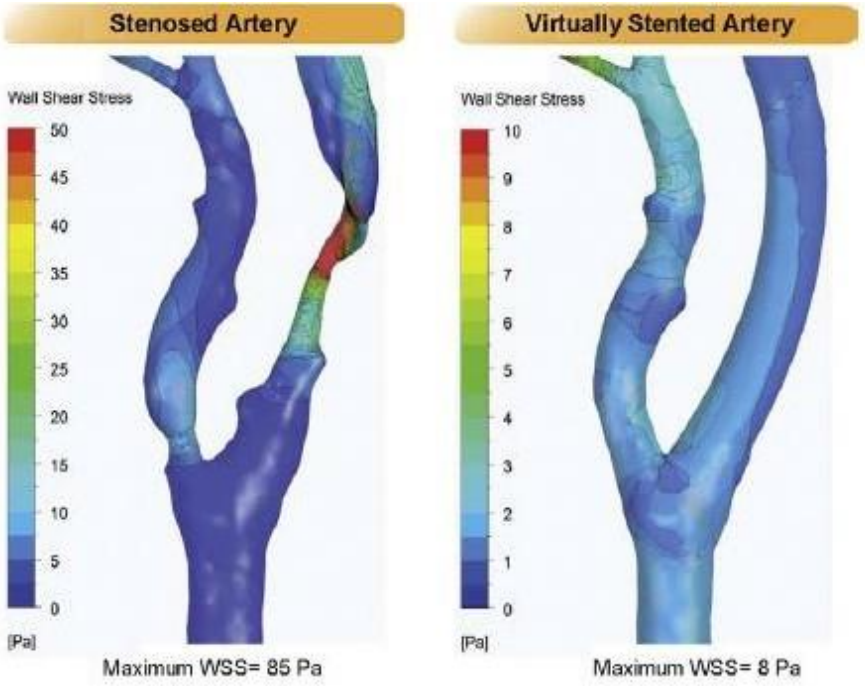

Figure 1.5 Example of CFD prediction of wall shear stress (WSS) for originally stenosed and virtually stented arteries

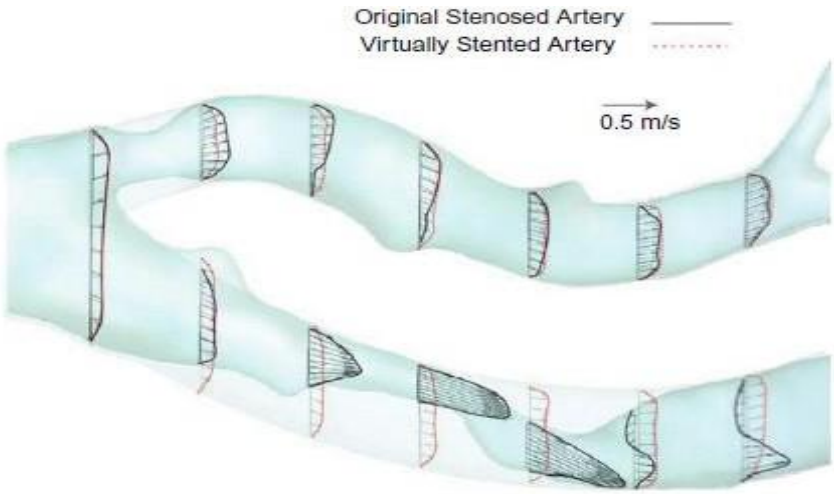

Figure 1.6 Example of predicted velocity profiles for originally stenosed and virtually stented arteries.

1.5.4. Chemical and Mineral Processing

World-wide, many necessities revolve around the chemical and mineralprocessing industries. By applying large quantities of heat and energy to physically or chemically deform raw materials, these industries have certainly helped to mould essential products for food and health as well as vital advanced technological equipment in computing and biotechno logy. In the face of increasing industrial competitiveness, these industries are confronted with major challenges in meeting the world's demands and present needs without compromising the future. This translates into making operational processes become more energy efficient, safer, andmore flexible whilst better containing and reducing emissions.

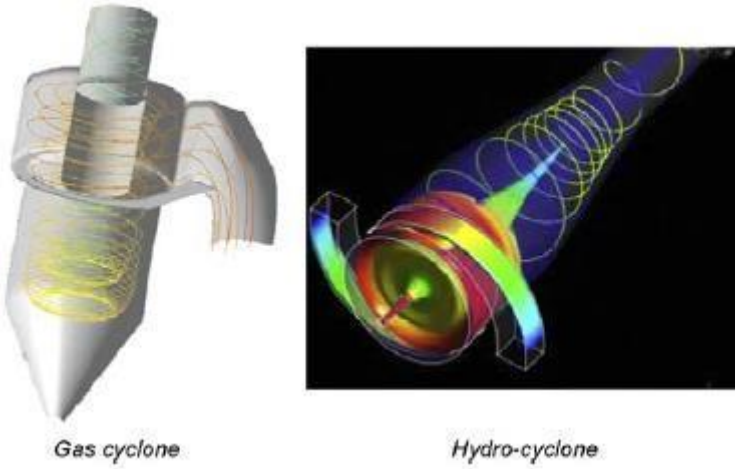

Figure 1.7 Example of CFD application in the simulation of a gas cyclone and a hydrocyclone.

The detailed information about the transport of liquid and gases gained through the use of CFD and population balance approaches ensures that engineers have the best available data to work with in order to increase yield by improving fluid flows, thereby reducing operating costs and increasing system efficiency. Figure 1.7 illustrates a separation process in mineral processing that involves the use of gas cyclones and hydro-cyclones. A gas cyclone is a commonly used apparatus that utilizes gravity and

centrifugal force to separate solid particles from a gas stream.

1.5.5. Civil and Environmental Engineering

CFD simulations have been at the heart of resolving many environmental issues. For instance, CFD has been used to predict the pollutant plume dispersion from a cooling tower subject to wind conditions, as shown in Figure 1.8. In addition,CFD can assist in ensuring compliance with strict regulat ions during the early design stages of construction. Figure 1.9 represents pre-construction simulation for a new 22- m tank at a water treatment plant. Owing to the huge construction cost, whichmay exceed millions of dollars, virtual computer-aided models can be built and analyzed that greatly save time and cost in exploring all aspects of design before construction is begun. To determine the feas ibility of such a construction, flowmodeling is also performed (also shown in Figure 1.9), which provides insights into the flow behavior for the proposed tank that would not have been possible through physical modeling.

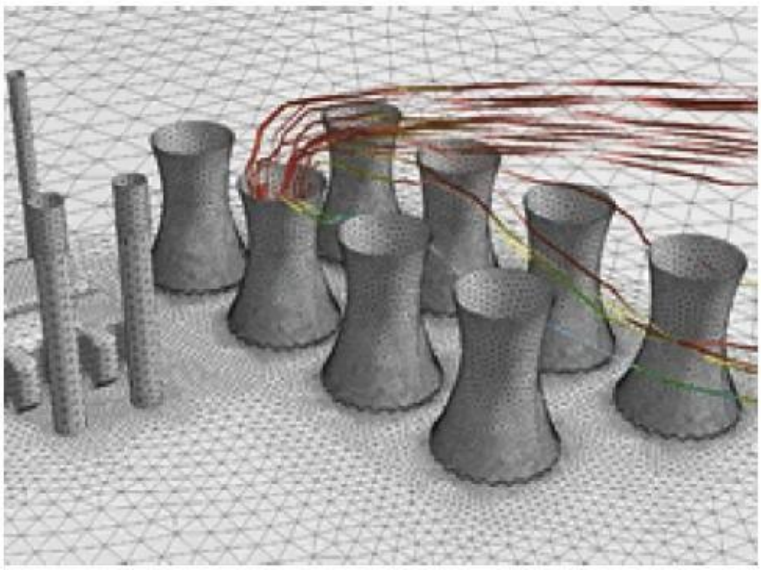

Figure 1.8 Example of CFD application to plume dispersion from a cooling tower.

Figure 1.9 Example of CFD application to the construction of a new tank at a water treatment plant. The top right-hand corner of the figure describes the CFD simulation of the water tank that will be installed within the excavated construction site

The added understanding gained from CFD simulation provides confidence in the design proposal, thus avoiding the added costs of over-sizing and over-specification, whilst reducing risk.

1.5.6. Metallurgy

CFD has been very useful in studying various metallurgical processes and various aspects of a specific process. CFD has been shown to provide an insightful understanding of an existing process, of modification and optimization of the operation and design in an existing process, and of new process development. It is worthwhile mentioning that metallurgical processes are challenging for CFD modeling since many of the phenomena have not yet been properly described or incorporated into the general CFD framework. Nevertheless, many new and significant developments of multi-physics models are taking place in aptly simulating increasingly complicated industrial processes involving flow and transport of mass, momentum, energy, and chemical species in multi-phase and high-temperature reactive systems. The use of CFD in simulating heterogeneous and slow dissolution of packed bed coke particles is illustrated in Figure 1.10.

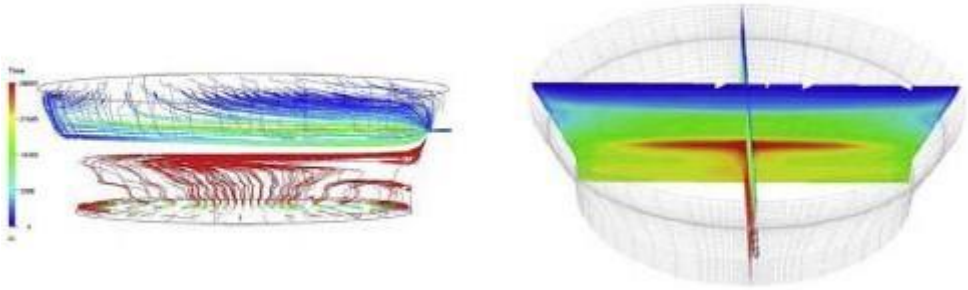

Figure 1.10 Example of CFD application to predict molten iron flow (left, timeline) and carbon dissolution (right, concentration) in the blast furnace hearth.

1.5.7. Nuclear Safety

During the last decade, the need for more accurate computational models for relevant safety analyses of nuclear facilities has sparked an escalating interest in CFD to feasibly predict a number of important flow phenomena that otherwise may not have been possible through other simplified approaches.

Some specific problems, such as those arising from pressurized thermal shock, coolant mixing, and thermal stripping, as well as containment issues in nuclear reactors, have certainly motivated enormous research activities for the application of CFD to analyze such problems.

Figure 1.11 Example of CFD application to the prediction of turbulent mixing in the ROCOM test facility during boron dilution transients

CFD calculations have been performed for coolant mixing in pressurized water reactors. This problem is of significant interest to the nuclear community, particularly in attempting to understand the stationary and transient mixing of coolant in streamlined break and boron dilution scenarios, where the mixing phenomena have tremendous impact on the economical operation and structural integrity of such facilities. Figure 1.11 illustrates the case of a pump start-up due to a strong impulse-driven flow at the inlet nozzle, where the horizontal part of the flow dominates in the down comer in a pressurized water reactor.

1.5.8. Power Generation

In an increasingly competitive energy market, utilities and equipment manufacturers are turning to CFD to provide a technological edge through a better understanding of the equipment and processes within these industries. Although traditional electric-power–generation sources are stillwidely used, renewable power sources, such as wind energy, are emerging as a potential alternative for power generation. To maximize return on investment, CFD is being employed to optimize the turbine blades for generating constant power under varying wind conditions, as demonstrated by a typical three-dimensional simulation of the hydraulics in a complete Francis turbine depicted in Figure 1.12.

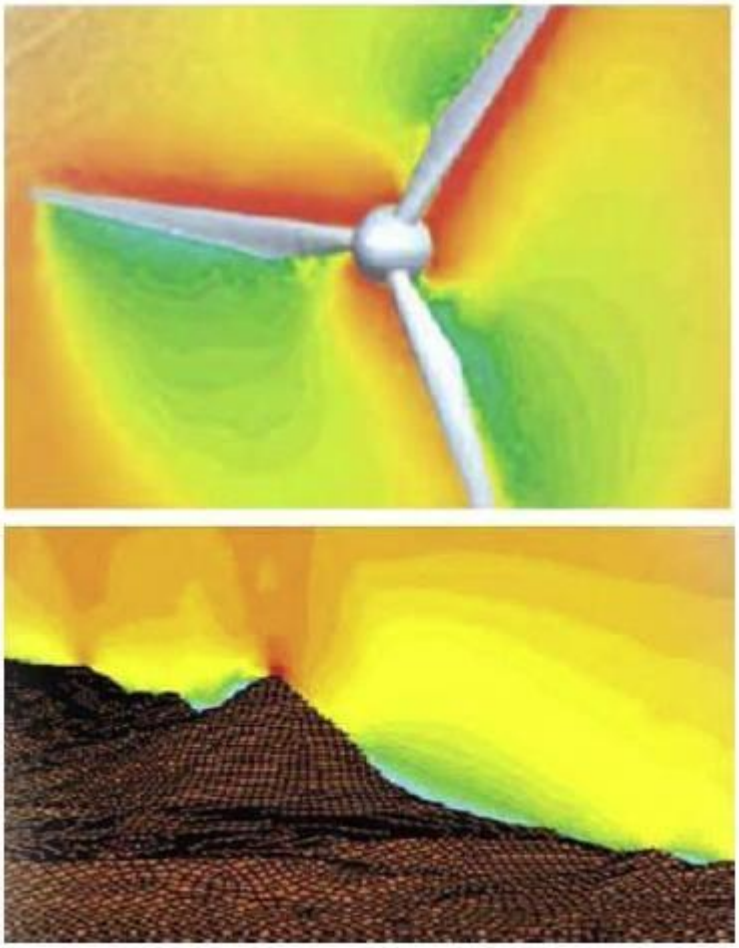

Figure 1.12 Example of CFD application to prediction of the velocity field of a wind turbine and in the vicinity of a proposed wind farm for power.

CFD is also the only technology that has proven to accurately model wind- farm resource distribution, especially for highly complex terrainwith steep inclines, as shown in the same figure. Signicantly, CFD has allowed the positioning of turbines throughout an area to achieve efficient wind capture and

tominimizewake interaction.

1.5.8. Sports Simualtion

Very recently, one of the most innovative uses of CFD in the sports arena is to "design" the optimum stroke to achieve peak propulsive performance for elite swimmers, as demonstrated by the example in Figure 1.13.

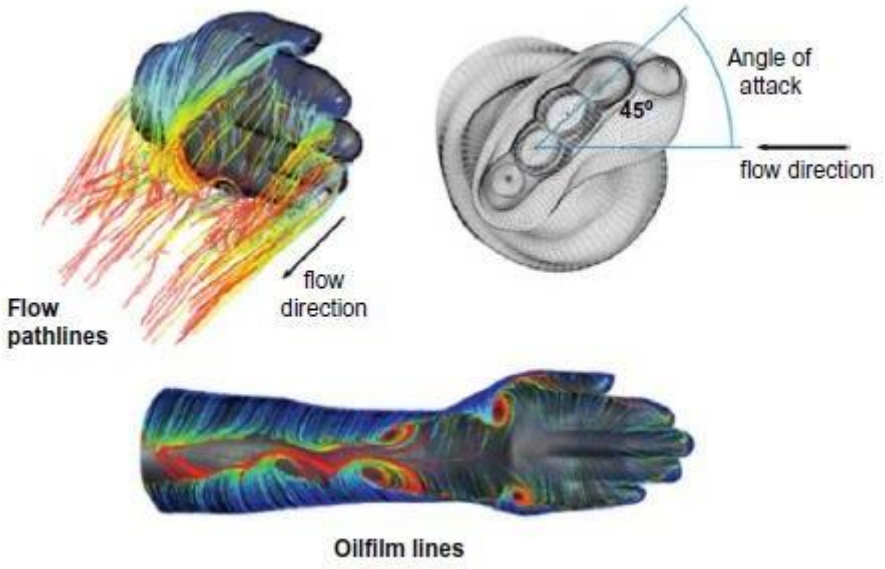

Figure 1.13 Example of CFD application for designing the optimum stroke.

In aspiring to attain an extra edge, USA Swimming, the national governing body for competitive swimming in the United States, commissioned CFD investigations to evaluate the flow around the hand and forearm of a swimmer during the propulsion phases of the freestyle and butterfly strokes. By applying CFD, steady-state lift and drag forces for the hand and arm are determined through a sophisticated turbulence model and adaptive meshing.

Through CFD, Sports Engineering Research Group (SERG) redesigned the Olympic bikes' forks and handlebar arrangement. CFD also helped the team to choose the most streamlined design for the aerodynamic helmet, as exemplified in Figure 1.14. By better understanding the flow pathlines over the aerodynamic helmet, a range of helmet designs were manufactured to accommodate different head styles, achieving the ultimate cycling efficiency. SERG's recommendations ensured the British cycling team had the competitive advantage in their quest for gold.

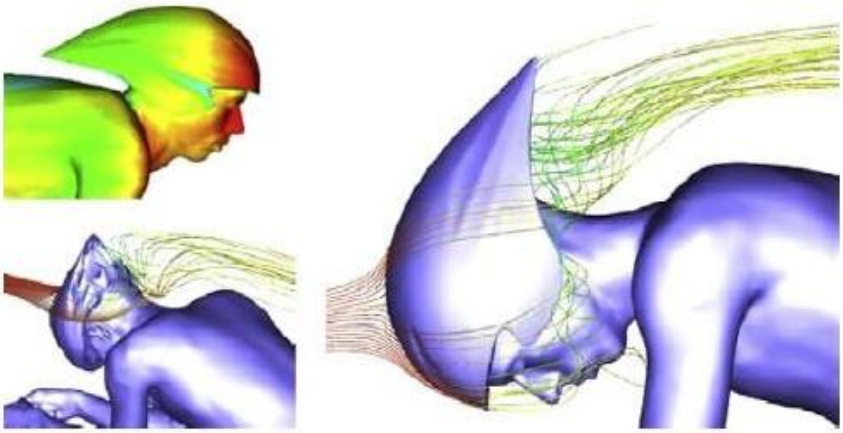

Figure 1.14 Example of CFD simulation in designing the ultimate aerodynamic helmet.

1.6 GENERAL PROCEDURE OF CFD

The codes provide a complete CFD analysis, consisting of three main elements:

- Pre-processor
- Solver
- Post-processor

Figure 1.15 presents a framework that illustrates the interconnectivity of the three aforementioned elements within the CFD analysis.

1.7 PROBLEM SETUP—PRE-PROCESS

1.7.1 Creation of Geometry—Step 1

The first step in any CFD analysis is the definition and creation of the geometry of the flow region, i.e., the computational domain for the CFD calculations. It is important that the reader should always acknowledge the real physical flow representation of the problem that is to be solved, as demonstrated by the respective physical domains in Figures 1.16. One important aspect that the reader should always note in the creation of the geometry for CFD calculations is to allow the flow dynamics to be sufficiently developed across the length L of the computational domains.

1.7.2 Mesh Generation—Step 2

The second step, mesh generation, is one of the most important steps in the preprocess stage after the definition of the domain geometry. CFD requires the subdivision of the domain into a number of smaller, non-overlapping subdomains in order to solve the flow physics within the domain geometry that has been created; this results in the generation of a mesh (or grid) of cells (elements or control volumes) overlying the whole domain geometry. The essential fluid flows that are described in each of these cells are usually solved numerically, so that the discrete values of the flow properties, such as the velocity, pressure, temperature, and other transport parameters of interest, are determined. This yields the CFD solution to the flow problem that is being solved. The accuracy of a CFD solution is strongly influenced by the number of cells in the mesh within the computational domain.

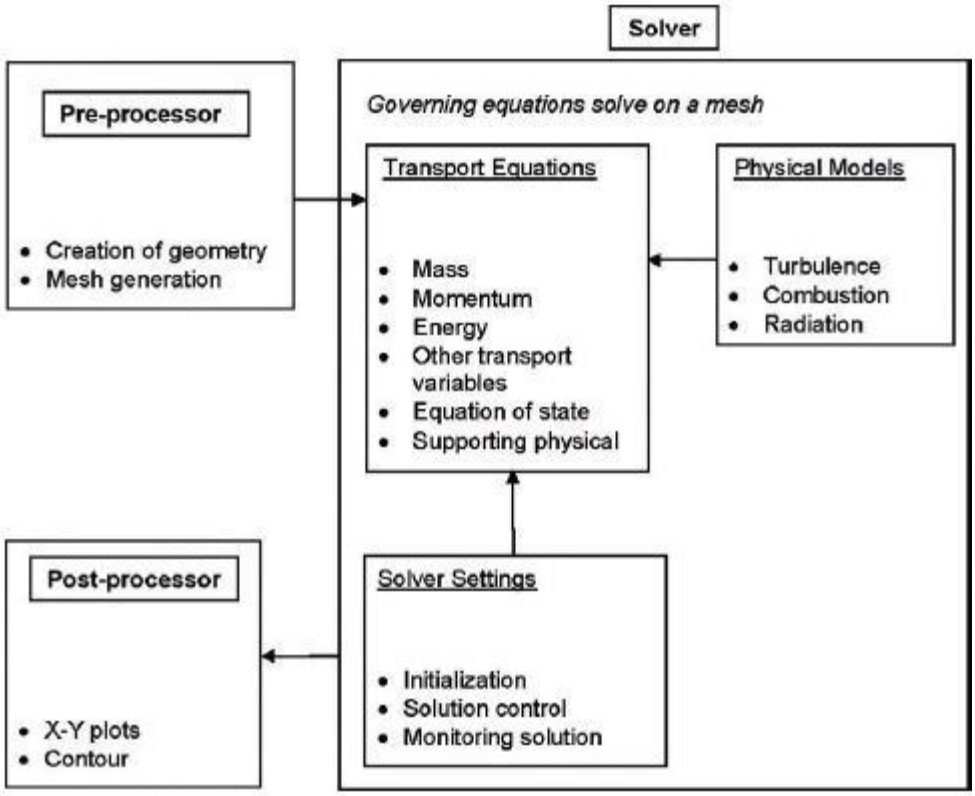

Figure 1.15 The interconnectivity functions of the three main elements within a CFD analysis framework.

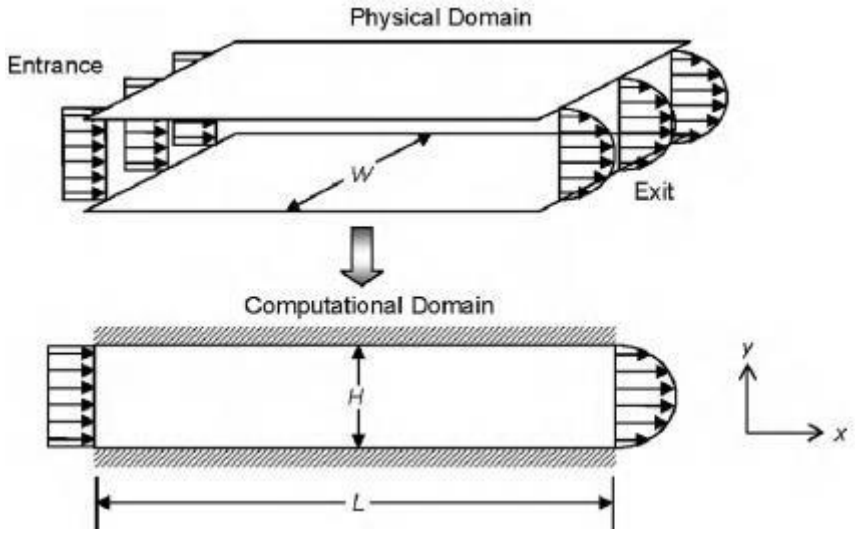

Figure 1.16 Fluid flowing between two stationary parallel plates.

Figure 1.17 shows a mesh of 20 (L) x 20 (H) cells, resulting in a total of 400 cells allocated for the Case of CFD problem between two stationary parallel plates. For more complex geometries, meshing by triangular cells allows flexibility in mesh generation for geometries having complicated shape boundaries. Figure 1.18 illustrates a typical distribution of triangular cells within the computational domain for the Case of problem of fluid passing over two cylinders, with a mesh totaling 16,637 cells mapping the whole flow domain.

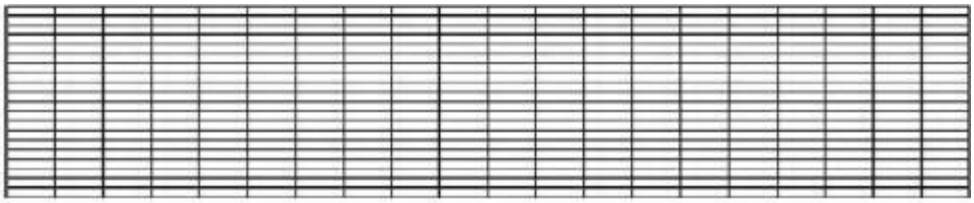

Figure 1.17 Structured meshing for fluid flowing between two stationary parallel plates.

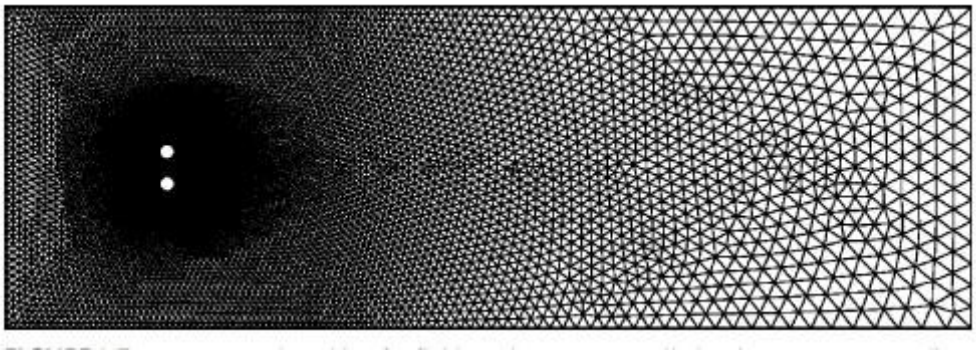

Figure 1.18 Unstructured meshing for fluid passing over two cylinders in an open surrounding

1.7.3 Selection of Physics and Fluid Properties—Step 3

Many industrial CFD flow problems may require solutions to very complex physical flow processes, such as the accommodation of complicated chemical reactions in combusting fluid flows. The inclusion of combustion and possibly radiation models in the CFD calculations is generally a prerequisite for successful modeling of these types of flows.

Combustion and radiation processes have the tendency to strongly influence the local and global heat transport, whichconsequently affects the overall fluid dynamics within the flow domain. It is therefore imperative that the CFD user carefully identify the underlying flow physics unique to the particular fluid-flow system. For clarity and ease of reference, a flowchart highlighting the various flow physics that may be encountered within the framework of CFD and heat transfer processes is presentedin Figure 1.19.

Under the main banner "Computational Fluid Dynamics & Heat Transfer," a CFD user declare s initially whether simulations of the fluid-flow system are to be attained for transient/unsteady or steady solutions. He/she subsequently defines which class of fluids that the flows belong to: inviscid or viscous.

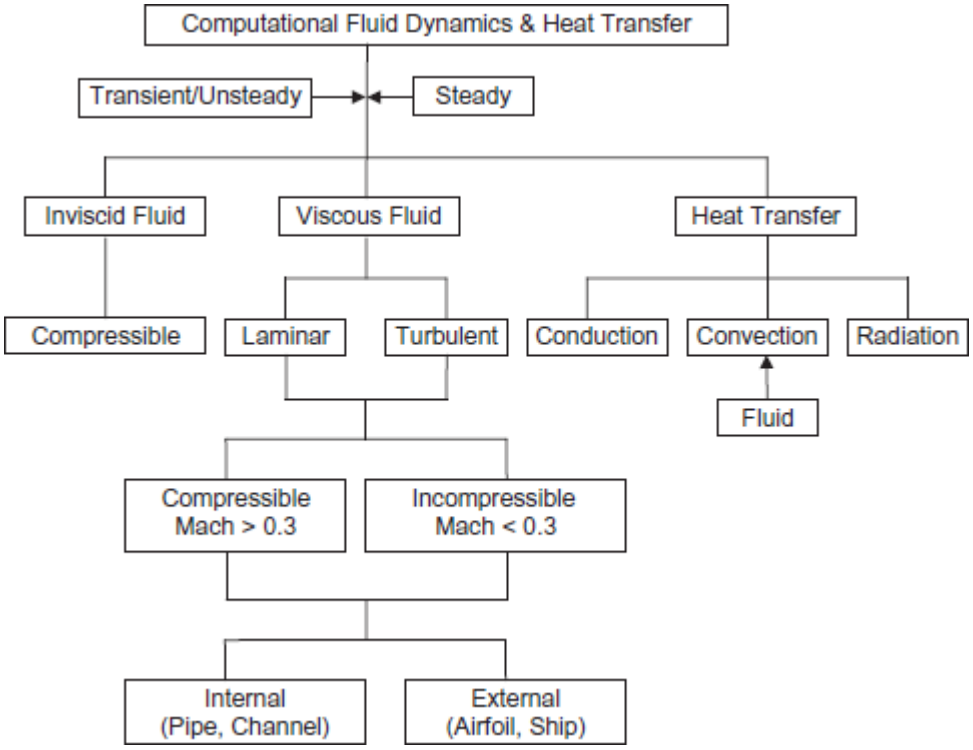

Figure 1.19 A flowchart encapsulating the various flow physics in CFD.

1.7.4 Specification of Boundary Conditions—Step 4

The complex nature of many fluid- flow behaviors has important implications for which boundary conditions are prescribed for the flow problem. A CFD user needs to define appropriate conditions that mimic the real physical representation of the fluid flow in a solvable CFD problem.

The fourth step in the pre-process stage deals with the specification of permissible boundary conditions that are available for impending simulations. Evidently, where inflow and outflow boundaries exist within the flow domain, suitable fluid-flow boundary conditions are required to accommodate the fluid behavior upon entering and leaving the flow domain.

Schematic descriptions of the boundary conditions are demonstrated in Figure 1.20 for Case of CFD problem between two stationary parallel plates.

1.8 NUMERICAL SOLUTION—CFD SOLVER

The appropriate use of either an in-house or a commercial CFD code requires a core understanding of the underlying numerical aspects of the CFD solver. This section focuses on the solver element. A CFD solver can usually be described and envisaged by the solution procedure presented in Figure 1.21.

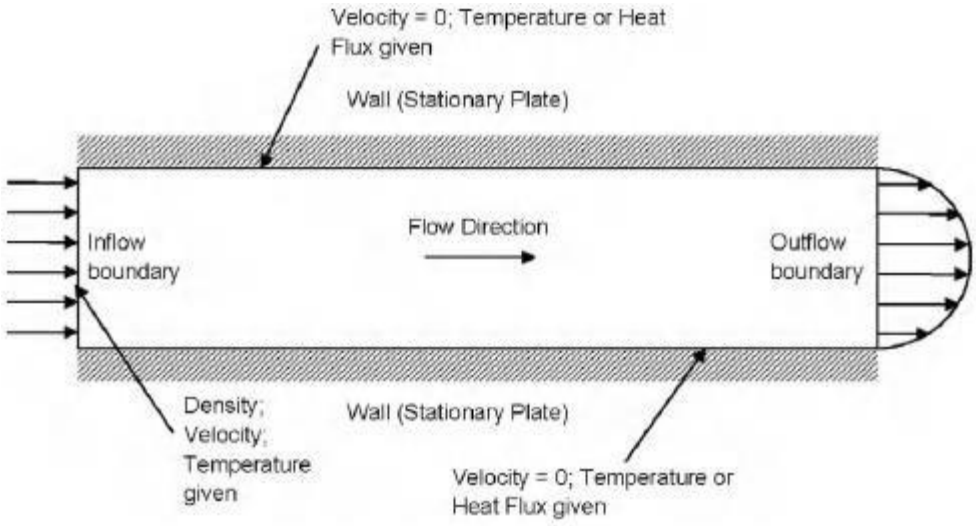

Figure 1.20 Boundary conditions for an internal flow problem: CFD problem of flow between two stationary parallel plates.

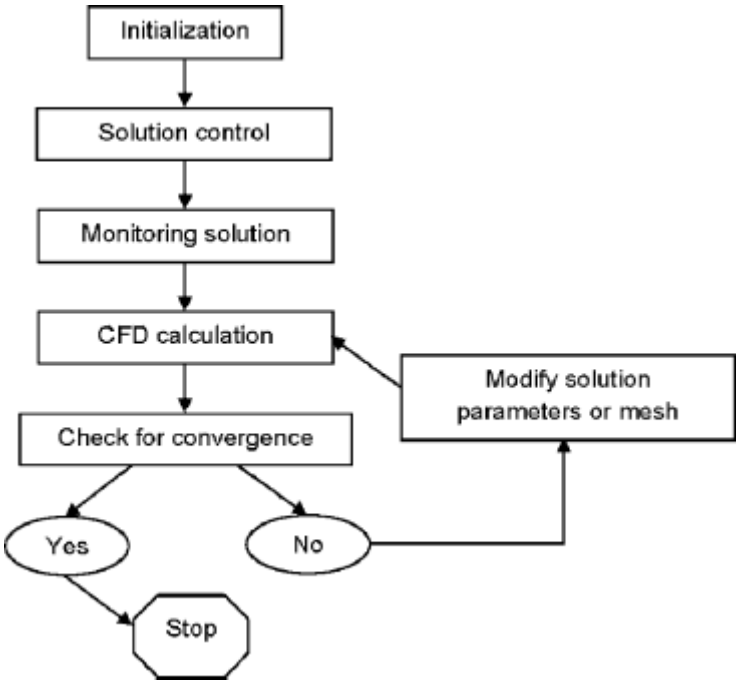

Figure 1.21 An overview of the solution procedure.

The prerequisite processes in the solution procedure that have implications for the computational solution are initialization, solution control, monitoring solution, CFD calculation, and checking for convergence.

1.8.1 Initialization and Solution Control—Step 5

The fifth step of the CFD analysis encompasses two prerequisite processes within the CFD solver: initialization and solution control. Two reasons that a CFD user should undertake the appropriate selection of initial conditions are

- If the initial conditions are close to the final steady-state solution, the

quicker the iterative procedure will converge and yield results in a shorter computational time.

- If the initial conditions are far away from reality, the computations will require longer computational efforts to reach the desired convergence. Also, improper initial conditions may lead to the iterative procedure's misbehaving and possibly "blowing up" or diverging.

Second, setting up appropriate parameters in the solution control usually entails the specification of appropriate discretization (interpolation) schemes and selection of suitable iterative solvers.

1.8.2 Monitoring Convergence—Step 6

The sixth step of the CFD solver involves the interlinking operations of three prerequisite processes: monitoring solution, CFD calculation, and checking for convergence. Two aspects that characterize a successful CFD computational solution are convergence of the iterative process and grid independence.

1.9 RESULT REPORT AND VISUALIZATION—POST-PROCESS

CFD has a reputation for generating vivid graphic images and, while some of the images are promotional and are usually displayed in stunning and superb colorful output, the ability to present the computational results effectively is an invaluable design tool.

1.9.1 X-Y Plots

X-Y plots are mainly two-dimensional graphs that represent the variation of one dependent transport variable as compared with another, independent variable. They can usually be drawn by hand or more conveniently by many plotting packages. Such plots are the most precise and quantitative way to present the numerical data. Often, laboratory data are gathered by straight- line traverses. An X-Y plot of a laminar velocity profile at the fully developed region for the Case of flow between two stationary parallel plates is shown in Figure 1.22.

1.9.2 Vector Plots

A vector plot provides the means whereby a vector quantity (usually velocity) is displayed at discrete points by an arrow, whose orientation indicates direction and whose size indicates magnitude. A vector plot generally presents a perspective view of the flow field in two dimensions. In a three-dimensional flow field, different slices of two-dimensional planes containing the vector quantities can be generated in different orientations to better scrutinize the global flow phenomena.

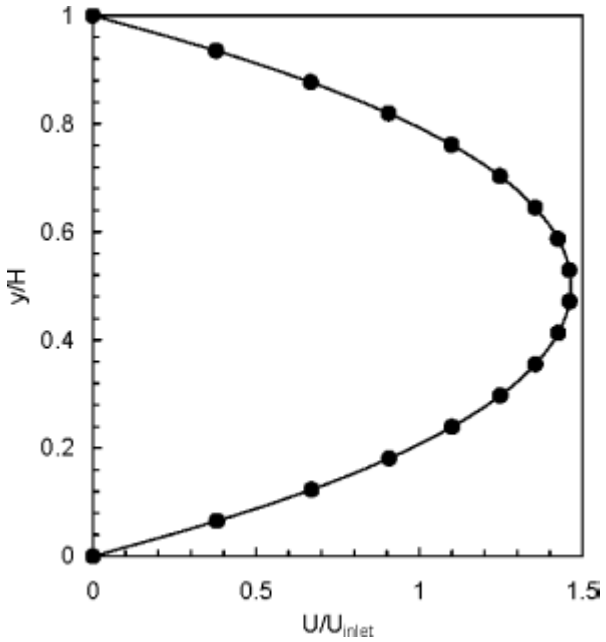

Figure 1.22 X-Y plot of a parabolic laminar velocity profile at the fully developed region for the case of flow between two stationery parallel plates

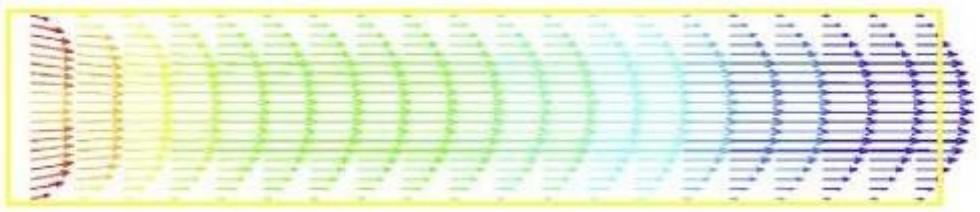

Figure 1.23 Velocity vectors showing the flow development along the parallel-plate channel for Case of flow between two stationery parallel plates

1.9.3 Contour Plots

Contour plotting is another useful and effective graphic technique that is frequently utilized in viewing CFD results. The proliferation of contour plots ever since the advent of the computer is not surprising. In CFD, contour plots are one of the most commonly found graphic representations of data. A contour line (also known as an isoline) can be described as a line indicative of some property that is constant in space. The equivalent representation in three dimensions is an isosurface. In contrast to X-Y plots, contour plots, like vector plots, provide
a global description of the fluid flow encapsulated in one view.

1.10 MODELS OF FLUID FLOW

In obtaining the basic equations of fluid motion, the following philosophy is always followed:

1. Choose the appropriate fundamental physical principles from the law of physics, such as:

a. Mass is conserved.

b. **F = ma** (Newton's second law).
c. Energy is conserved.

2. Apply these physical principles to a suitable model of the flow.
3. From this application, extract the mathematical equations which embody such physical principles.

A solid body is rather easy to see and define· on the other hand, a fluid is a "squishy" substance that is hard to grab hold of. If a solid body is in translational motion, the veloc ity of each part of the body is the same; on the other hand, if a fluid is in motion, the velocity may be different at each location in the fluid. How then do we visualize a moving fluid so as to apply to it the fundamental physical principles?

For a continuum fluid, the answer is to construct one of the four models described below.

1.10.1 Finite Control Volume

Consider a general flow field as represented by the streamlines in Figure 1.24. Let us imagine a closed volume drawn within a *finite* region of the flow. This volume defines a *control volume Y;* a *control surface* Sis defined as the closed surface which bounds the volume. The control volume may be *fixed* in space with the fluid moving through it, as shown at the left of Figure 1.24.

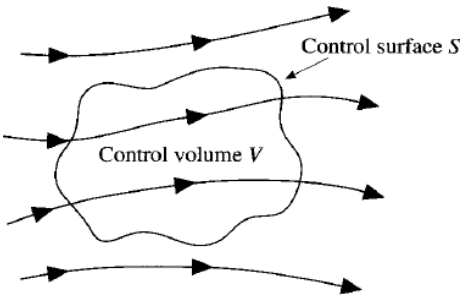

Finite control volume fixed in space with the fluid moving through it

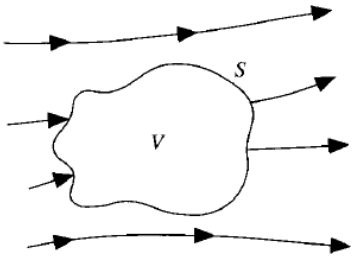

Finite control volume moving with the fluid such that the same fluid particles are always in the same control volume

Left figure **Right Figure**

Figure 1.24 Models of a flow - Finite control volume approach

Alternatively, the control volume may be moving with the fluid such that the same fluid particles are always inside it as shown at the right of Figure 1.24. In either case, the control volume is a reasonably large, finite region of the flow. The fundamental physical principles are applied to the fluid inside the control volume and to the fluid crossing the control surface (if the control volume is fixed in space).

Therefore, instead of lookmg at the whole flow field at once, with the control volume model we limit our attention to just the fluid in the finite region of the volume itself. The fluid-flow equations that we *directly* obtain by applying the fundamental physical principles to a finite control volume are in *integral form.* These integral forms of the governing equations can be manipulated to *indirectly* obtain partial differential equations. The equations so obtained from the **finite control volume fixed in space** (left side of Figure 1.24*),* in either integral or partial differential form, are called the ***conservation* form of the**

governing equations.

The equations obtained from the **finite control volume moving with the fluid** (right side of Figure *1.24*), in either integral or partial differential form, are called the ***nonconservation* form of the governing equations.**

1.10.2 Infinitesimal Fluid Element

Consider a general flow field as represented by the streamlines in Figure 1.25. Let us imagine an infinitesimally small fluid element in the flow with a differential volume dV. The fluid element is infinitesimal in the same sense as differential calculus; however, it is large enough to contain a huge number of molecules so that it can be viewed as a continuous medium.

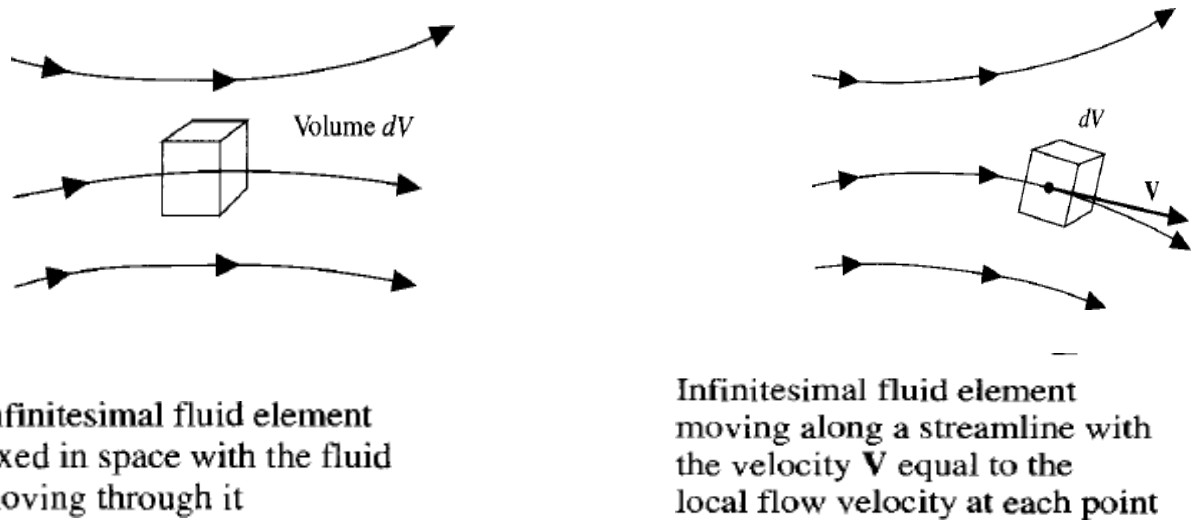

Left figure **Right Figure**

Figure 1.25 Models of a flow - infinitesimal fluid element approach

The fluid element may be fixed in space with the fluid moving through it, as shown at the left of Figure 1.25. Alternatively, it may be moving along a streamline with a velocity vector V equal to the flow velocity at each point. Again, instead of looking at the whole flow field at once, the fundamental physical principles are applied to just the infinitesimally small fluid element itself.

This application leads *directly* to the fundamental equations in *partial differential equation form.* Moreover, the particular partial differential equations obtained directly from **the fluid element fixed in space (left side of Figure 1.25*)* are again the *conservation form* of the equations**.

The partial differential equations obtained *directly* **from the moving fluid element (right side of Figure *1.25)* are again called the *nonconservation form* of the equations.**

1.11 SUBSTANTIAL DERIVATIVE (TIME RATE OF CHANGE FOLLOWING A MOVING FLUID ELEMENT)

Before deriving the governing equations, we need to establish a notation which is common in aerodynamics - that of the substantial derivative.

As the model of the flow, we will adopt the picture shown at the right of Figure 1.25. Here we consideran infinitesimally small fluid element moving with the flow. The motion of this fluid element is shown in more detail in figure 1.26.

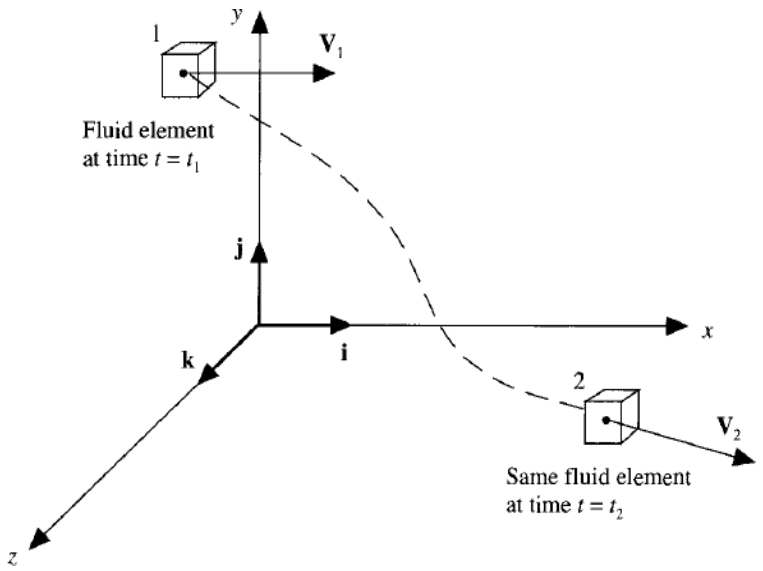

Figure 1.26 Fluid element moving in the fluid flow-illustration for the substantial derivative

Here, the fluid element is moving through cartesian space. The unit vectors along the *x*, *y*, and *z* axes are **i, j,** and **k,** respectively. The vector velocity field in this cartesian space is given by equation (1)

$$V = ui + vj + wk \quad \textbf{(1)}$$

where the x, y, and z components of velocity (Equation 1) are given, respectively, by

$$\begin{aligned} u &= u(x, y, z, t) \\ v &= v(x, y, z, t) \\ w &= w(x, y, z, t) \end{aligned} \quad \textbf{(2)}$$

Note that we are considering in general an unsteady flow, where u, v, and w are functions of both space and time t. In addition, the scalar density field is given by

$$\rho = \rho(x, y, z, t) \quad \textbf{(3)}$$

At time t_1, the fluid element is located at point 1 as in Figure 1.26. At this point and time, the density of the fluid element is

$$\rho_1 = \rho(x_1, y_1, z_1, t_1) \quad \textbf{(4)}$$

At time t_2, the fluid element is located at point 2 as in Figure 1.26. Hence at time t_2, the density of the fluid element is

$\rho_2 = \rho(x_2, y_2, z_2, t_2)$ ..... **(5)**

Since ρ = ρ (x, y, z, t), we can expand this function in a Taylor series about point 1 as follows: The General Expression for Taylor's series of a function f(x) with respect to point a

$$f(x) = f(a) + f'(a)(x-a) + \frac{f^{FF}(a)}{2!}(x-a)^2$$

$$\rho_2 = \rho_1 + \left(\frac{\partial \rho}{\partial x}\right)_1 (x_2 - x_1) + \left(\frac{\partial \rho}{\partial y}\right)_1 (y_2 - y_1) + \left(\frac{\partial \rho}{\partial z}\right)_1 (z_2 - z_1) + \left(\frac{\partial \rho}{\partial t}\right)_1 (t_2 - t_1) + (\text{higher-order terms})$$

……..(6)

Dividing equation (6), by $t_2 - t_1$ and ignoring higher-order terms, we obtain

$$\frac{\rho_2 - \rho_1}{t_2 - t_1} = \left(\frac{\partial \rho}{\partial x}\right)_1 \frac{x_2 - x_1}{t_2 - t_1} + \left(\frac{\partial \rho}{\partial y}\right)_1 \frac{y_2 - y_1}{t_2 - t_1} + \left(\frac{\partial \rho}{\partial z}\right)_1 \frac{z_2 - z_1}{t_2 - t_1} + \left(\frac{\partial \rho}{\partial t}\right)_1$$

……..(7)

Examine the left side of the Equation (7). This is physically the *average* time rate of change in density of the fluid element as it moves from point 1 to point 2. In the limit, as t_2 approaches t_1, this term becomes

$$\lim_{t_2 \to t_1} \frac{\rho_2 - \rho_1}{t_2 - t_1} \equiv \frac{D\rho}{Dt}$$

…….. (8)

In equation (8) the term , $D\rho/Dt$ is a symbol for the *instantaneous* time rate of change of density of the fluid element as it moves through point 1. By definition, this symbol is called the *substantial derivative D/Dt.*

Note that $D\rho/Dt$ is the time rate of change of density of the *given fluid element* as it moves through space. Here, our eyes are locked on the fluid element as it is moving, and we are watching the density of the element change as it moves through point 1.

This is different from $(\partial\rho/\partial t)_1$, which is physically the time rate of change of density at the fixed point 1. For $(\partial\rho/\partial t)_1$, we fix our eyes on the stationary point 1 and watch the density change due to transient fluctuations in the flow field. Thus, $D\rho/Dt$ *and* $\partial\rho/\partial t$ are physically and numerically different quantities.

Now in equation (7), note that

$$\lim_{t_2 \to t_1} \frac{x_2 - x_1}{t_2 - t_1} \equiv u$$
$$\lim_{t_2 \to t_1} \frac{y_2 - y_1}{t_2 - t_1} \equiv v$$
$$\lim_{t_2 \to t_1} \frac{z_2 - z_1}{t_2 - t_1} \equiv w$$

……(9)

Substitute equation (8) and equation (9) in to equation (7) and thus, taking the limit of Eq. (2.1) as $t_2 \; t_1$, we obtain

$$\frac{D\rho}{Dt} = u\frac{\partial \rho}{\partial x} + v\frac{\partial \rho}{\partial y} + w\frac{\partial \rho}{\partial z} + \frac{\partial \rho}{\partial t}$$

……(10)

Examine Equation (10) closely. From it, we can obtain an expression for the substantial derivative in Cartesian coordinates:

$$\frac{D}{Dt} \equiv \frac{\partial}{\partial t} + u\frac{\partial}{\partial x} + v\frac{\partial}{\partial y} + w\frac{\partial}{\partial z}$$

……(11)

Furthermore, in Cartesian coordinates, the vector operator ❑ is defined as

$$\nabla \equiv \mathbf{i}\frac{\partial}{\partial x} + \mathbf{j}\frac{\partial}{\partial y} + \mathbf{k}\frac{\partial}{\partial z}$$

……(12)

we know that V =ui + vj +wk , then V . ❑ = $\cdot \; u\frac{\partial}{\partial x} + v\frac{\partial}{\partial y} + w\frac{\partial}{\partial z}$ **(13)**

Hence equation (11) becomes $\frac{D}{Dt} \equiv \frac{\partial}{\partial t} + (\mathbf{V} \cdot \nabla)$ **(14)**

Equation (14) represents a definition of the substantial derivative operator in vector notation; thus, it is valid for any coordinate system.

D/Dt is the substantial derivative, which is physically that time rate of change following a moving fluid element;

∂/∂t is called the *local derivative,* which is physically the time rate of change at a fixed point;

V. ∇ is called the *convective derivative,* which is physically the time rate of change due to the movement of the fluid element from one location to another in the flow field where the flow properties are spatially different.

The substantial derivative applies to any flow-field variable, for example, *Dp/Dt, DT/Dt, Du/Dt,* etc., where *p* and T are the static pressure and temperature, respectively.

1.9 DIVERGENCE OF VELOCITY : ITS PHYSICAL MEANING

Let us consider the divergence of the velocity, ❑ · V .This term appears frequently in the equations of fluid dynamics, and it is well to consider its physical meaning. Consider a control volume moving with the fluid as sketched below

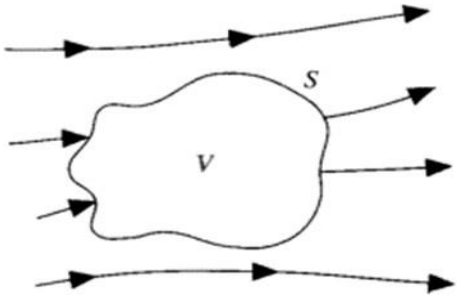

Finite control volume moving with the fluid such that the same fluid particles are always in the same control volume

This control volume is always made up of the same fluid particles as it moves with the flow; hence, its mass is fixed, invariant with time. However, its volume and control surface S are changing with time as it moves to different regions of the flow where different values of ρ exist. That is, this moving control volume of fixed mass is constantly increasing or decreasing its volume and is changing its shape, depending on the characteristics of the flow.

This control volume is shown in Figure below and at some instant in time. Consider an infinitesimal element of the surface *dS* moving at the local velocity V, as shown in below figure1.27.

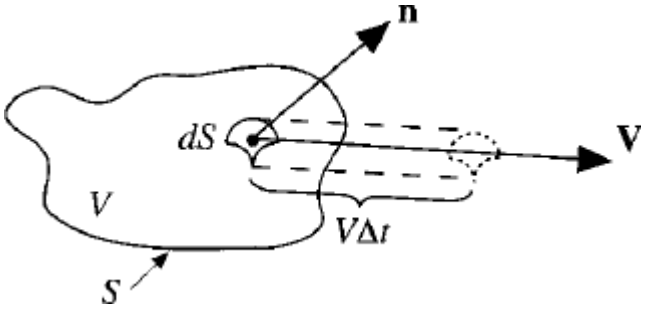

Figure 1.27 Moving control volume used for the physical interpretation of the divergence of velocity.

(Note: velocity = displacement / time ; and displacement = velocity x time)

The change in the volume of the control volume, $\Delta \forall$, due to just the movement of *dS* over a time increment Δ*t* is, from Figure 1.27, equal to the volume of the long, thin cylinder with base area *dS* and altitude (V *Δt)* · n, where n is a unit vector perpendicular to the surface at *dS.*

$$\Delta \mathscr{V} = [(\mathbf{V}\,\Delta t)\cdot \mathbf{n}]\,dS = (\mathbf{V}\,\Delta t)\cdot \mathbf{dS}$$

……(15)

Note: Volume of Cylinder V = base x height ;Here as in previous figure the base is *dS and height is* (V *Δt)* · n *Hence volume is [*(V *Δt)* · n] *dS*

Over the time increment *Δt,* the total change in volume of the whole control volume is equal to the summation of Equation (15) over the total control surface. In the limit as *dS*→ 0, the sum becomes the surface integral

$$\iint_S (\mathbf{V}\,\Delta t)\cdot \mathbf{dS}$$

……(16)

If this integral (equation 2) is divided by *Δt,* the result is physically the time rate of change of the control volume, denoted by $D\mathscr{V}/Dt$;

$$\frac{D\mathscr{V}}{Dt} = \frac{1}{\Delta t}\iint_S (\mathbf{V}\cdot\Delta t)\cdot \mathbf{dS} = \iint_S \mathbf{V}\cdot \mathbf{dS}$$

…….(17)

Note that we have written the left side of Equation (17) as the substantial derivative of $\mathscr{V}$, because we are dealing with the time rate of change of the control volume *as the volume moves with the flow* (we are using the picture of model 2). and this is physically what is meant by the substantial derivative.

Applying the divergence theorem from vector calculus (equation 18) to the right side of Equation (17)we obtain equation 19,

(Note: General form of Divergence Theorem is given in equation (18)

$$\iiint_V (\nabla\cdot\mathbf{F})\,dV = \oiint_S (\mathbf{F}\cdot\hat{\mathbf{n}})\,dS.$$

……(18)

$$\frac{D\mathscr{V}}{Dt} = \iiint_{\mathscr{V}} (\nabla\cdot\mathbf{V})\,d\mathscr{V}$$

……(19)

Now, let us imagine that the moving control volume in Figure (slide no.23) is shrunk to a very small volume $\delta\mathscr{V}$, essentially becoming an infinitesimal moving fluid element. Then Equation (19) can be written as

$$\frac{D(\delta\forall)}{Dt} = \iiint_{\delta\forall} (\nabla \cdot \mathbf{V})\, d\forall$$

……..(20)

Assume that $\delta\forall$ is small enough such that ❑ · V is essentially the same value through out . $\delta\forall$ .Then the integral in Equation (20), in the limit shrinks to zero is given by (∇.V) $\delta\forall$

From equation (20), we have,

$$\frac{D(\delta\forall)}{Dt} = (\nabla \cdot \mathbf{V})\, \delta\forall$$

……..(21)

$$\boxed{\nabla \cdot \mathbf{V} = \frac{1}{\delta\forall} \frac{D(\delta\forall)}{Dt}}$$

…….(22)

Examine Equation (22) closely. on the left side we have the divergence of the velocity; On the right side we have its physical meaning. That is, ∇ .V is physically the time rate of change of the volume of a moving fluid element, per unit volume.

UNIT – II
Governing Equations of Fluid dynamics

2.1 THE CONTINUITY EQUATION

In obtaining the basic equations of fluid motion, the following philosophy is always followed:

(I) Write down a fundamental physical principle (mass is conserved for continuity equation)
(2) Apply it to a suitable model of the flow, and
(3) Obtain an equation which represents the fundamental physical principle.

In this section, we will treat the following case:

Physical principle: Mass is conserved.

The governing flow equation which results from the application of this physical principle to any one of the four models of the flow is called the *continuity equation.*Moreover, in this section we will carry out in detail the application of this physical principle using *all four* of the flow models.

That is, we will derive the continuity equation four different ways, obtaining in a direct fashion four different forms of the equation. Then, by indirect manipulation of these four different forms, we will show that they are all really the *same* equation. In addition, we will invoke the idea of conservation versus nonconservation forms, helping to elucidate the meaning of those words.

2.1.1 MODEL OF THE FINITE CONTROL VOLUME FIXED IN SPACE

Consider the flow model, namely, a control volume of arbitrary shape and of finite size. The volume is fixed in space. The surface that bounds this control volume is called the control surface. The fluid moves through the fixed control volume (Model 1), flowing across the control surface. This flow model is shown in more detail in Fig. 2.1. At a point on the control surface in Fig. 2.1, the flow velocity is V and the vector elemental surface area is **dS.** Also let $d\forall$ be an elemental volume inside the finite control volume. Applied to this control volume, our fundamental physical principle that mass is conserved means

$$\begin{array}{ll} \text{Net mass flow } \textit{out} & \text{time rate of} \\ \text{of control volume} = & \text{decrease of mass} \\ \text{through surface } S & \text{inside control volume} \end{array}$$

or

$$B = C \qquad \text{.....(1)}$$

where *B* and C are just convenient symbols for the left and right sides, respectively.

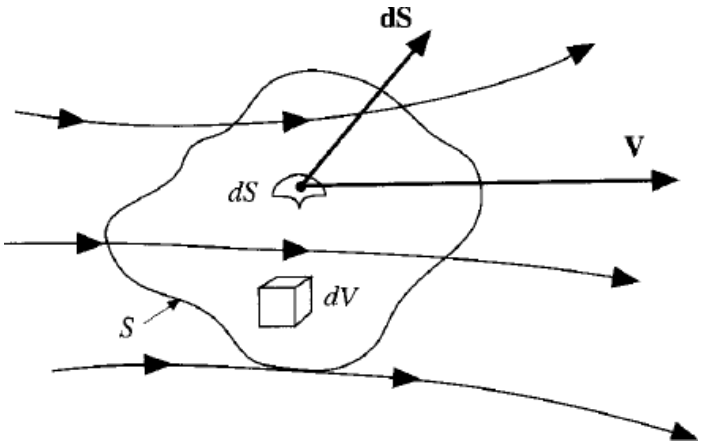

Fig. 2.1 Finite control volume fixed in space

First, let us obtain an expression for *B* in terms of the quantities shown in Fig. 2.1. The mass flow of a moving fluid across any fixed surface (say, in kilograms per second or slugs per second) is equal to the product of (density) x (area of surface) x (component of velocity perpendicular to the surface). Hence the elemental mass flow across the area *dS* is

$$\rho V_n \, dS = \rho \mathbf{V} \cdot \mathbf{dS} \qquad \text{.....(2)}$$

The net mass flow *out* of the entire control volume through the control surface S is the summation over *S* of the elemental mass flow expressed in equation (2)

$$B = \int\int_S \rho \mathbf{V} \cdot \mathbf{dS} \qquad \text{.....(3)}$$

Now let us consider the right side of equation (1), The mass contained within the elemental volume $d\mathscr{V}$ is $\rho \, d\mathscr{V}$. The total mass inside the control volume is therefore

$$\int\int\int_{\mathscr{V}} \rho \, d\mathscr{V} \qquad \text{.....(4)}$$

The time rate of *increase* of mass inside $\mathscr{V}$ is then

$$\frac{\partial}{\partial t}\int\int\int_{\mathscr{V}} \rho \, d\mathscr{V} \qquad \text{.....(5)}$$

In turn, the time rate of decrease of mass inside is the negative of the above; i.e.,

$$-\frac{\partial}{\partial t}\iiint_{\forall} \rho \, d\forall = C$$

…….(6)

Substitute equation (3) and equation (6) in to equation (1), we get

$$\iint_{S} \rho \mathbf{V} \cdot \mathbf{dS} = -\frac{\partial}{\partial t}\iiint_{\forall} \rho \, d\forall$$

…….(7)

$$\boxed{\frac{\partial}{\partial t}\iiint_{\forall} \rho \, d\forall + \iint_{S} \rho \mathbf{V} \cdot \mathbf{dS} = 0}$$

……..(8)

Equation (8) is an *integral form of the continuity equation*. It was derived on the basis of a ***finite* control volume *fixed* in space.**

The fact that the **control volume was *fixed*** *in space* leads to the specific integral form given by Eq. (8), which is called the ***conservation form.***

2.1.2 MODEL OF THE FINITE CONTROL VOLUME MOVING WITH THE FLUID

Consider the flow model, namely, a control volumee of finite size moving with the fluid. This control volume, as it moves with the fluid, is always composed of the same identifiable elements of mass; i.e., the moving control volume has a *fixed mass.* On the other hand, as this fixed mass moves downstream, the shape and volume of the finite control volume can, in general, change. Consider an infinitesimally small element of volume $d\forall$ inside this finite control volume; the mass of this small element is $\rho \, d\forall$, , where ρ *is* the local density.

Then, the total mass of the finite control volume is given by

$$\text{Mass} = \iiint_{\forall} \rho \, d\forall$$

…….(9)

Now recall the physical meanmg of the substantial denvatlve ; it expresses the time rate of change of any

property of a fluid element as it moves with the flow. Since our finite control volumee is made up of an infinite number of infinitesimally small fluid elements, all with a fixed, unchanging mass, and hence all with substantial denvatives of these unchanging masses equal to zero, we can write for the finite control volume, from Eq. (9),

$$\frac{D}{Dt}\int\int\int_{\mathscr{V}} \rho \, d\mathscr{V} = 0 \qquad \text{.....(10)}$$

Equation (10) is an ***integral form of the continuity equation*** It was derived on the basis of a ***finite* control volume *moving* with the fluid.** The fact that the control volume is *moving* with the fluid leads to the specific integral form given by Eq. (10), which is called the ***Non-conservation form.***

2.1.3 MODEL OF AN INFINITESIMALLY SMALL ELEMENT FIXED IN SPACE

Consider the flow model, namely, an infinitesimally small element fixed in space, with the fluid moving through it (Model 3). This flow model is shown in more detail in Fig. 2.2. Here, for convenience we adopt a cartesian coordinate system, where the velocity and density are functions of *(x, y,* z) space and time *t.* Fixed in this *(x, y,* z) space is an infinitesimally small element of sides *dx, dy,* and *dz* (Fig. 2.2a). There is mass flow through this fixed element, as shown in Fig. 2.2*b.* Consider the left and right faces of the element which are perpendicular to the *x* axis. The area of these faces is *dy dz.* The mass flow through the left face is *(ρu) dy dz.* Since the velocity and density are functions of spatial location, the values of the mass flux across the right face will be different from that across the left face; indeed, the difference in mass flux between the two faces is simply *[(∂ (ρu) ∂ x] dx.* Thus, the mass flow across the right face can be expressed as *{ρu + [∂ (ρu)/ ∂ x] dy dz.* The mass flow across both the left and right faces is shown in Fig. *2.2b.* In a similar vein, the mass flow through both the bottom and top faces, which are perpendicular to the y axis, is *(ρv) dx dz* and *{ρv + [∂ (ρv)/ ∂ y] dy} dx dz,* respectively. The mass flow through both the front and back faces, which are perpendicular to the *z* axis, is *(ρw) dx dy* and
{ρw + [∂ (ρw) ∂ z] dz} dx dy, respectively.

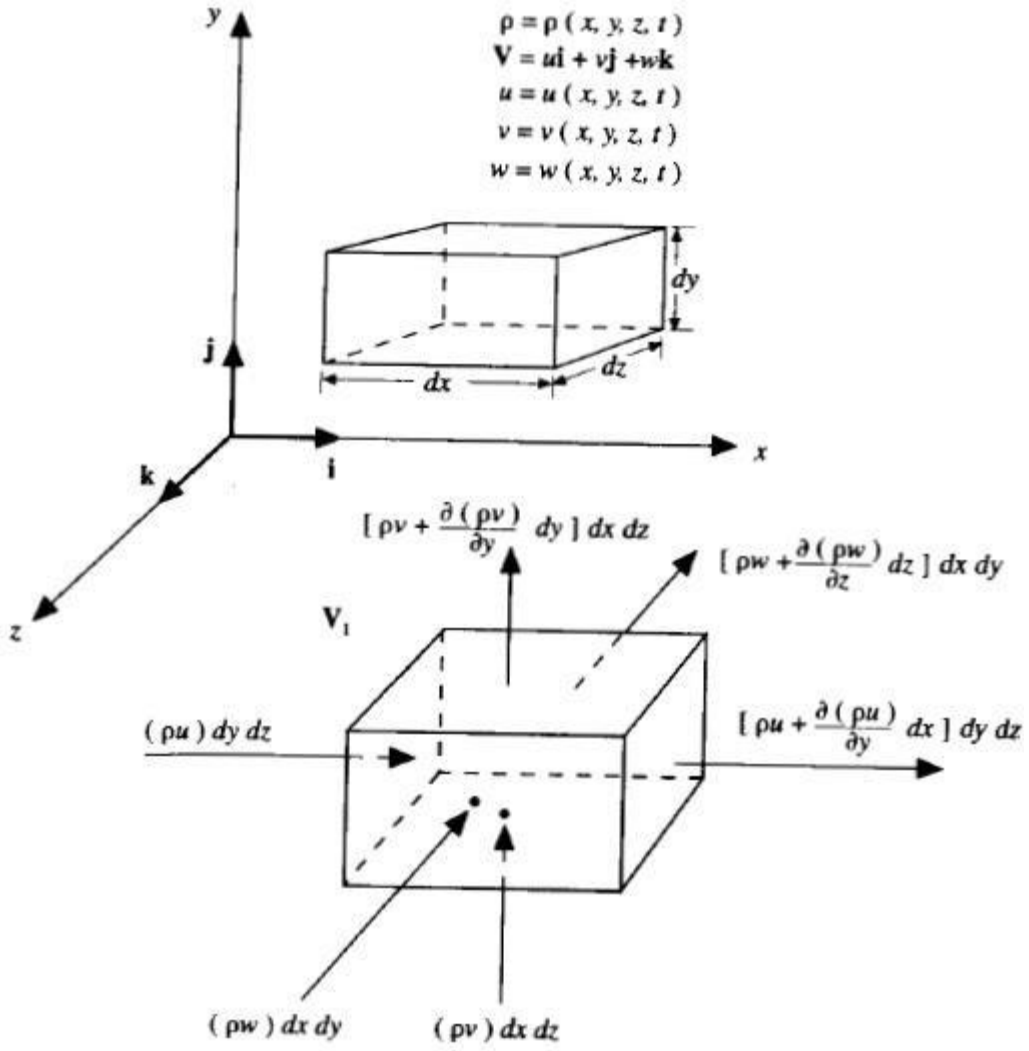

Fig. 2.2 Model of the infinitesimally small element fixed in space and a diagram of the mass fluxes through the various faces of the element for a denvation of the continuity equation.

Note that *u*, *v*, and *w* are positive, by convention, in the positive *x*, *y*, and *z* directions, respectively. Hence, the arrows in Fig. 2. 2 show the contributions to the inflow and outflow of mass through the sidesof the fixed element. If we denote a net outflow of mass as a positive quantity, then from Fig. 2.2, we have

Net outflow in x direction:

$$\left[\rho u + \frac{\partial(\rho u)}{\partial x}\,dx\right] dy\,dz - (\rho u)\,dy\,dz = \frac{\partial(\rho u)}{\partial x}\,dx\,dy\,dz \qquad \text{…….(11)}$$

Net outflow in y direction:

$$\left[\rho v + \frac{\partial(\rho v)}{\partial y}\,dy\right] dx\,dz - (\rho v)\,dx\,dz = \frac{\partial(\rho v)}{\partial y}\,dx\,dy\,dz \qquad \text{…….(12)}$$

Net outflow in z direction:

$$\left[\rho w + \frac{\partial(\rho w)}{\partial z}\,dz\right] dx\,dy - (\rho w)\,dx\,dy = \frac{\partial(\rho w)}{\partial z}\,dx\,dy\,dz$$

…….(13)

Hence, the net mass flow out of the element is given by

$$\text{Net mass flow} = \left[\frac{\partial(\rho u)}{\partial x} + \frac{\partial(\rho v)}{\partial y} + \frac{\partial(\rho w)}{\partial z}\right] dx\,dy\,dz$$

…….(14)

The total mass of fluid in the infinitesimally small element is $\rho\ (dx\,dy\,dz)$; hence the time rate of increase of mass inside the element is given by

$$\text{Time rate of mass increase} = \frac{\partial \rho}{\partial t}\,(dx\,dy\,dz)$$

…….(15)

Physical Principle of mass conservation: The net mass flow out of the element must equal the time rate of *decrease* of mass inside the element. Denoting the mass decrease by a negative quantity

$$\left[\frac{\partial(\rho u)}{\partial x} + \frac{\partial(\rho v)}{\partial y} + \frac{\partial(\rho w)}{\partial z}\right] dx\,dy\,dz = -\frac{\partial \rho}{\partial t}(dx\,dy\,dz)$$

…….(16)

$$\frac{\partial \rho}{\partial t} + \left[\frac{\partial(\rho u)}{\partial x} + \frac{\partial(\rho v)}{\partial y} + \frac{\partial(\rho w)}{\partial z}\right] = 0$$

…….(17)

We Know that,

$$\mathbf{V} \cdot \nabla = u\frac{\partial}{\partial x} + v\frac{\partial}{\partial y} + w\frac{\partial}{\partial z}$$

…….(18)

Substitute equation (18) to equation (17)

$$\boxed{\frac{\partial \rho}{\partial t} + \nabla \cdot (\rho \mathbf{V}) = 0}$$

…….(19)

Equation (19) is a ***partial differential equation form of the continuity equation.*** The fact that the element was fixed in space leads to the specific differential form given by Eq. (19), **which is called the conservation form.**

2.1.4 MODEL OF AN INFINITESIMALLY SMALL ELEMENT MOVING WITH THE FLUID

Consider the flow model, namely, an infinitesimally small fluid element moving with the flow. This fluid element has a fixed mass, but in general its shape and volume will change as it moves downstream.

Denote the fixed mass and variable volume of this moving fluid element by δm and $\delta \forall$, respectively. Then

$$\delta m = \rho \, \delta \forall \qquad \text{.....(20)}$$

Since mass is conserved, we can state that the time rate of change of the mass of the fluid element is zero as the element moves along with the flow.

$$\frac{D(\delta m)}{Dt} = 0 \qquad \text{.....(21)}$$

Sub. Equation (20) in to equation (21) and differentiating, we have

$$\frac{D(\rho \, \delta \forall)}{Dt} = \delta \forall \frac{D\rho}{Dt} + \rho \frac{D(\delta \forall)}{Dt} = 0$$

$$\frac{D\rho}{Dt} + \rho \left[\frac{1}{\delta \forall} \frac{D(\delta \forall)}{Dt} \right] = 0 \qquad \text{.....(22)}$$

Note: W.K.T Divergence of velocity is

$$\boxed{\nabla \cdot \mathbf{V} = \frac{1}{\delta \forall} \frac{D(\delta \forall)}{Dt}} \qquad \text{.....(23)}$$

Substitute equation (23) in equation (22),

$$\boxed{\frac{D\rho}{Dt} + \rho \nabla \cdot \mathbf{V} = 0} \qquad \text{.....(24)}$$

Equation (24) is a **partial differential equation form of the continuity equation**, The fact that the **element is *moving* with the flow leads** to the specific differential form given by Eq. (23), which is called the **non-conservation form.**

2.1.5 ALL THE EQUATIONS ARE ONE: SOME MANIPULATIONS

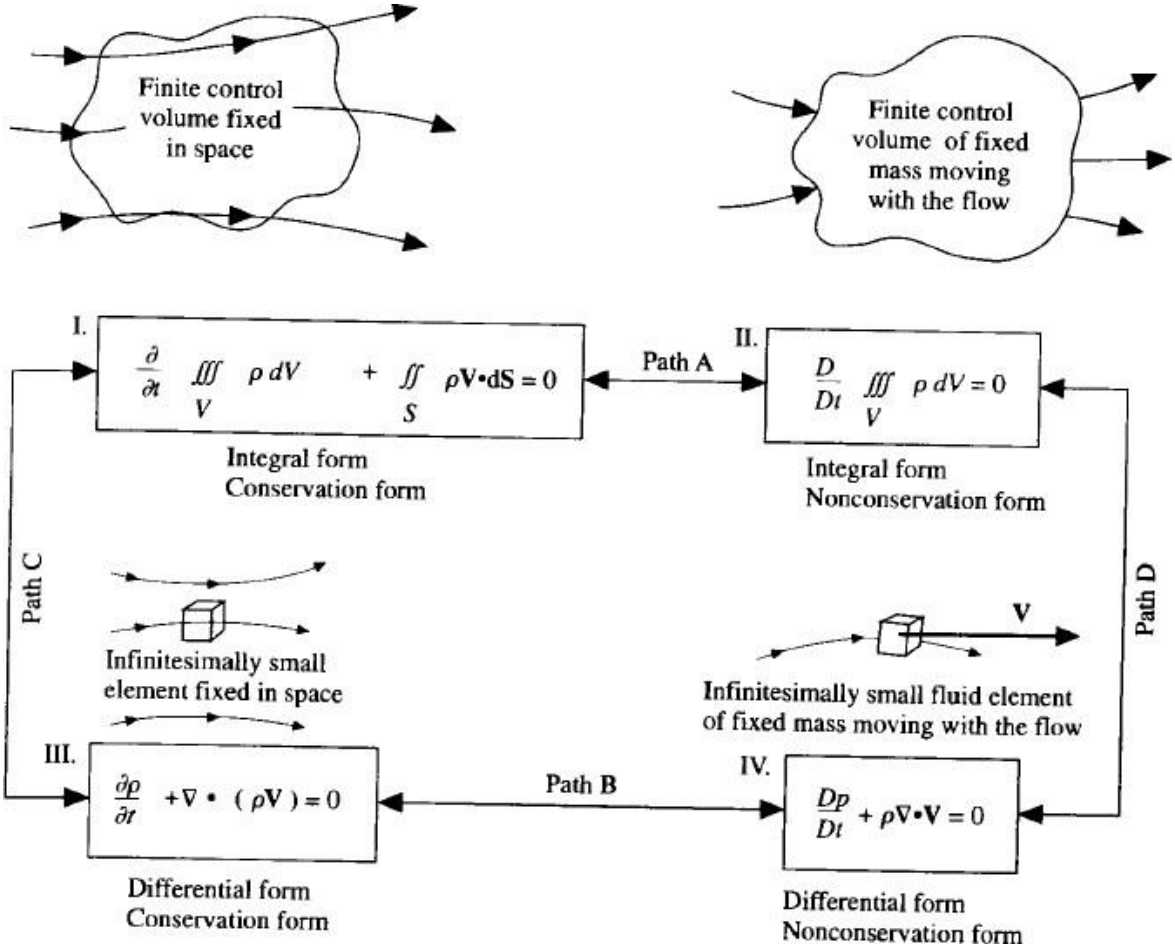

Fig. 2.3 The different forms of the continuity equation, their relationship to the different models of the flow, and the schematic emphasis that all four equations are essentially the same -they can each be obtained from the other.

Now consider Fig. 2.3, which shows the same four flow models. However, in Fig. 2.3 the specific form of the continuity equation obtained *directly* from each model is displayed underneath the sketch of the particular model. Then, we will show, **by mampulation, that the equations in all four boxes (I to IVin figure 2.3) are simply different forms of the same equation.**

Examining Fig. 2.3, we see four different forms of the continuity equation, each one a direct product of the flow model used in its derivation. Two of the forms are integral equations; the other two are partial differential equations. **Two of the equations are in conservation form**; **the other two are in nonconservation form.** However, these **four equations are not fundamentally different equations;** rather, **they are four different forms of the *same* equation**, namely, the continuity equation. Any of these four forms can be derived by manipulation from any of the others. This is symbolized by paths A through *D* sketched in Fig. 2.3.

First, let us examine how the partial differential equation form can be obtained from the integral equation form; i.e., **let us examine path C in Fig. 2.6.** we know,

$$\frac{\partial}{\partial t}\iiint_{\mathscr{V}} \rho \, d\mathscr{V} + \iint_{S} \rho \mathbf{V} \cdot \mathbf{dS} = 0 \qquad \text{…….(25)}$$

Since the control volume used for the derivation of Eq. (25) is fixed in space, the limits of integration for the integrals in Eq. (25) are constant, and hence the time derivative $\partial / \partial t$ can be placed inside the integral.

$$\iiint_{\mathscr{V}} \frac{\partial \rho}{\partial t} \, d\mathscr{V} + \iint_{S} \rho \mathbf{V} \cdot \mathbf{dS} = 0 \qquad \text{…….(26)}$$

Applying the divergence theorem from vector calculus, the surface integral in Eq. (26) can be expressed as a volume integral:

$$\iint_{S} (\rho \mathbf{V}) \cdot \mathbf{dS} = \iiint_{\mathscr{V}} \nabla \cdot (\rho \mathbf{V}) \, d\mathscr{V} \qquad \text{…….(27)}$$

Substituting Eq. (27) into (26), we have

$$\iiint_{\mathscr{V}} \frac{\partial \rho}{\partial t} \, d\mathscr{V} + \iiint_{\mathscr{V}} \nabla \cdot (\rho \mathbf{V}) \, d\mathscr{V} = 0 \qquad \text{…….(28)}$$

$$\iiint_{\mathscr{V}} \left[\frac{\partial \rho}{\partial t} + \nabla \cdot (\rho \mathbf{V}) \right] d\mathscr{V} = 0$$

Or ..... (29)

Since the finite control volume is *arbitrarily* drawn in space, the only way for the integral in Eq. (29) to equal zero is for the integrand to be zero at every point within the control volume. Hence, from Eq. (29)

$$\boxed{\frac{\partial \rho}{\partial t} + \nabla \cdot (\rho \mathbf{V}) = 0} \qquad \text{…….(30)}$$

Equation (30) is precisely the continuity equation in partial differential equation form that is displayed in box III in Fig. 2.3. Hence, we have shown how the integral form in box I can, after some manipulation, yield the differential form in box III. Again, note that both the equations in boxes I and III are in conservation form; the above manipulation does not change that situation.

Energy equation

Nonconservation form

$$\rho\frac{D}{Dt}\left(e+\frac{V^2}{2}\right)=\rho\dot{q}+\frac{\partial}{\partial x}\left(k\frac{\partial T}{\partial x}\right)+\frac{\partial}{\partial y}\left(k\frac{\partial T}{\partial y}\right)+\frac{\partial}{\partial z}\left(k\frac{\partial T}{\partial z}\right)$$
$$-\frac{\partial(up)}{\partial x}-\frac{\partial(vp)}{\partial y}-\frac{\partial(wp)}{\partial z}+\frac{\partial(u\tau_{xx})}{\partial x}$$
$$+\frac{\partial(u\tau_{yx})}{\partial y}+\frac{\partial(u\tau_{zx})}{\partial z}+\frac{\partial(v\tau_{xy})}{\partial x}+\frac{\partial(v\tau_{yy})}{\partial y}$$
$$+\frac{\partial(v\tau_{zy})}{\partial z}+\frac{\partial(w\tau_{xz})}{\partial x}+\frac{\partial(w\tau_{yz})}{\partial y}+\frac{\partial(w\tau_{zz})}{\partial z}+\rho\mathbf{f}\cdot\mathbf{V}\quad(2$$

Conservation form

$$\frac{\partial}{\partial t}\left[\rho\left(e+\frac{V^2}{2}\right)\right]+\nabla\cdot\left[\rho\left(e+\frac{V^2}{2}\right)\mathbf{V}\right]=\rho\dot{q}+\frac{\partial}{\partial x}\left(k\frac{\partial T}{\partial x}\right)+\frac{\partial}{\partial y}\left(k\frac{\partial T}{\partial y}\right)$$
$$+\frac{\partial}{\partial z}\left(k\frac{\partial T}{\partial z}\right)-\frac{\partial(up)}{\partial x}-\frac{\partial(vp)}{\partial y}-\frac{\partial(wp)}{\partial z}+\frac{\partial(u\tau_{xx})}{\partial x}$$
$$+\frac{\partial(u\tau_{yx})}{\partial y}+\frac{\partial(u\tau_{zx})}{\partial z}+\frac{\partial(v\tau_{xy})}{\partial x}+\frac{\partial(v\tau_{yy})}{\partial y}$$
$$+\frac{\partial(v\tau_{zy})}{\partial z}+\frac{\partial(w\tau_{xz})}{\partial x}+\frac{\partial(w\tau_{yz})}{\partial y}+\frac{\partial(w\tau_{zz})}{\partial z}+\rho\mathbf{f}\cdot\mathbf{V}\quad(2$$

physical boundary conditions

- The near wall flow is considered as laminar and the velocity varies linearly with distance from the wall
- No slip condition: u = v = 0.
- The velocity is constant along parallel to the wall and varies only in the direction normal to the wall.
- No pressure gradients in the flow direction.

Types of boundary conditions: In general, boundary conditions for any PDE can be classified into 4 major categories:

Dirichlet boundary condition: - in which the dependent variables themselves are prescribed along the domain boundary. 2) Von Neumann boundary condition: - in which the normal gradient of the dependent variables is prescribed along the boundary. 3) Robin boundary condition: - in which the boundary conditions are a linear combination of the Dirichlet and Von Neumann type. 4) Mixed boundary conditions: - in which certain portions of the boundary are defined as Dirichlet type, while others as Von Neumann type.

Shock fitting and shock capturing

In computational fluid dynamics, **shock-capturing methods** are a class of techniques for computing inviscid flows with shock waves. The computation of flow containing shock waves such flows result in sharp, discontinuous changes in flow variables such as pressure, temperature, density, and is an extremely difficult task because

velocity across the shock. In shock-capturing methods, the governing equations of inviscid flows (i.e. Euler equations) are cast in conservation form and any shock waves or discontinuities are computed as part of the solution. Here, no special treatment is employed to take care of the shocks themselves, which is in contrast to the shock-fitting method, where shock waves are explicitly introduced in the solution using appropriate shock relations (Rankine–Hugoniot relations). The shock waves predicted by shock-capturing methods are generally not sharp and may be smeared over several grid elements. Also, classical shock-capturing methods have the disadvantage that unphysical oscillations (Gibbs phenomenon) may develop near strong shocks.

Impact of partial differential eqautions on CFD.

1. They are a coupled system of nonlinear partial differential equations, and hence are very difficult to solve analytically. To date, there is no general closed-form solution to these equations. (This does not mean that no general solution exists—we just have not been able to find one.)
2. For the momentum and energy equations, the difference between the non-conservation and conservation forms of the equations is just the left-hand side. The right-hand side of the equations in the two different forms is the same.
3. Note that the conservation forms of the equations contain terms on the left-hand side which include the divergence of some quantity, such as $\nabla \cdot (\rho \mathbf{V})$ or $\nabla \cdot (\rho u \mathbf{V})$. For this reason, the conservation form of the governing equations is sometimes called the *divergence form*.

Classification of Quasi-Linear Partial differential equation,

In CFD applications, computational schemes and specification of boundary conditions depend on the types of PARTIAL DIFFERENTIAL EQUATIONS. In many cases, the governing equations in fluids and heat transfer are of mixedtypes. For this reason, selection of computational schemes and methods to apply boundary conditions are important subjects in CFD.

Description

Partial differential equations (PDEs) in general, or the governing equations in fluid dynamics in particular, areclassified into three categories:

(1) elliptic

(2) parabolic

(3) hyperbolic

Consider a system of quasi linear equations given below

$$a_1 \frac{\partial u}{\partial x} + b_1 \frac{\partial u}{\partial y} + c_1 \frac{\partial v}{\partial x} + d_1 \frac{\partial v}{\partial y} = f_1$$

$$a_2 \frac{\partial u}{\partial x} + b_2 \frac{\partial u}{\partial y} + c_2 \frac{\partial v}{\partial x} + d_2 \frac{\partial v}{\partial y} = f_2$$

Where u and

$$du = \frac{\partial u}{\partial x}\,dx + \frac{\partial u}{\partial y}\,dy$$
$$dv = \frac{\partial v}{\partial x}\,dx + \frac{\partial v}{\partial y}\,dy$$

$$\begin{bmatrix} a_1 & b_1 & c_1 & d_1 \\ a_2 & b_2 & c_2 & d_2 \\ dx & dy & 0 & 0 \\ 0 & 0 & dx & dy \end{bmatrix} \begin{bmatrix} \partial u/\partial x \\ \partial u/\partial y \\ \partial v/\partial x \\ \partial v/\partial y \end{bmatrix} = \begin{bmatrix} f_1 \\ f_2 \\ du \\ dv \end{bmatrix}$$

Let $[A]$ denote the coefficient matrix.

$$[A] \equiv \begin{bmatrix} a_1 & b_1 & c_1 & d_1 \\ a_2 & b_2 & c_2 & d_2 \\ dx & dy & 0 & 0 \\ 0 & 0 & dx & dy \end{bmatrix}$$

Solve the above matrix for unknown like ∂u/∂x using cramer's rule. So, replacing first column of matrix [A] withconstants column vector defining new mareix [B]

$$[B] = \begin{bmatrix} f_1 & b_1 & c_1 & d_1 \\ f_2 & b_2 & c_2 & d_2 \\ du & dy & 0 & 0 \\ dv & 0 & dx & dy \end{bmatrix}$$

Cramers rules give the solution for ∂u/∂xas

$$\frac{\partial u}{\partial x} = \frac{|B|}{|A|}$$
$$|A| = 0$$
$$\begin{vmatrix} a_1 & b_1 & c_1 & d_1 \\ a_2 & b_2 & c_2 & d_2 \\ dx & dy & 0 & 0 \\ 0 & 0 & dx & dy \end{vmatrix} = 0$$

$$(a_1c_2 - a_2c_1)(dy)^2 - (a_1d_2 - a_2d_1 + b_1c_2 - b_2c_1)\,dx\,dy + (b_1d_2 - b_2d_1)(dx)^2 = 0$$

$$a = (a_1c_2 - a_2c_1)$$
$$b = -(a_1d_2 - a_2d_1 + b_1c_2 - b_2c_1)$$
$$c = (b_1d_2 - b_2d_1)$$
$$a\left(\frac{dy}{dx}\right)^2 + b\,\frac{dy}{dx} + c = 0$$

$$\frac{dy}{dx} = \frac{-b \pm \sqrt{b^2 - 4ac}}{2a}$$
$$D = b^2 - 4ac$$

Elliptic Equations

- A PDE is elliptic in a region if ($b^2 - 4ac < 0$) at all points of the region.
-

- A disturbance is propagated instantly in all directions within the region.
- Examples of Elliptic PDEs are Laplace equation and Poisson equation.
- The domain of solution for an elliptic PDE is a closed Region *R*.

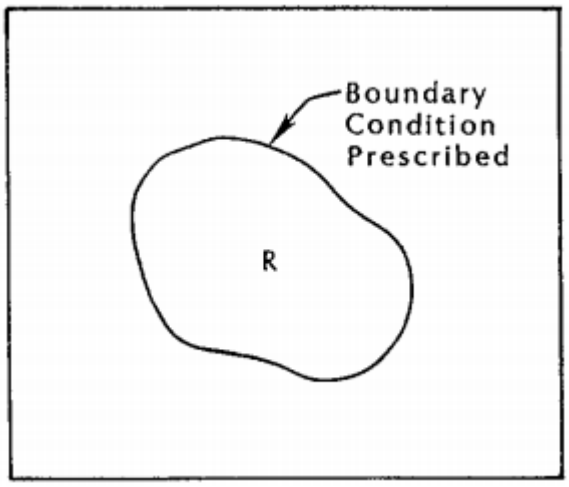

- **Boundary value problem:** Only boundary conditions are required to get the solution of elliptic equation.
- Steady state temperature distribution of a insulated solid rod.

2. Parabolic Equations

- A PDE is parabolic in a region if ($b^2 - 4ac = 0$) at all points of the region.
- Time dependent problem: Example of parabolic PDEs is unsteady heat diffusion equation.

$$\frac{\partial \phi}{\partial t} = \alpha \frac{\partial^2 \phi}{\partial x^2}$$

- *Marching type problem*: The domain of solution for an parabolic PDE is an open Region.

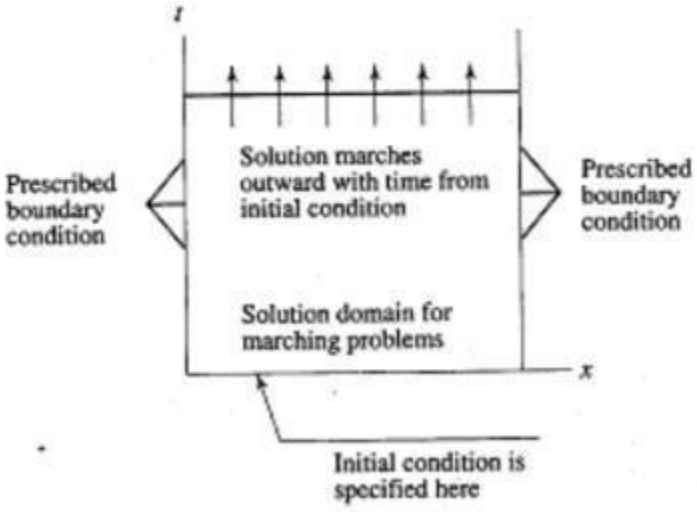

- **Initial-Boundary value problems:** Initial condition and two boundary conditions are required.
- Examples: Boundary layers, jets, mixing layers, wakes, fully developed duct flows.

3. Hyperbolic Equations

- A PDE is hyperbolic in a region if ($b^2 - 4ac > 0$) at all points of the region.

- Example of hyperbolic PDEs is wave equation.

$$\frac{\partial^2 \phi}{\partial t^2} = c^2 \frac{\partial^2 \phi}{\partial x^2}$$

- The domain of solution for an parabolic PDE is an open Region.

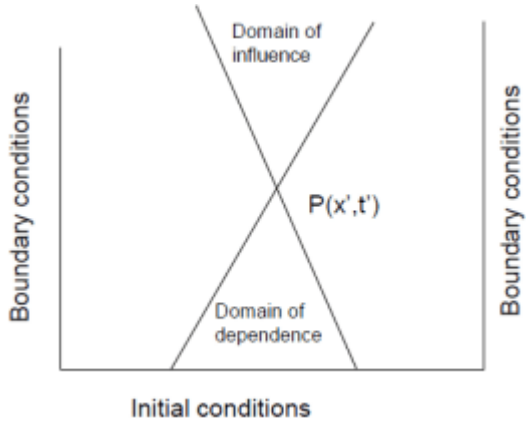

- Initial boundary value problem: Two Initial conditions and two boundary conditions are required.
- Solution may be discontinuous (shock waves) : steady/unsteady compressible flows at supersonic speeds.
- **Method of Characteristics:** A classical method to solve hyperbolic equations with two independent variables: Applicable to two-dimensional, steady, isentropic, adiabatic, irrotational flow of a perfect gas.

Physical Interpretation

- Consider the flow of a body having velocity **u** in a quiescent fluid.
- The movement of this body disturbs the fluid particles ahead of the body.
- The propagation speed of disturbance would be equal to speed of sound, **a**.
- The ratio of the speed of body to the speed of sound is called Mach number **M=u/a.**
- Consider the steady two-dimensional velocity potential equation:

$$(1 - M^2)\phi_{xx} + \phi_{yy} = 0$$

Now $A = (1 - M^2)$, $B = 0$ and $C = 1$

Thus, $(B^2 - 4AC = -4(1 - M^2))$

- There are three types of PDEs for the three types of flows.

1 Elliptic PDEs: Subsonic($M < 0$).

2 Parabolic PDEs: Sonic($M = 0$).

3 Hyperbolic PDEs: Supersonic($M > 0$).

The physical situations these types of equations represent can be illustrated by the flow velocity relative to the speed of sound as shown in Figure 2.1.1. Consider that the flow velocity u is the velocity of a body moving in the quiescent fluid.The movement of this body disturbs the fluid particles ahead of the body, setting off the

propagation velocity equal to the speed of sound a. The ratio of these two competing speeds is defined as Mach number, **M=u/a.**

For subsonic speed, M < 1, as time t increases, the body moves a distance, ut, which is always shorter than the distance at of the sound wave (Figure 2.1.1a). The sound wave reaches the observer, prior to the arrival of the body, thus warning the observer that an object is approaching. The zones outside and inside of the circles are known as the zone of silence and zone of action, respectively.

If, on the other hand, the body travels at the speed of sound, M = 1, then the observer does not hear the body approaching him prior to the arrival of the body, as these two actions are simultaneous (Figure 2.1.lb). All circles representing the distance traveled by the sound wave are tangent to the vertical line at the position of the observer. For supersonic speed, M > 1, the velocity of the body is faster than the speed of sound (Figure 2.1.1c). The line tangent to the circles of the speed of sound, known as a Mach wave, forms the boundary between the zones of silence (outside) and action (inside). Only after the body has passed by does the observer become aware of it.

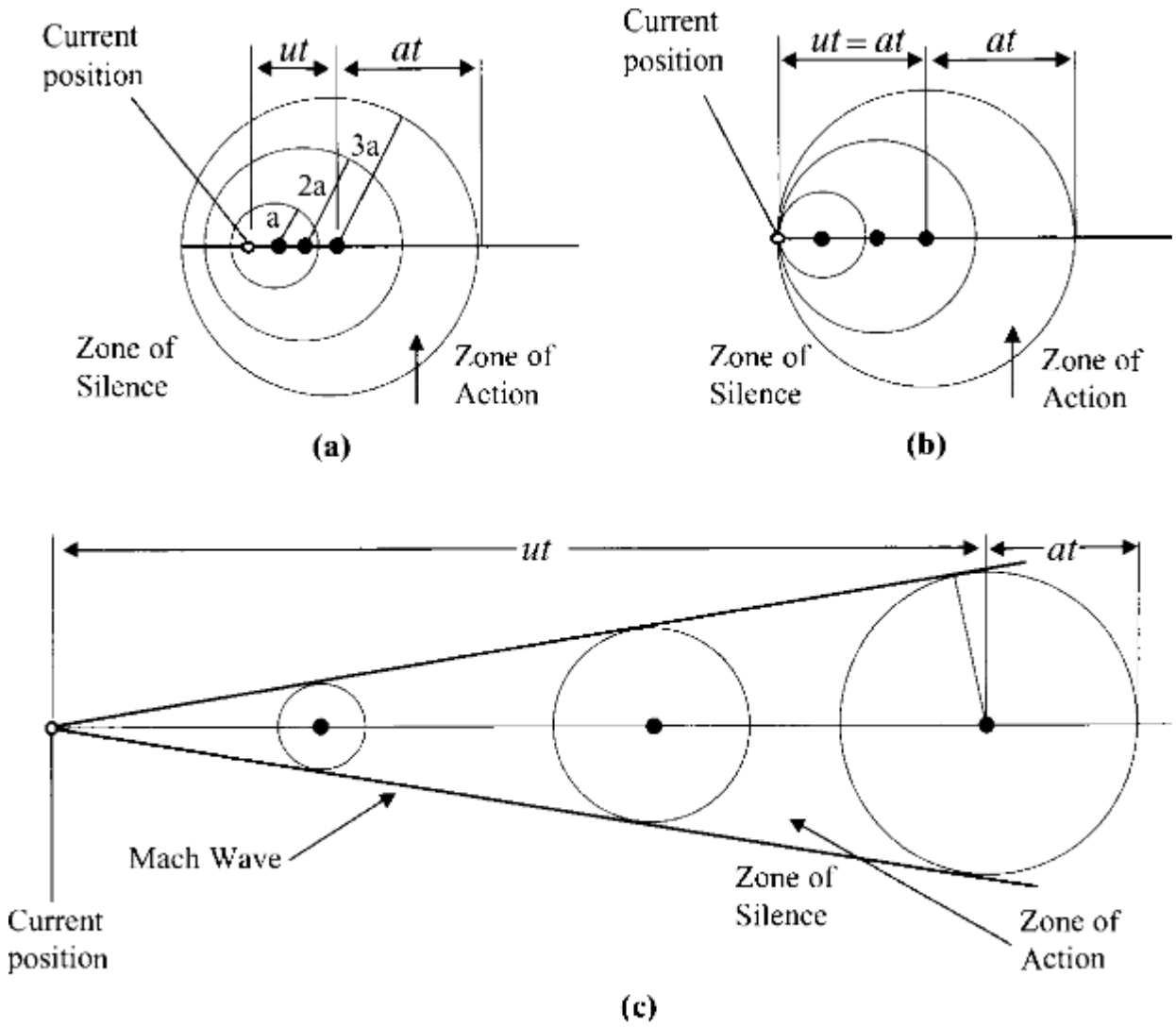

Figure 2.1.1 Subsonic, sonic, and supersonic flows. **(a)** Subsonic ($u < a$, $M < 1$). **(b)** S ($u = a$, $M = 1$). **(c)** Supersonic ($u > a$, $M > 1$).

The governing equations for subsonic flow, transonic flow, and supersonic flow are classified as elliptic, parabolic, and hyperbolic, respectively. We shall elaborate on these equations below. Most of the governing equations in fluid dynamics are second order partial differential equations. For generality, let us consider the partial differential equation of the form [Sneddon, 1957] in a two-dimensional domain.

$$A\frac{\partial^2 u}{\partial x^2} + B\frac{\partial^2 u}{\partial x \partial y} + C\frac{\partial^2 u}{\partial y^2} + D\frac{\partial u}{\partial x} + F\frac{\partial u}{\partial y} + Fu + G = 0 \qquad (2.1.1)$$

Where the coefficients A, B, C, D, E, and F are constants or may be functions of both independent

and/ordependent variables. To assure the continuity of the first derivative of u, $\mathbf{u_x = \partial u/\partial x}$ **and** $\mathbf{uy=\partial u/\partial y}$**.** We write

$$du_x = \frac{\partial u_x}{\partial x}dx + \frac{\partial u_x}{\partial y}dy = \frac{\partial^2 u}{\partial x^2}dx + \frac{\partial^2 u}{\partial x \partial y}dy \tag{2.1.2a}$$

$$du_y = \frac{\partial u_y}{\partial x}dx + \frac{\partial u_y}{\partial y}dy = \frac{\partial^2 u}{\partial x \partial y}dx + \frac{\partial^2 u}{\partial y^2}dy \tag{2.1.2b}$$

Here u forms a solution surface above or below the $x - y$ plane and the slope dy/dx representing the solution surface is defined as the characteristic curve.

Equations (2.1.1), (2.1.2a). and (2.1.2b) can be combined to form a matrix equation

$$\begin{bmatrix} A & B & C \\ dx & dy & 0 \\ 0 & dx & dy \end{bmatrix} \begin{bmatrix} u_{xx} \\ u_{xy} \\ u_{yy} \end{bmatrix} = \begin{bmatrix} H \\ du_x \\ du_y \end{bmatrix} \tag{2.1.3}$$

where

$$H = -\left(D\frac{\partial u}{\partial x} + E\frac{\partial u}{\partial y} + Fu + G \right) \tag{2.1.4}$$

Since it is possible to have discontinuities in the second order derivatives of the dependent variable along the characteristics, these derivatives are indeterminate.

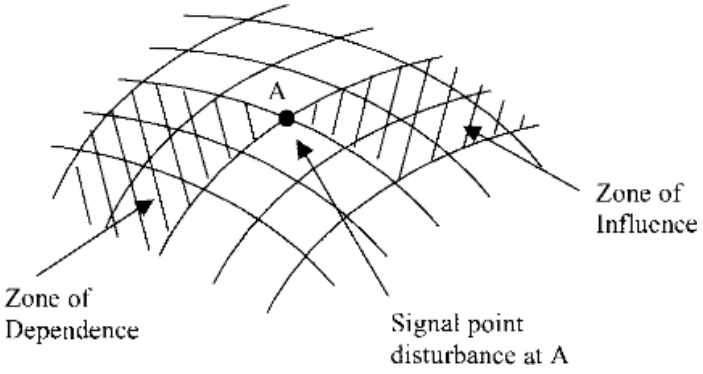

Figure 2.1.2 Propagation of disturbance and characteristics.

This happens when the determinant of the coefficient matrix in (2.1.3) is equal to zero.

$$\begin{vmatrix} A & B & C \\ dx & dy & 0 \\ 0 & dx & dy \end{vmatrix} = 0 \qquad (2.1.5)$$

which yields

$$A\left(\frac{dy}{dx}\right)^2 - B\left(\frac{dy}{dx}\right) + C = 0 \qquad (2.1.6)$$

Solving this quadratic equation yields the equation of the characteristics in physical space,

$$\frac{dy}{dx} = \frac{B \pm \sqrt{B^2 - 4AC}}{2A} \qquad (2.1.7)$$

Depending on the value of $B^2 - 4AC$, characteristic curves can be real or imaginary.

For problems in which real characteristics exist, a disturbance propagates only over a finite region (Figure 2.1.2). The downstream region affected by this disturbance at point A is called the zone of influence. A signal at point Awill be felt only if it originates from a finite region called the zone of dependence of point A.

The second order PDE is classified according to the sign of the expression ($B^2 - 4AC$).

(a) Elliptic if $B^2 - 4AC < 0$

In this case, the characteristics do not exist.

(b) Parabolic if $B^2 - 4AC = 0$

In this case, one set of characteristics exists.

(c) Hyperbolic if $B^2 - 4AC > 0$

In this case, two sets of characteristics exist.

Note that (2.1.1) resembles the general expression of a conic section, $AX^2 + BXY + CY^2 + DX + EY + F = 0$

(2.1.8)

in which one can identify the following geometrical properties: $B^2 - 4AC < 0$ ellipse

$B^2 - 4AC = 0$

parabola $B^2 - 4AC$

> 0 hyperbola

This is the origin of terms used for classification of partial differential equations.

Examples

(a) Elliptic equation

$$\frac{\partial^2 u}{\partial x^2} + \frac{\partial^2 u}{\partial y^2} = 0 \tag{2.1.9}$$

$$A = 1, \quad B = 0, \quad C = 1$$

$$B^2 - 4AC = -4 < 0$$

(b) Parabolic equation

$$\frac{\partial u}{\partial t} - \alpha \frac{\partial^2 u}{\partial x^2} = 0 \quad (\alpha > 0) \tag{2.1.10}$$

$$A = -\alpha, \quad B = 0, \quad C = 0$$

$$B^2 - 4AC = 0$$

(c) Hyperbolic equation

1-D First Order Wave Equation

$$\frac{\partial u}{\partial t} + a \frac{\partial u}{\partial x} = 0 \quad (a > 0) \tag{2.1.11}$$

1-D Second Order Wave Equation

Differentiating (2.1.11) with respect to x and t,

$$\frac{\partial^2 u}{\partial t \partial x} + a \frac{\partial^2 u}{\partial x^2} = 0 \tag{2.1.12a}$$

$$\frac{\partial^2 u}{\partial t^2} + a \frac{\partial^2 u}{\partial t \partial x} = 0 \tag{2.1.12b}$$

Combining (2.1.12a) and (2.1.12b) yields

$$\frac{\partial^2 u}{\partial t^2} - a^2 \frac{\partial^2 u}{\partial x^2} = 0 \tag{2.1.13}$$

where

$$A = 1, \quad B = 0, \quad C = -a^2$$

$$B^2 - 4AC = 4a^2 > 0$$

The Eigen value method, General behavior of different classes of Partial differential equation – elliptic, parabolicand hyperbolic.

$$a_1 \frac{\partial u}{\partial x} + b_1 \frac{\partial u}{\partial y} + c_1 \frac{\partial v}{\partial x} + d_1 \frac{\partial v}{\partial y} = 0$$

$$a_2 \frac{\partial u}{\partial x} + b_2 \frac{\partial u}{\partial y} + c_2 \frac{\partial v}{\partial x} + d_2 \frac{\partial v}{\partial y} = 0$$

Defining W as the column vector

$$W = \begin{Bmatrix} u \\ v \end{Bmatrix}$$

$$\begin{bmatrix} a_1 & c_1 \\ a_2 & c_2 \end{bmatrix} \frac{\partial W}{\partial x} + \begin{bmatrix} b_1 & d_1 \\ b_2 & d_2 \end{bmatrix} \frac{\partial W}{\partial y} = 0$$

$$[K]\frac{\partial W}{\partial x} + [M]\frac{\partial W}{\partial y} = 0$$

$$\frac{\partial W}{\partial x} + [K]^{-1}[M]\frac{\partial W}{\partial y} = 0$$

$$\frac{\partial W}{\partial x} + [N]\frac{\partial W}{\partial y} = 0$$

where by definition $[N] = [K]^{-1}[M]$.

If the eigen values are all real, the equations are hyperbolic.
If the eigen values are all complex the equations are elliptic or else they are parabolic.

WELL POSED PROBLEMS

The mathematical term **well-posed problem** stems from a definition given by Jacques Hadamard. He believed that mathematical models of physical phenomena should have the properties that:

1. a solution exists,
2. the solution is unique,
3. the solution's behavior changes continuously with the initial conditions.

If the problem is well-posed, then it stands a good chance of solution on a computer using a stable algorithm. If it is not well-posed, it needs to be re-formulated for numerical treatment. Typically thisinvolves including additional assumptions, such as smoothness of solution.

UNIT-III – DISCRETIZATION TECHNIQUES

Introduction, Finite differences

In mathematics, **finite-difference methods** (FDM) are numerical methods for solving differential equations by approximating them with difference equations, in which finite differences approximate the derivatives. FDMs are thus discretization methods.

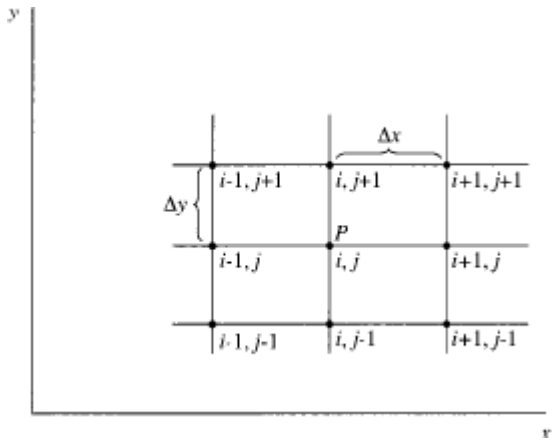

Formulas for first and second derivatives

First, assuming the function whose derivatives are to be approximated is properly-behaved, by Taylor's theorem,we can create a Taylor series expansion

If $u_{i,j}$ denotes velocity at point (I,j) then the velocity $u_{i+1,j}$ at point (i+1,j) can be expressed in terms of Taylor series expanded about point (I,j) as follows:

$$u_{i+1,j} = u_{i,j} + \left(\frac{\partial u}{\partial x}\right)_{i,j} \Delta x + \left(\frac{\partial^2 u}{\partial x^2}\right)_{i,j} \frac{(\Delta x)^2}{2} + \left(\frac{\partial^3 u}{\partial x^3}\right)_{i,j} \frac{(\Delta x)^3}{6} + \cdots$$

Solving above equation for derivative gives

$$\left(\frac{\partial u}{\partial x}\right)_{i,j} = \underbrace{\frac{u_{i+1,j} - u_{i,j}}{\Delta x}}_{\text{Finite-difference representation}} - \underbrace{\left(\frac{\partial^2 u}{\partial x^2}\right)_{i,j} \frac{\Delta x}{2} - \left(\frac{\partial^3 u}{\partial x^3}\right)_{i,j} \frac{(\Delta x)^2}{6} + \cdots}_{\text{Truncation error}}$$

$$\left(\frac{\partial u}{\partial x}\right)_{i,j} \approx \frac{u_{i+1,j} - u_{i,j}}{\Delta x}$$

The lowest order term in truncation error involves Δx to the first power; hence the finite difference expression

$$\left(\frac{\partial u}{\partial x}\right)_{i,j} = \frac{u_{i+1,j} - u_{i,j}}{\Delta x} + O(\Delta x)$$

Is called first order accurate and the symbol O(Δx) is a formal mathematical notation which represents terms of order Δx. The above equation uses information to the right of grid point (i,j) i.e it uses $u_{i+1,j}$ and $u_{i,j}$. As a result it is

First, consider a continuous function of x, namely, $f(x)$, with all derivatives defined at x. Then, the value of f at a location $x + \Delta x$ can be estimated from a Taylor series expanded about point x, that is,

$$f(x+\Delta x) = \underbrace{f(x)}_{\text{First guess (not very good)}} + \underbrace{\frac{\partial f}{\partial x}\Delta x}_{\text{Add to capture slope}} + \underbrace{\frac{\partial^2 f}{\partial x^2}\frac{(\Delta x)^2}{2}}_{\text{Add to account for curvature}} + \cdots$$

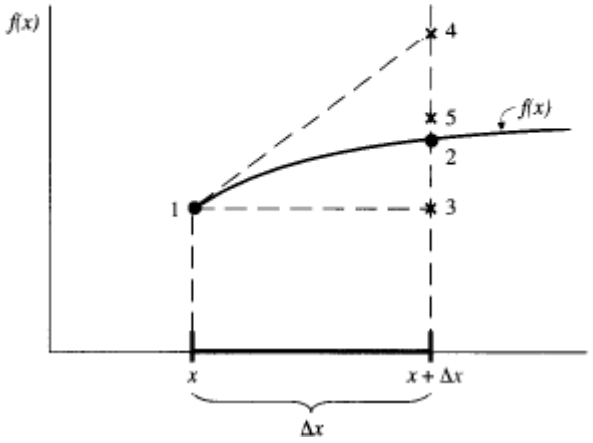

$$f(x) = \sin 2\pi x$$

$$\text{At } x = 0.2: \qquad f(x) = 0.9511$$

$$\text{At } x = 0.22: \qquad f(x) = 0.9823$$

$$f(0.22) \approx f(0.2) = 0.9511$$

$$f(x+\Delta x) \approx f(x) + \frac{\partial f}{\partial x}\Delta x$$

$$f(0.22) \approx f(0.2) + 2\pi \cos[2\pi(0.2)](0.02)$$

$$\simeq 0.9511 + 0.388 = 0.9899$$

$$f(x+\Delta x) \approx f(x) + \frac{\partial f}{\partial x}\Delta x + \frac{\partial^2 f}{\partial x^2}\frac{(\Delta x)^2}{2}$$

$$f(0.22) \approx f(0.2) + 2\pi \cos[2\pi(0.2)](0.02) \quad 4\pi^2 \sin[2\pi(0.2)]\frac{(0.02)^2}{2}$$

$$\approx 0.9511 + 0.0388 - 0.0075$$

$$\approx 0.9824$$

Let us now write a Taylor series expansion for $u_{i-1,j}$, expanded about $u_{i,j}$.

$$u_{i-1,j} = u_{i,j} + \left(\frac{\partial u}{\partial x}\right)_{i,j}(-\Delta x) + \left(\frac{\partial^2 u}{\partial x^2}\right)_{i,j}\frac{(-\Delta x)^2}{2} + \left(\frac{\partial^3 u}{\partial x^3}\right)_{i,j}\frac{(-\Delta x)^3}{6} + \cdots$$

$$u_{i-1,j} = u_{i,j} - \left(\frac{\partial u}{\partial x}\right)_{i,j}\Delta x + \left(\frac{\partial^2 u}{\partial x^2}\right)_{i,j}\frac{(\Delta x)^2}{2} - \left(\frac{\partial^3 u}{\partial x^3}\right)_{i,j}\frac{(\Delta x)^3}{6} + \cdots$$

Solving for $(\partial u/\partial x)_{i,j}$, we obtain

$$\boxed{\left(\frac{\partial u}{\partial x}\right)_{i,j} = \frac{u_{i,j} - u_{i-1,j}}{\Delta x} + O(\Delta x)}$$

The above equation uses information to the left of grid point (i,j) i.e it uses $u_{i-1,j}$ and $u_{i,j}$. As a result it is known as first order backward or rearward difference

In most CFD applications first order accuracy is not sufficient second order difference are obtained by subtract forward and backward differences as follows:

$$u_{i+1,j} - u_{i-1,j} = 2\left(\frac{\partial u}{\partial x}\right)_{i,j}\Delta x + 2\left(\frac{\partial^3 u}{\partial x^3}\right)_{i,j}\frac{(\Delta x)^3}{6} + \cdots$$

$$\boxed{\left(\frac{\partial u}{\partial x}\right)_{i,j} = \frac{u_{i+1,j} - u_{i-1,j}}{2\Delta x} + O(\Delta x)^2}$$

The lowest order term in truncation error involves Δx to the first power; hence the finite difference expression is of second order. The above equation uses information to the left and right of grid point (i,j) i.e it uses $u_{i+1,j}$, $u_{i-1,j}$ and $u_{i,j}$. As a result it is known as second order central difference.

Similarly the finite differences for y derivatives are given as

$$\left(\frac{\partial u}{\partial y}\right)_{i,j} = \begin{cases} \dfrac{u_{i,j+1} - u_{i,j}}{\Delta y} + O(\Delta y) & \textit{Forward difference} \\ \dfrac{u_{i,j} - u_{i,j-1}}{\Delta y} + O(\Delta y) & \textit{Rearward difference} \\ \dfrac{u_{i,j+1} - u_{i,j-1}}{2\Delta y} + O(\Delta y)^2 & \textit{Central difference} \end{cases}$$

$$u_{i+1,j} + u_{i-1,j} = 2u_{i,j} + \left(\frac{\partial^2 u}{\partial x^2}\right)_{i,j}(\Delta x)^2 + \left(\frac{\partial^4 u}{\partial x^4}\right)_{i,j}\frac{(\Delta x)^4}{12} + \cdots$$

Solving for $(\partial^2 u/\partial x)_{i,j}$,

$$\boxed{\left(\frac{\partial^2 u}{\partial x^2}\right)_{i,j} - \frac{u_{i+1,j} - 2u_{i,j} + u_{i-1,j}}{(\Delta x)^2} + O(\Delta x)^2}$$

$$\left(\frac{\partial^2 u}{\partial y^2}\right)_{i,j} = \frac{u_{i,j+1} - 2u_{i,j} + u_{i,j-1}}{(\Delta y)^2} + \mathrm{O}(\Delta y)^2$$

These are examples of second derivative finite differences are known as second differences.

For mixed derivatives

$$\left(\frac{\partial u}{\partial y}\right)_{i+1,j} = \left(\frac{\partial u}{\partial y}\right)_{i,j} + \left(\frac{\partial^2 u}{\partial x\,\partial y}\right)_{i,j} \Delta x + \left(\frac{\partial^3 u}{\partial x^2\,\partial y}\right)_{i,j} \frac{(\Delta x)^2}{2} + \left(\frac{\partial^4 u}{\partial x^3\,\partial y}\right)_{i,j} \frac{(\Delta x)^3}{6} + \cdots$$

$$\left(\frac{\partial u}{\partial y}\right)_{i-1,j} = \left(\frac{\partial u}{\partial y}\right)_{i,j} - \left(\frac{\partial^2 u}{\partial x\,\partial y}\right)_{i,j} \Delta x + \left(\frac{\partial^3 u}{\partial x^2\,\partial y}\right)_{i,j} \frac{(\Delta x)^2}{2} + \left(\frac{\partial^4 u}{\partial x^3\,\partial y}\right)_{i,j} \frac{(\Delta x)^3}{6} + \cdots$$

Subtracting above two equations

$$\left(\frac{\partial u}{\partial y}\right)_{i+1,j} - \left(\frac{\partial u}{\partial y}\right)_{i-1,j} = 2\left(\frac{\partial^2 u}{\partial x\,\partial y}\right)_{i,j} \Delta x + \left(\frac{\partial^4 u}{\partial x^3\,\partial y}\right)_{i,j} \frac{(\Delta x)^3}{6} + \cdots$$

$$\left(\frac{\partial^2 u}{\partial x\,\partial y}\right)_{i,j} = \frac{(\partial u/\partial y)_{i+1,j} - (\partial u/\partial \tilde{y})_{i-1,j}}{2\Delta x} - \left(\frac{\partial^4 u}{\partial x^3\,\partial y}\right)_{i,j} \frac{(\Delta x)^2}{12} + \cdots$$

$$\left(\frac{\partial u}{\partial y}\right)_{i+1,j} = \frac{u_{i+1,j+1} - u_{i+1,j-1}}{2\Delta y} + \mathrm{O}(\Delta y)^2$$

$$\left(\frac{\partial u}{\partial y}\right)_{i-1,j} = \frac{u_{i-1,j+1} - u_{i-1,j-1}}{2\Delta y} + \mathrm{O}(\Delta y)^2$$

$$\left(\frac{\partial^2 u}{\partial x\,\partial y}\right)_{i,j} = \frac{u_{i+1,j+1} - u_{i+1,j-1} - u_{i-1,j+1} + u_{i-1,j-1}}{4\Delta x\,\Delta y} + \mathrm{O}[(\Delta x)^2, (\Delta y)^2]$$

This known as second order central difference for mixed derivative.

First-order forward difference with respect to x

$$\left(\frac{\partial u}{\partial x}\right)_{i,j} = \frac{u_{i+1,j} - u_{i,j}}{\Delta x}$$

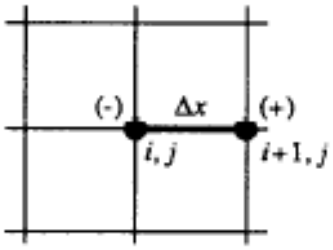

First-order rearward difference with respect to x

$$\left(\frac{\partial u}{\partial x}\right)_{i,j} = \frac{u_{i,j} - u_{i-1,j}}{\Delta x}$$

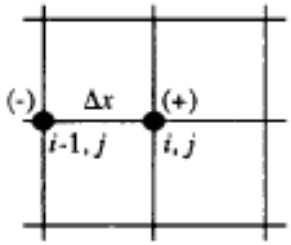

Second-order central difference with respect to x

$$\left(\frac{\partial u}{\partial x}\right)_{i,j} = \frac{u_{i+1,j} - u_{i-1,j}}{2\Delta x}$$

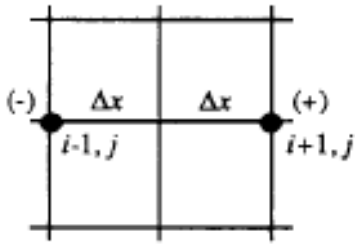

Second-order central second difference with respect to x

$$\left(\frac{\partial^2 u}{\partial x^2}\right)_{i,j} = \frac{u_{i+1,j} - 2u_{i,j} + u_{i-1,j}}{(\Delta x)^2}$$

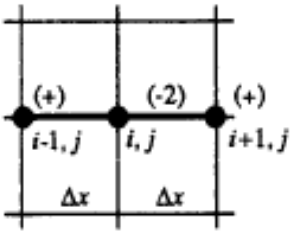

First-order forward difference with respect to y

$$\left(\frac{\partial u}{\partial y}\right)_{i,j} = \frac{u_{i,j+1} - u_{i,j}}{\Delta y}$$

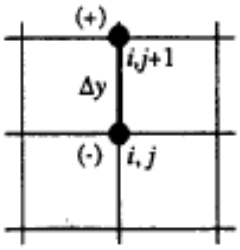

First-order rearward difference with respect to y

$$\left(\frac{\partial u}{\partial y}\right)_{i,j} = \frac{u_{i,j} - u_{i,j-1}}{\Delta y}$$

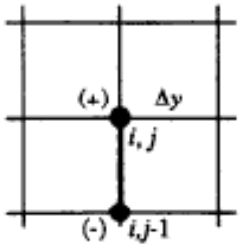

Second-order central difference with respect to y

$$\left(\frac{\partial u}{\partial y}\right)_{i,j} = \frac{u_{i,j+1} - u_{i,j-1}}{2\Delta y}$$

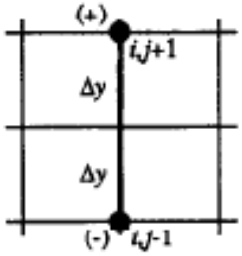

Second-order central second difference with respect to y

$$\left(\frac{\partial^2 u}{\partial y^2}\right)_{i,j} = \frac{u_{i,j+1} - 2u_{i,j} + u_{i,j-1}}{(\Delta y)^2}$$

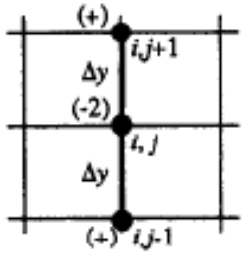

Second-order central mixed difference with respect to x and y

$$\left(\frac{\partial^2 u}{\partial x \partial y}\right)_{i,j} = \frac{u_{i+1,j+1} + u_{i-1,j-1} - u_{i-1,j+1} - u_{i+1,j-1}}{4\Delta x\, \Delta y}$$

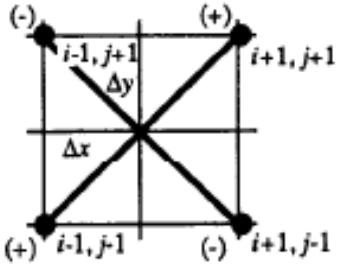

Difference equations

When all the partial derivatives in agiven PDE are replaced by finite difference the algebraic equation is known asdifference equation.

Consider a one dimensional heat conduction equation with constant thermal diffusivity

$$\frac{\partial T}{\partial t} = \alpha \frac{\partial^2 T}{\partial x^2}$$

This equation is parabolic in nature. So we use marching solution with respect to time. Here time is representd byprefix n to grid point.

$$\left(\frac{\partial T}{\partial t}\right)_i^n = \frac{T_i^{n+1} - T_i^n}{\Delta t} - \left(\frac{\partial^2 T}{\partial t^2}\right)_i^n \frac{\Delta t}{2} + \cdots$$

$$\left(\frac{\partial^2 T}{\partial x^2}\right)_i^n = \frac{T_{i+1}^n - 2T_i^n + T_{i-1}^n}{(\Delta x)^2} - \left(\frac{\partial^4 T}{\partial x^4}\right)_i^n \frac{(\Delta x)^2}{12} + \cdots$$

$$\frac{\partial T}{\partial t} - \alpha \frac{\partial^2 T}{\partial x^2} = 0$$

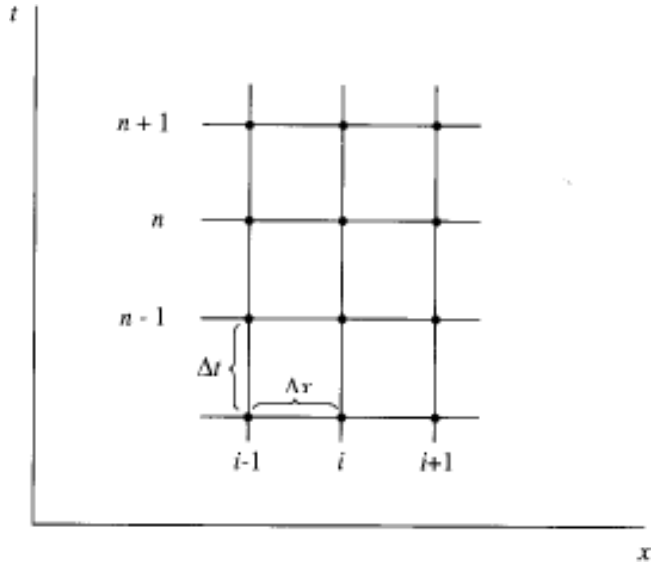

$$\overbrace{\frac{\partial T}{\partial t} - \alpha \frac{\partial^2 T}{\partial x^2} = 0}^{\text{Partial differential equation}} = \underbrace{\frac{T_i^{n+1} - T_i^n}{\Delta t} - \frac{\alpha(T_{i+1}^n - 2T_i^n + T_{i-1}^n)}{(\Delta x)^2}}_{\text{Difference equation}} + \underbrace{\left[-\left(\frac{\partial^2 T}{\partial t^2}\right)_i^n \frac{\Delta t}{2} + \alpha \left(\frac{\partial^4 T}{\partial x^4}\right)_i^n \frac{(\Delta x)^2}{12} + \cdots \right]}_{\text{Truncation error}}$$

$$\frac{T_i^{n+1} - T_i^n}{\Delta t} = \frac{\alpha(T_{i+1}^n - 2T_i^n + T_{i-1}^n)}{(\Delta x)^2}$$

The above equation is known as difference equation for one dimensional heat conduction governing equation.

Explicit and implicit approaches

Consider the same 1D heat conduction equation

$$\frac{T_i^{n+1} - T_i^n}{\Delta t} = \frac{\alpha(T_{i+1}^n - 2T_i^n + T_{i-1}^n)}{(\Delta x)^2}$$

With some rearrangements of above equation gives

$$T_i^{n+1} = T_i^n + \alpha \frac{\Delta t}{(\Delta x)^2}(T_{i+1}^n - 2T_i^n + T_{i-1}^n)$$

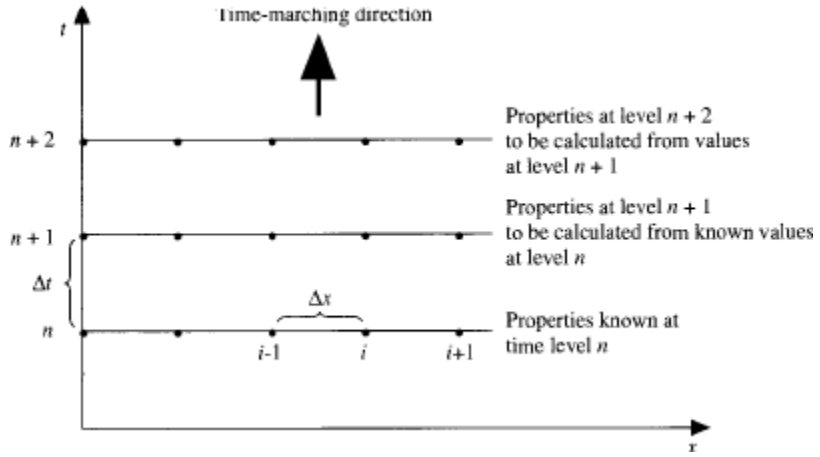

In the above equation left hand side is unkown and all the right side terms in n level are known by boundary conditions. Thus by marching in time direction with varying n levels as shown in above figure the solution is obtained .

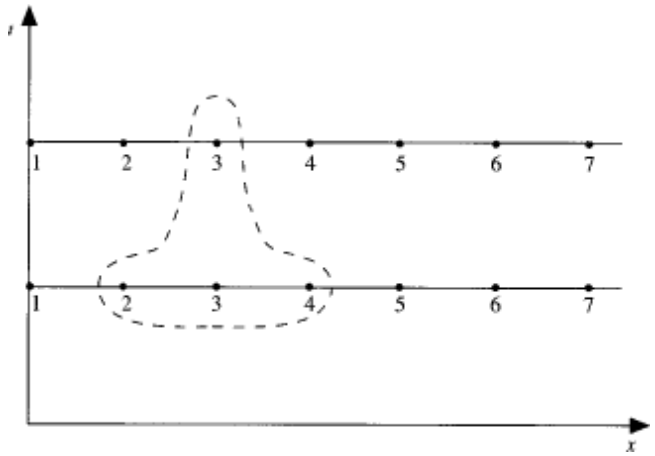

$$T_2^{n+1} = T_2^n + \alpha \frac{\Delta t}{(\Delta x)^2}(T_3^n - 2T_2^n + T_1^n)$$

$$T_3^{n+1} = T_3^n + \alpha \frac{\Delta t}{(\Delta x)^2}(T_4^n - 2T_3^n + T_2^n)$$

Similarly we can get for T^{n+4}, T^{n+5} and T^{n+6} . As these equations are solving for only one single unknown then it is known as explicit method.

For a given PDE we can write n number of difference equations with various methods like the following

$$\frac{T_i^{n+1} - T_i^n}{\Delta t} = \alpha \frac{\frac{1}{2}(T_{i+1}^{n+1} + T_{i+1}^n) + \frac{1}{2}(-2T_i^{n+1} - 2T_i^n) + \frac{1}{2}(T_{i-1}^{n+1} + T_{i-1}^n)}{(\Delta x)^2}$$

The above finite difference method is known as Crank Nicholoson form.

In the above both left and right handside terms are unknowns i.e. n+1 level terms. So to obtain the solution for a equation with more than one unknown it requires equations equal to number of unknowns. Thus solving simulkataneous euqtions or unknowns is known as implicit method.

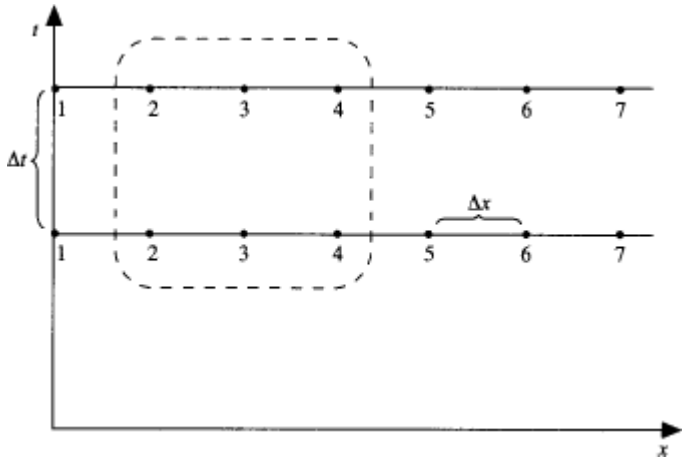

$$\frac{\alpha\,\Delta t}{2(\Delta x)^2} T_{i-1}^{n+1} - \left[1 + \frac{\alpha\,\Delta t}{(\Delta x)^2}\right] T_i^{n+1} + \frac{\alpha\,\Delta t}{2(\Delta x)^2} T_{i+1}^{n+1}$$

$$= -T_i^n - \frac{\alpha\,\Delta t}{2(\Delta t)^2}(T_{i+1}^n - 2T_i^n + T_{i-1}^n)$$

$$A = \frac{\alpha\,\Delta t}{2(\Delta x)^2}$$

$$B = 1 + \frac{\alpha\,\Delta t}{(\Delta x)^2}$$

$$K_i = -T_i^n - \frac{\alpha\,\Delta t}{2(\Delta x)^2}(T_{i+1}^n - 2T_i^n + T_{i-1}^n)$$

$$AT_{i-1}^{n+1} - BT_i^{n+1} + AT_{i+1}^{n+1} = K_i$$

At grid point 2 : $AT_1 - BT_2 + AT_3 = K_2$

$$-BT_2 + AT_3 = K_2 - AT_1$$

At grid point 3 : $AT_2 - BT_3 + AT_4 - K_3$

At grid point 4 : $AT_3 - BT_4 + AT_5 = K_4$

At grid point 5 : $AT_4 - BT_5 + AT_6 = K_5$

At grid point 6 : $AT_5 - BT_6 + AT_7 = K_6$

$$AT_5 - BT_6 = K_6 - AT_7 = K'_6$$

$$\begin{bmatrix} B & A & 0 & 0 & 0 \\ A & B & A & 0 & 0 \\ 0 & A & B & A & 0 \\ 0 & 0 & A & B & A \\ 0 & 0 & 0 & A & B \end{bmatrix} \begin{bmatrix} T_2 \\ T_3 \\ T_4 \\ T_5 \\ T_6 \end{bmatrix} = \begin{bmatrix} K'_2 \\ K_3 \\ K_4 \\ K_5 \\ K'_6 \end{bmatrix}$$

1. To obtain a steady state solution by means of assuming some arbitrary initial conditions for a flow field, and then calculating the flow in steps of time, going out to a sufficiently large number of time steps until a final steady-state flow is approached at large values of time. In this situation, the final steady state is the desired result, and the time marching is simply a means to that end. The solution to the supersonic blunt body problem is a case in point, as discussed in Sec.

Explicit approach

Advantage	Relatively simple to set up and program.
Disadvantage	In terms of our above example, for a given Δx, Δt must be less than some limit imposed by stability constraints. In some cases, Δt must be very small to maintain stability; this can result in long computer running times to make calculations over a given interval of t.

Implicit approach

Advantage	Stability can be maintained over much larger values of Δt, hence using considerable fewer time steps to make calculations over a given interval of t. This results in less computer time.
Disadvantage	More complicated to set up and program.

Disadvantage	Since massive matrix manipulations are usually required at each time step, the computer time per time step is much larger than in the explicit approach.
Disadvantage	Since large Δt can be taken, the truncation error is large, and the use of implicit methods to follow the exact transients (time variations of the independent variable) may not be as accurate as an explicit approach. However, for a time-dependent solution in which the steady state is the desired result, this relative timewise inaccuracy is not important.

Basis of finite volume method-

The **finite volume method** (**FVM**) is a method for representing and evaluating partial differential equations in the form of algebraic equations [LeVeque, 2002; Toro, 1999]. Similar to the finite difference method or finite element method, values are calculated at discrete places on a meshed geometry. "Finite volume" refers to the small volume surrounding each node point on a mesh. In the finite volume method, volume integrals in a partial differential equation that contain a divergence term are converted to surface integrals, using the divergence theorem. These terms are then evaluated as fluxes at the surfaces of each finite volume. Because the flux entering a given volume is identical to that leaving the adjacent volume, these methods are conservative. Another advantage of the finite volume method is that it is easily formulated to allow for unstructured meshes. The method is used in many computational fluid dynamics packages.

4

Finite-Volume Methods

Finite-volume methods (FVM) – sometimes also called box methods – are mainly employed for the numerical solution of problems in fluid mechanics, where they were introduced in the 1970s by McDonald, MacCormack, and Paullay. However, the application of the FVM is not limited to flow prob- lems. An important property of finite-volume methods is that the balance principles, which are the basis for the mathematical modelling of continuum mechanical problems, per definition, also are fulfilled for the discrete equations (conservativity). In this chapter we will discuss the most important basics of finite-volume discretizations applied to continuum mechanical problems. For clarity in the presentation of the essential principles we will restrict ourselves mainly to the two-dimensional case.

4.1 General Methodology

In general, the FVM involves the following steps:

(1) Decomposition of the problem domain into control volumes.
(2) Formulation of integral balance equations for each control volume.
(3) Approximation of integrals by numerical integration.
(4) Approximation of function values and derivatives by interpolation with nodal values.
(5) Assembling and solution of discrete algebraic system.

In the following we will outline in detail the individual steps (the solution of algebraic systems will be the topic of Chap. 7). We

$$\partial x_i \quad \rho v_i \varphi - \alpha_{\partial x} \quad = f \tag{4.1}$$

for some problem domain Ω. We remark that a generalization of the FVM to other types of equations as given in Chap. 2 is straightforward (in Chap. 10 this will be done for the Navier-Stokes equations).

The starting point for a finite-volume discretization is a decomposition of the problem domain Ω into a finite number of subdomains V_i ($i = 1, \ldots, N$), called *control volumes* (CVs), and related nodes where the unknown variables are to be computed. The union of all CVs should cover the whole problem domain. In general, the CVs also may overlap, but since this results in un- necessary complications we consider here the non-overlapping case only. Since finally each CV gives one equation for computing the nodal values, their final number (i.e., after the incorporation of boundary conditions) should be equal to the number of CVs. Usually, the CVs and the nodes are defined on the basis of a numerical grid, which, for instance, is generated with one of the techniques described in Chap. 3. In order to keep the usual terminology of the FVM, we always talk of volumes (and their surfaces), although strictly speaking this is only correct for the three-dimensional case.

For one-dimensional problems the CVs are subintervals of the problem interval and the nodes can be the midpoints or the edges of the subintervals (see Fig. 4.1).

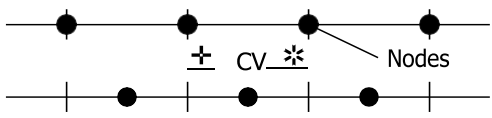

Fig. 4.1. Definitions of CVs and edge (top) and cell-oriented (bottom) arrangement of nodes for one-dimensional grids

In the two-dimensional case, in principle, the CVs can be arbitrary poly-gons. For quadrilateral grids the CVs usually are chosen identically with the grid cells. The nodes can be defined as the vertices or the centers of the CVs (see Fig. 4.2), often called edge or cell-centered approaches, respectively. For triangular grids, in principle, one could do it similarily, i.e., the triangles define the CVs and the nodes can be the vertices or the centers of the triangles. How- ever, in this case other CV definitions are usually employed. One approach is closely related to the Delaunay

as *Voronoi polygons* andin the case of convex problems domains and non-obtuse triangles there is a one-to-one correspondance to a Delaunay triangulation with its “nice” prop- erties. However, this approach may fail for arbitrary triangulations. Another more general approach is to define a polygonal CV by joining the centroids and the midpoints of the edges of the triangles surrounding a node leading to the so-called *Donald polygons* (see Fig. 4.4).

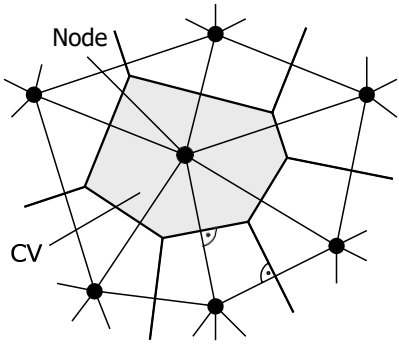

Fig. 4.3. Definition of CVs and nodes for tri-angular grids with Voronoi polygons

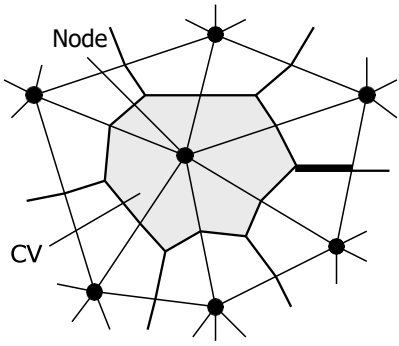

Fig. 4.4. Definition of CVs and nodes for tri-angular grids with Donald polygons

For three-dimensional problems on the basis of hexahedral or tetrahedral grids similar techniques as in the two-dimensional case can be applied (see, e.g., [26]).

After having defined the CVs, the balance equations describing the prob- lem are formulated in integral form for each CV. Normally, these equations are directly available from the corresponding continuum mechanical conservation laws (applied to a CV), but they can also be derived by integration from the corresponding differential equations. By integration of (4.1) over an arbitrary control volume V and application of the Gauß integral theorem, one obtains:

$$\int \frac{\partial \varphi}{} \int$$

$$\rho v_i \varphi - \alpha \frac{\partial}{\partial x_i} \Big) n_i \, \mathrm{d}S = \int_V f \, \mathrm{d}V \,, \tag{4.2}$$

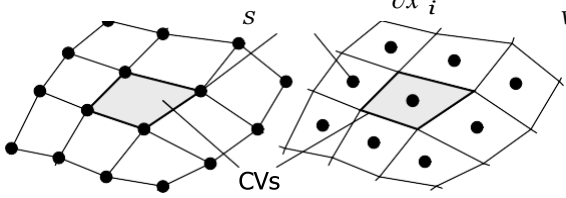

Fig. 4.2. Edge-oriented (left) and cell-oriented (right) arrangements of nodes for quadrilateral grids

where S is the surface of the CV and n_i are the components of the unit normal vector to the surface. The integral balance equation (4.2) constitutes the starting point for the further discretization of the considered problem with an FVM.

As an example we consider quadrilateral CVs with a cell-oriented arrange- ment of nodes (a generalization to arbitrary polygons poses no principal dif- ficulties). For a general quadrilateral CV we use the notations of the distin- guished points (midpoint, midpoints of faces, and edge points) and the unit normal vectors according to the so-called compass notation as indicated in Fig. 4.5. The midpoints of the directly neighboring CVs we denote – again in compass notation – with capital letters S, SE, etc. (see Fig. 4.6).

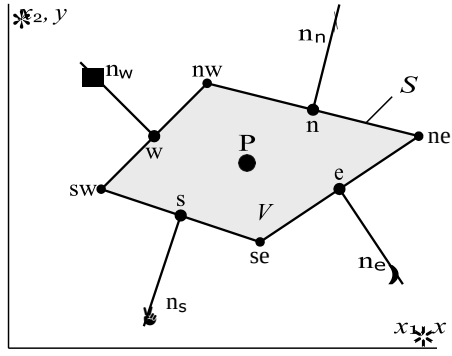

Fig. 4.5. Quadrilateral control volume with notations

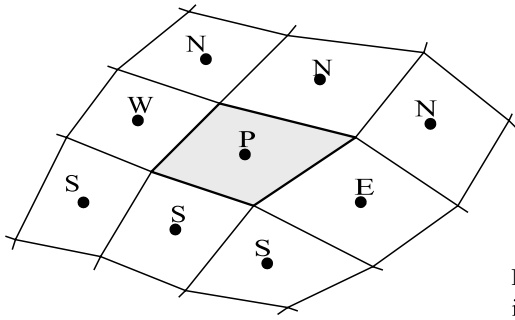

Fig. 4.6. Notations for neighbor- ing control volumes

The surface integral in (4.2) can be split into the sum of the four surface integrals over the cell faces S_c (c = e, w, n, s) of the CV, such that the balance equation (4.2) can be written

equivalently in the form

$$\sum_{c} \int_{S_c} \left(\rho v_i \varphi - \alpha \frac{\partial \varphi}{\partial x_i} \right) n_{ci} \, \mathrm{d}S_c = \int_V f \, \mathrm{d}V \, . \qquad (4.3)$$

The expression (4.3) represents a balance equation for the convective and diffusive fluxes F^C and F^D through the CV faces, respectively, with

$$F_c^C = \int_{S_c} (\rho v_i \varphi)_{ci} n_{ci} \, dS \quad \text{and} \quad F_c^D = \int_{S_c} \alpha \frac{\partial \varphi}{\partial x_i} n_{ci} \, dS \, .$$

For the face S_e, for instance, the unit normal vector $n_e = (n_{e1}, n_{e2})$ is defined by the following (geometric) conditions:

$$(x_{ne} - x_{se}) \cdot n_e = 0 \quad \text{und} \quad |n_e| = \sqrt{n_{e1}^2 + n_{e2}^2} = 1 \, .$$

From this one obtains the representation

$$n_e = \frac{(y_{ne} - y_{se})}{\delta S_e} e_1 - \frac{(x_{ne} - x_{se})}{\delta S_e} e_2 \, , \qquad (4.4)$$

where

$$\delta S_e = |x_{ne} - x_{se}| = \sqrt{(x_{ne} - x_{se})^2 + (y_{ne} - y_{se})^2}$$

denotes the length of the face S_e. Analogous relations result for the other CV faces.

For neighboring CVs with a common face the absolute value of the total flux $F_c = F_c^C + F_c^D$ through this face is identical, but the sign differs. For instance, for the CV around point P the flux F_e is equal to the flux F_w for the CV around point E (since $(n_e)_P = (n_w)_E$). This is exploited for the implementation of the method in order to avoid on the one hand a double computation for the fluxes and on the other hand to ensure that the corresponding absolute fluxes really are equal (important for conservativity, see Sect. 8.1.4). In the case of quadrilateral CVs the computation can be organized in such a way that, starting from a CV face at the boundary of the problem

the surface integrals and the vol- ume integral in (4.3) by suitable averages of the corresponding integrands at the CV faces. Afterwards, these have to be put into proper relation to the unknown function values in the nodes.

4.2 Approximation of Surface and Volume Integrals

We start with the approximation of the surface integrals in (4.3), which for a cell-centered variable arrangement suitably is carried out in two steps:

(1) Approximation of the surface integrals (fluxes) by values on the CV faces.

(2) Approximation of the variable values at the CV faces by node values.

As an example let us consider the approximation of the surface integral

$$\int_{S_e} w_i n_{ei}\, \mathrm{d}S_e$$

over the face S_e of a CV for a general integrand function w = (w_1(x), w_2(x)) (the other faces can be treated in a completely analogous way).

The integral can be approximated in different ways by involving more or less values of the integrand at the CV face. The simplest possibility is an approximation by just using the midpoint of the face:

$$\int_{S_e} w_i n_{ei}\, \mathrm{d}S_e \approx g_e\, \delta S_e\,, \tag{4.5}$$

where we denote with $g_e = w_{ei} n_{ei}$ the normal component of w at the loca- tion e. With this, one obtains an approximation of 2nd order (with respect to the face length δS_e) for the surface integral, which can be checked by means of a Taylor series expansion (Exercise 4.1). The integration formula (4.5) cor-responds to the *midpoint rule* known from numerical integration.

Other common integration formulas, that can be employed for such ap- proximations are, for instance, the *trapezoidal rule* and the *Simpson rule*. The corresponding formulas are summarized in Table 4.1 with their respective orders (with respect to δS_e).

Table 4.1. Approximations for surface integrals over the face S_e

Name	Formula	Order
Midpoint rule	$\delta S_e g_e$	2
Trapezoidal rule	$\delta S_e(g_{ne} + g_{se})/2$	2
Simpson rule	$\delta S_e(g_{ne} + 4g_e + g_{se})/6$	4

For instance, by applying the midpoint rule for the approximation of the convective and diffusive fluxes through the CV faces in (4.3), we obtain the approximations:

$$F_c^{\mathrm{C}} \approx \rho v_i n_{ci} \delta S_c\, \varphi_c \quad \text{and} \quad F_c^{\mathrm{D}} \approx -\alpha n_{ci} \delta S_c \quad \frac{\partial \varphi}{}$$

$$\dot{m}_c \qquad \partial x_i \Big|_c \,,$$

where, for simplicity, we have assumed that v_i, ρ, and α are constant across the CV. $\dot{m}_c$ denotes the mass flux through the face S_c. Inserting the definition

of the normal vector, we obtain, for instance, for the convective flux through the face S_e, the approximation

$$F_e^C \approx \dot{m}_e \varphi_e = \rho[v_1(y_{ne} - y_{se}) - v_2(x_{ne} - x_{se})] .$$

Before we turn to the further discretization of the fluxes, we first deal with the approximation of the volume integral in (4.3), which normally also is carried out by means of numerical integration. The assumption that the value f_P of f in the CV center represents an average value over the CV leads to the two-dimensional midpoint rule:

$$\int_V f \, dV \approx f_P \, \delta V ,$$

where δV denotes the volume of the CV, which for a quadrilateral CV is given by

$$\delta V = \frac{1}{2} |(x_{se} - x_{nw})(y_{ne} - y_{sw}) - (x_{ne} - x_{sw})(y_{se} - y_{nw})| .$$

An overview of the most common two-dimensional integration formulas for Cartesian CVs with the corresponding error order (with respect to δV) is given in Fig. 4.7 showing a schematical representation with the corresponding location of integration points and weighting factors. As a formula this means, e.g., in the case of the Simpson rule, an approximation of the form:

$$\int_V f \, dV \approx \frac{\delta V}{36} (16 f_P + 4 f_e + 4 f_w + 4 f_n + 4 f_s + f_{ne} + f_{se} + f_{ne} + f_{se}) .$$

It should be noted that the formulas for the two-dimensional numerical inte- gration can be used to approximate the surface integrals occurring in three- dimensional applications. For three-dimensional volume integrals analogous integration formulas as for the two-dimensional case are available.

In summary, by applying the midpoint rule (to which we will retrict ourselves) we now have the following approximation for the balance equa- tion (4.3):

$$\sum_c \dot{m}_c \varphi_c - \sum_i \alpha n_{ci} \delta S_c \frac{\partial \varphi}{\partial x}\Big|_{ci} = f_P \, \delta V . \qquad (4.6)$$

conv. fluxes — diff. fluxes — source

In the next step it is necessary to approximate the function values and deriva- tives of φ at the CV faces occurring in the convective and diffusive flux ex- pressions, respectively, by variable values in the nodes (here the CV centers). In order to clearly outline the essential principles, we will first explain the corresponding approaches for a two-dimensional Cartesian CV as indicated in Fig. 4.8. In this case the unit normal vectors $\mathbf{n}_c$ along the CV faces are given by

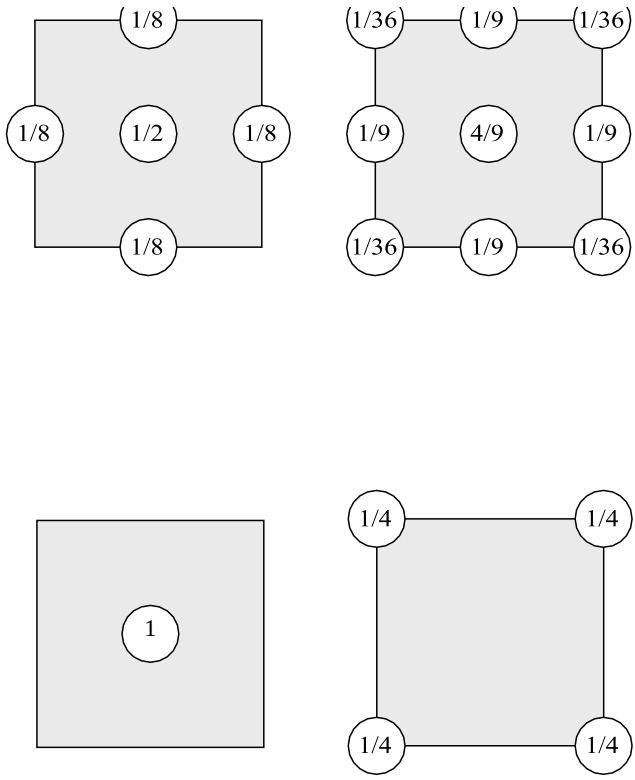

Fig. 4.7. Schematic representation of numerical integration formulas for two-dimensional volume integrals over a Cartesian CV

$$\mathbf{n}_e = \mathbf{e}_1\,,\ \mathbf{n}_w = -\mathbf{e}_1\,,\ \ \mathbf{n}_n = \mathbf{e}_2\,,\ \ \mathbf{n}_s = -\mathbf{e}_2$$

and the expressions for the mass fluxes through the CV faces simplify to

$$\dot{m}_e = \rho v_1 (y_n - y_s) \quad \dot{m}_n = \rho v_2 (x_e - x_w)\,,$$
$$\dot{m}_w = \rho v_1 (y_s - y_n)\,, \quad \dot{m}_s = \rho v_2 (x_w - x_e)\,.$$

Particularities that arise due to non-Cartesian grids will be considered in Sect. 4.5.

4.3 Discretization of Convective Fluxes

For the further approximation of the convective fluxes F_c^C, it is

where we can restrict ourselves to one-dimensional considerations for the face S_e, since the other faces and the second (or third) spatial dimension can be treated in a fully analogous way. Traditionally, the corre- sponding approximations are called differencing techniques, since they result

in formulas analogous to finite-difference methods. Strictly speaking, these areinterpolation techniques.

4.3.1 Central Differences

For the *central differencing scheme (CDS)* φ_e is approximated by linear interpolation with the values in the neighboring nodes P und E (see Fig. 4.9):

$$\varphi_e \approx \gamma_e \varphi_E + (1 - \gamma_e)\varphi_P \,. \tag{4.7}$$

The interpolation factor γ_e is defined by

$$\gamma_e = \frac{x_e - x_P}{x_E - x_P} \,.$$

The approximation (4.7) has, for an equidistant grid as well as for a non- equidistant grid, an interpolation error of 2nd order. This can be seen from a Taylor series expansion of φ around the point x_P:

$$\varphi(x) = \varphi_P + (x - x_P)\left(\frac{\partial \varphi}{\partial x}\right)_P + \frac{(x - x_P)^2}{2}\left(\frac{\partial^2 \varphi}{\partial x^2}\right)_P + T_H \,,$$

where T_H denotes the terms of higher order. Evaluating this series at thelocations x_e and x_E and taking the difference leads to the relation

$$\varphi_e = \gamma_e \varphi_E + (1 - \gamma_e)\varphi_P - \frac{(x_e - x_P)(x_E - x_e)}{2}\left(\frac{\partial^2 \varphi}{\partial x^2}\right)_P + T_H \,,$$

which shows that the leading error term depends quadratically on the grid spacing.

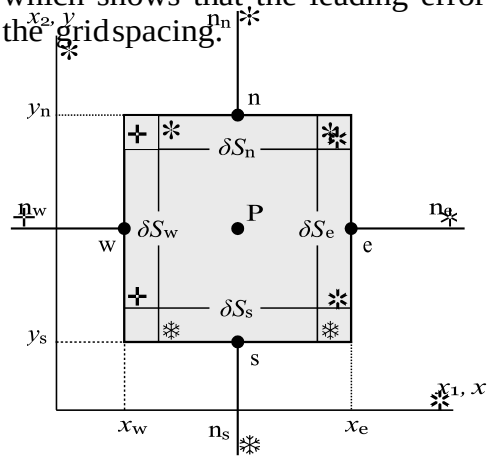

Fig. 4.8. Cartesian control volume with notations

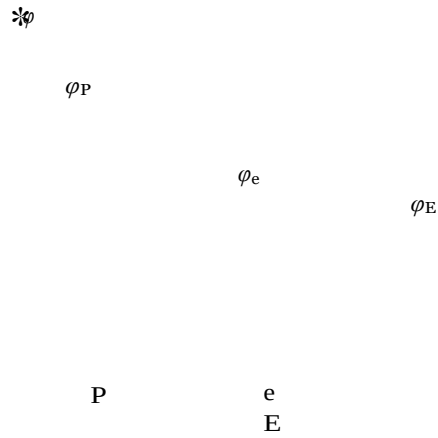

Fig. 4.9. Approximation of φ_e with CDS method

By involving additional grid points, central differencing schemes of higher order can be defined. For instance, an approximation of 4th order for an equidistant grid is given by

$$\varphi_e = \frac{1}{48}(-3\varphi_{EE} + 27\varphi_E + 27\varphi_P - 3\varphi_W),$$

where EE denotes the "east" neighboring point of E (see Fig. 4.11). Note that an application of this formula only makes sense if it is used together with an integration formula of 4th order, e.g., the Simpson rule. Only in this case is the total approximation of the convective flux also of 4th order.

When using central differencing approximations unphysical oscillations may appear in the numerical solution (the reasons for this problem will be discussed in detail in Sect. 8.1). Therefore, one often uses so-called *upwind approximations*, which are not sensitive or less sensitive to this problem. The principal idea of these methods is to make the interpolation dependent on the direction of the velocity vector. Doing so, one exploits the transport property of convection processes, which means that the convective transport of φ only takes place "downstream". In the following we will discuss two of the most important upwind techniques.

4.3.2 Upwind Techniques

The simplest upwind method results if φ is approximated by a step function. Here, φ_e is determined depending on the direction of the mass flux as follows (see Fig. 4.10):

$$\varphi_e = \varphi_P \text{ , if } \dot{m}_e > 0 \text{ ,}$$
$$\varphi_e = \varphi_E \text{ , if } \dot{m}_e < 0 \text{ .}$$

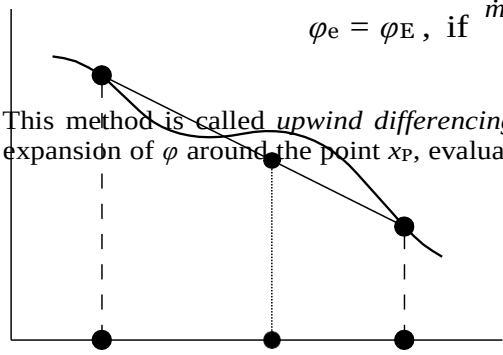

This method is called *upwind differencing scheme (UDS)*. A Taylor series expansion of φ around the point x_P, evaluated at the point x_e, gives:

$$\varphi_e = \varphi_P + (x_e - x_P)\left(\frac{\partial \varphi}{\partial x}\right)_P + \frac{(x_e - x_P)^2}{2}\left(\frac{\partial^2 \varphi}{\partial x^2}\right)_P + T_H .$$

This shows that the UDS method (independent of the grid) has an interpola-tion error of 1st order. The leading error term in the resulting approximation of the convective flux F^C becomes

$$\underbrace{\dot{m}_e (x_e - x_P)}_{\alpha_{num}} \left(\frac{\partial \varphi}{\partial x}\right)_P .$$

The error caused by this is called *artificial* or *numerical diffusion*, since the error term can be interpreted as a diffusive flux. The coefficient α_{num} is a measure for the amount of the numerical diffusion. If the transport direction is nearly perpendicular to the CV face, the approximation of the convective fluxes resulting with the UDS method is comparably good (the derivative $(\partial\varphi/\partial x)_P$ is then small). Otherwise the approximation can be quite inaccurate and for large mass fluxes (i.e., large velocities) it can then be necessary to employ very fine grids (i.e., $x_e - x_P$ very small) for the computation in order to achieve a solution with an adequate accuracy. The disadvantage of the relatively poor accuracy is confronted by the advantage that the UDS method leads to an unconditionally bounded solution algorithm. We will discuss this aspect in more detail in Sect. 8.1.5.

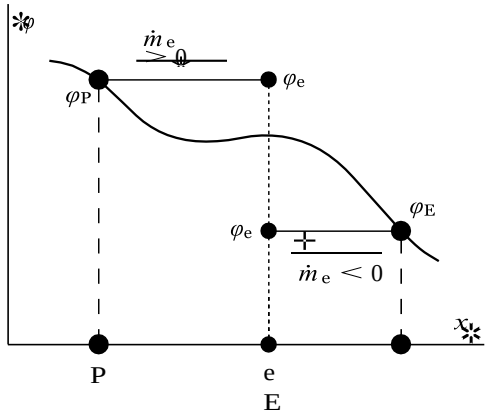

Fig. 4.10. Mass flux dependent approximation of φ_e with UDS method

An upwind approximation frequently employed in practice is the quadratic upwind interpolation, which in the literature is known as the QUICK method (Quadratic Upwind Interpolation for Convective Kinematics). Here, a quadratic polynomial is fitted through the two neighboring points P and E, and a third point, which is located upstream (W or EE depending on the flow direction). Evaluating this polynomial at point e one obtains the approximation (see also Fig. 4.11):

$$\varphi_e = a_1\varphi_E + a_2\varphi_W + (1 - a_1 + a_2)\varphi_P, \quad \dot{m}_e > 0,$$

$$\varphi_e = b_1\varphi_P - b_2\varphi_{EE} + (1 - b_1 + b_2)\varphi_E, \quad \dot{m}_e < 0,$$

where

$$a_1 = \frac{(2-\gamma_w)\gamma_e^2}{(1+\gamma_w)(1-\gamma_e)^2}, \quad a_2 = \frac{(1-\gamma_e)(1-\gamma_w)^2}{1+\gamma_e-\gamma_w},$$

$$b_1 = \frac{1+\gamma_{ee}-\gamma_e}{1+\gamma_{ee}-\gamma_e}, \quad b_2 = \frac{\gamma_{ee}^2\gamma_e}{1+\gamma_{ee}-\gamma_e}.$$

For an equidistant grid one has:

$$a_1 = \frac{3}{8}, \quad a_2 = \frac{1}{8}, \quad b_1 = \frac{3}{8}, \quad b_2 = \frac{1}{8}.$$

In this case the QUICK method possesses an interpolation error of 3rd order. However, if it is used together with numerical integration of only 2nd order the overall flux approximation also is only of 2nd order, but it is somewhat more accurate than with the CDS method.

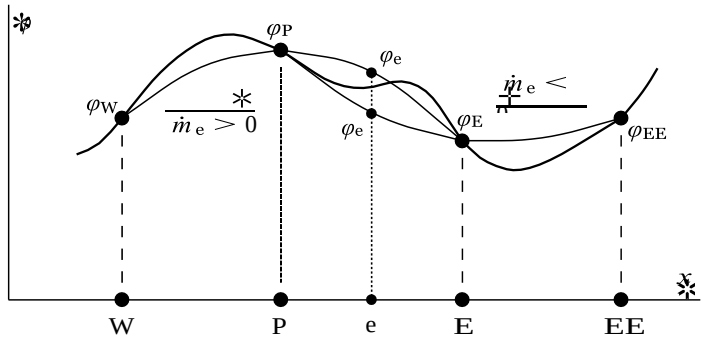

Fig. 4.11. Mass flux dependent approximation of φ_e with QUICK method

Before we turn to the discretization of the diffusive fluxes, we

The principal idea of *flux-blending*, which goes back to Khosla und Rubin(1974), is to mix different approximations for the convective flux. In this way one attempts to combine the advantages of an accurate approximation of a higher order scheme with the better robustness and boundedness properties of a lower order scheme (mostly the UDS method).

To explain the method we again consider exemplarily the face S_e of a CV. The corresponding approximations for φ_{ee} in the convective flux F^C for the

two methods to be combined are denoted by φ^{ML} and φ^{MH}, where ML and
MH are the lower and higher order methods, respectively. The approximation
for the combined method reads:

$$\varphi_e \approx (1-\beta)\varphi_e^{ML} + \beta\varphi_e^{MH} = \varphi_e^{ML} + \beta(\varphi_e^{MH} - \varphi_e^{ML}) \quad (4.8)$$

From (4.8) for $\beta = 0$ and $\beta = 1$ the methods ML and MH, respectively, result. However, it is possible to choose for β any other value between 0 and 1, allowing to control the portions of the corresponding methods according to the needs of the underlying problem. However, due to the loss in accuracy, values $\beta < 1$ should be selected only if with $\beta = 1$ on the given grid no "reasonable" solution can be obtained (see Sect. 8.1.5) and a finer grid is not possible due to limitations in memory or computing time.

Also, if $\beta = 1$ (i.e., the higher order method) is employed, it can be be- neficial to use the splitting according to (4.8) in order to treat the term $b^{\varphi,e}$ "explicitly" in combination with an iterative solver. This means that this term is computed with (known) values of φ from the preceding iteration and added to the source term. This may lead to a more stable iterative solution procedure, since this (probably critical) term then makes no contribution to the system matrix, which becomes more diagonally dominant. It should be pointed out that this modification has no influence on the converged solution, which is identical to that obtained with the higher order method MH alone. We will discuss this approach in some more detail at the end of Sect. 7.1.4.

4.4 Discretization of Diffusive Fluxes

For the approximation of diffusive fluxes it is necessary to approximate the values of the normal derivative of φ at the CV faces by nodal values in the CV centers. For the east face S_e of the CV, which we will again consider exemplarily, one has to approximate (in the Cartesian case) the derivative $(\partial\varphi/\partial x)_e$. For this, difference formulas as they are common in the framework of the finite-difference method can be used (see, e.g., [9]).

The simplest approximation one obtains when using a central differencing formula

$$\frac{\partial\varphi}{\partial x}_e$$

$$\frac{\varphi_E - \varphi_P}{x_E - x_P}, \qquad (\approx 4.9)$$

which is equivalent to the assumption that φ is a linear function between the points x_P and x_E (see Fig. 4.12). For the discussion of the error of this ap- proximation, we consider the difference of the Taylor series expansion aroundx_e at the locations x_P and x_E:

$$\left(\frac{\partial\varphi}{\partial x}\right)_e = \frac{\varphi_E - \varphi_P}{x_E - x_P} + \frac{(x_e - x_P)^2 - (x_E - x_e)^2}{2(x_E - x_P)}\left(\frac{\partial^2\varphi}{\partial x^2}\right)_e - \frac{(x_e - x_P)^3 + (x_E - x_e)^3}{6(x_E - x_P)}\left(\frac{\partial^3\varphi}{\partial x^3}\right)_e + T_H .$$

One can observe that for an equidistant grid an error of 2nd order results, since in this case the coefficient in front of the second derivative is zero. In the case of non-equidistant grids, one obtains by a simple algebraic rearrange-ment that this leading error term is proportional to the grid spacing and the expansion rate ξ_e of neighboring grid spacings:

$$\frac{(1-\xi_e)(x_e - x_P)}{2}\left(\frac{\partial^2\varphi}{\partial x^2}\right)_e \quad \text{with} \quad \xi_e = \frac{x_E - x_e}{x_e - x_P} .$$

This means that the portion of the 1st order error term gets larger the more the expansion rate deviates from 1. This aspect should be taken into account in the grid generation such that neighboring CVs do not differ that much in the corresponding dimensions (see also Sect. 8.3).

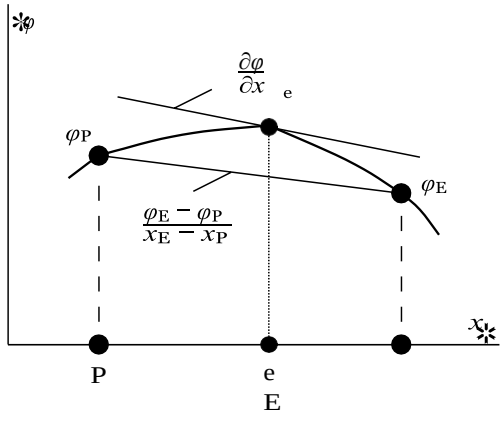

Fig. 4.12. Central differencing formula for approximation of 1st derivative at CV face

One obtains a 4th order approximation of the derivative at the CV face for an equidistant grid by

$$\left(\frac{\partial\varphi}{\partial x}\right)_e$$

$$\approx \frac{1}{24\Delta x}(\varphi_{\mathrm{W}} - 27\varphi_{\mathrm{P}} + 27\varphi_{\mathrm{E}} - \varphi_{\mathrm{EE}})\,, \tag{4.10}$$

which, for instance, can be used together with the Simpson rule to obtain an overall approximation for the diffusive flux of 4th order.

Although principally there are also other possibilities for approximating the derivatives (e.g., forward or backward differencing formulas), in practice almost only central differencing formulas are employed, which possess the best accuracy for a given number of grid points involved in the discretization. Problems with boundedness, as for the convective fluxes, do not exist. Thus,

there is no reason to use less accurate approximations. For CVs located at the boundary of the problem domain, it might be necessary to employ forward or backward differencing formulas because there are no grid points beyond the boundary (see Sect. 4.7).

4.5 Non-Cartesian Grids

The previous considerations with respect to the discretization of the convective and diffusive fluxes were confined to the case of Cartesian grids. In this section we will discuss necessary modifications for general (quadrilateral) CVs.

For the convective fluxes, simple generalizations of the schemes introduced in Sect. 4.3 (e.g., UDS, CDS, QUICK, . . .) can be employed for the approxi- mation of φ_c. For instance, a corresponding CDS approximation for φ_e reads:

$$\varphi_e \approx \frac{|\mathbf{x}_{\tilde{e}} - \mathbf{x}_P|}{|\mathbf{x}_E - \mathbf{x}_P|}\varphi_E + \frac{|\mathbf{x}_E - \mathbf{x}_{\tilde{e}}|}{|\mathbf{x}_E - \mathbf{x}_P|}\varphi_P , \tag{4.11}$$

where $\mathbf{x}_{\tilde{e}}$ is the intersection of the connnecting line of the points P and E with the (probably extended) CV face S_e (see Fig. 4.13). For the convective flux through S_e this results in the following approximation:

$$F_e^C \approx \frac{\dot{m}_e}{|\mathbf{x}_E - \mathbf{x}_P|}\left(|\mathbf{x}_{\tilde{e}} - \mathbf{x}_P|\varphi_E + |\mathbf{x}_E - \mathbf{x}_{\tilde{e}}|\varphi_P\right) .$$

When the grid at the corresponding face has a “kink”, an additional error results because the points $\mathbf{x}_{\tilde{e}}$ and $\mathbf{x}_e$ do not coincide (see Fig. 4.13). This aspect should be taken into account for the grid generation (see also Sect. 8.3).

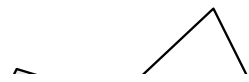

Let us turn to the approximation of the diffusive fluxes, for which farther reaching distinctions to the Cartesian case arise as for the convective fluxes. Here, for the required approximation of the normal derivative of φ in the center of the CV face there are a variety of different possibilities, depending on the directions in which the derivative is approximated, the locations where the appearing derivatives are evaluated, and the node values which are used

for the interpolation. As an example we will give here one variant and consider only the CV face S_e.

Since along the normal direction in general there are no nodal points, the normal derivative has to be expressed by derivatives along other suitable directions. For this we use here the coordinates $\tilde{\xi}$ and $\tilde{\eta}$ defined according to Fig. 4.14. The direction $\tilde{\xi}$ is determined by the connecting line between points P and E, and the direction $\tilde{\eta}$ is determined by the direction of the CV face. Note that $\tilde{\xi}$ and $\tilde{\eta}$, because of a distortion of the grid, can deviate from the directions ξ und η, which are defined by the connecting lines of P with the CV face centers e and n. The larger these deviations are, the larger the discretization error becomes. This is another aspect that has to be taken into account when generating the grid (see also Sect. 8.3).

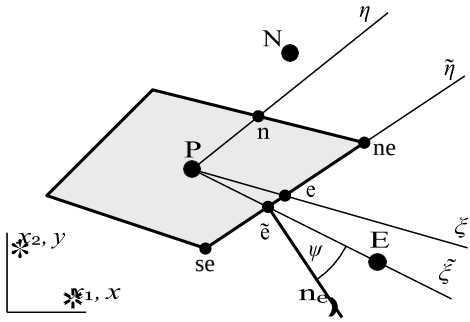

Fig. 4.14. Approximation of diffusive fluxes for non-Cartesian control volumes

A coordinate transformation $(x, y) \rightarrow (\tilde{\xi}, \tilde{\eta})$ results for the normal derivative in the following representation:

$$\frac{\partial \varphi}{\partial x} n_{e1} + \frac{\partial \varphi}{\partial y} n_{e2} = \frac{1}{J} \left(\frac{\partial y}{\partial \tilde{\eta}} n_{e1} - \frac{\partial x}{\partial \tilde{\eta}} n_{e2} \right) \frac{\partial \varphi}{\partial \tilde{\xi}} + \left(\frac{\partial x}{\partial \tilde{\xi}} n_{e2} - \frac{\partial y}{\partial \tilde{\xi}} n_{e1} \right) \frac{\partial \varphi}{\partial \tilde{\eta}} \quad (4.12)$$

with the Jacobi determinant

$$J = \frac{\partial x}{\partial \tilde{\xi}} \frac{\partial y}{\partial \tilde{\eta}} - \frac{\partial y}{\partial \tilde{\xi}} \frac{\partial x}{\partial \tilde{\eta}}.$$

The metric quantities can be approximated according to

$$\frac{\partial \mathrm{X}}{\partial \mathrm{P}} \approx \frac{\mathrm{X_E} - }{} \quad \text{and} \quad \frac{\partial \mathrm{X}}{} \approx \frac{\mathrm{x_{ne}} - \mathrm{x_{se}}}{}, \tag{4.13}$$

$$\partial \tilde{\xi} \quad |\mathrm{x}_E - \mathrm{x}_P| \qquad \partial \tilde{\eta} \qquad \delta S_\mathrm{e}$$

which results for the Jacobi determinant in the approximation

$$J_\mathrm{e} \approx \frac{(x_\mathrm{E} - x_\mathrm{P})(y_\mathrm{ne} - y_\mathrm{se}) - (y_\mathrm{E} - y_\mathrm{P})(x_\mathrm{ne} - x_\mathrm{se})}{|\mathrm{x}_E - \mathrm{x}_P|\, \delta S_\mathrm{e}} = \cos\psi\,,$$

where ψ denotes the angle between the direction $\tilde{\xi}$ and n_e (see Fig. 4.14). ψ is a measure for the deviation of the grid from orthogonality ($\psi = 0$ for an orthogonal grid).

The derivatives with respect to $\tilde{\xi}$ and $\tilde{\eta}$ in (4.12) can be approximated in the usual way with a finite-difference formula. For example, the use of a central difference of 2nd order gives:

$$\frac{\partial \varphi}{\partial \tilde{\xi}} \approx \frac{\varphi_E - \varphi_P}{|x_E - x_P|} \quad \text{and} \quad \frac{\partial \varphi}{\partial \tilde{\eta}} \approx \frac{\varphi_{ne} - \varphi_{se}}{\delta S_e}. \tag{4.14}$$

Inserting the approximations (4.13) and (4.14) into (4.12) and using the com- ponent representation (4.4) of the unit normal vector n_e we finally obtain the following approximation for the diffusive flux through the CV face S_e:

$$F_e^D \approx D_e(\varphi_E - \varphi_P) + N_e(\varphi_{ne} - \varphi_{se}) \tag{4.15}$$

with

$$D_e = \frac{\alpha}{(x_{ne} - x_{se})(y_E - y_P) - (y_{ne} - y_{se})(x_E - x_P)}, \tag{4.16}$$

$$N_e = \frac{\alpha\,[(y_{ne} - y_{se})(y_E - y_P) + (x_{ne} - x_{se})(x_E - x_P)]}{(y_{ne} - y_{se})(x_E - x_P) - (x_{ne} - x_{se})(y_E - y_P)}. \tag{4.17}$$

The coefficient N_e represents the portion that arise due to the non-orthogo-nality of the grid. If the grid is orthogonal, n_e and $x_E - x_P$ have the same direction such that $N_e = 0$. The coefficient N_e (and the corresponding values for the other CV faces) should be kept as small as possible (see als Sect. 8.3).

The values for φ_{ne} and φ_{se} in (4.15) can be approximated, for instance, by linear interpolation of four neighboring nodal values:

$$\varphi_{ne} = \gamma_P\varphi_P + \gamma_E\varphi_E + \gamma_N\varphi_N + \gamma_{NE}\varphi_{NE}$$

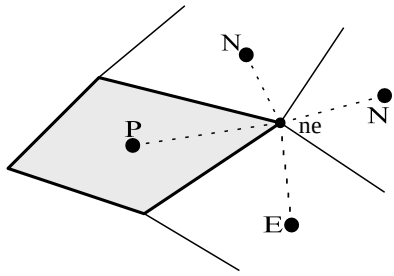

Fig. 4.15. Interpolation of values in CV edges for discretization of diffusive fluxes for non-Cartesian CV

4.6 Discrete Transport Equation

Let us now return to our example of the general two-dimensional transport equation (4.3) and apply the approximation techniques introduced in the pre- ceding sections to it.

We employ exemplarily the midpoint rule for the integral approximations, the UDS method for the convective flux, and the CDS method for the diffusive flux. Additionally, we assume that we have velocity components $v_1, v_2 > 0$ and that the grid is a Cartesian one. With these assumptions one obtains the following approximation of the balance equation (4.3):

$$\begin{aligned}
&\rho v_1 \varphi_P - \alpha \frac{\varphi_E - \varphi_P}{x_E - x_P} (y_n - y_s) \\
-\ &\rho v_1 \varphi_W - \alpha \frac{\varphi_P - \varphi_W}{x_P - x_W} (y_n - y_s) \\
+\ &\rho v_2 \varphi_P - \alpha \frac{\varphi_N - \varphi_P}{y_N - y_P} (x_e - x_w) \\
-\ &\rho v_2 \varphi_S - \alpha \frac{\varphi_P - \varphi_S}{y_P - y_S} (x_e - x_w) = f_P (y_n - y_s)(x_e - x_w) .
\end{aligned}$$

A simple rearrangement gives a relation of the form

$$a_P \varphi_P = a_E \varphi_E + a_W \varphi_W + a_N \varphi_N + a_S \varphi_S + b_P \tag{4.18}$$

with the coefficients

$$\begin{aligned}
a_E &= \frac{\alpha}{(x_E - x_P)(x_e - x_w)} , \\
a_W &= \frac{\rho v_1}{x_e - x_w} + \frac{\alpha}{(x_P - x_W)(x_e - x_w)} , \\
a_N &= \frac{\alpha}{(y_N - y_P)(y_n - y_s)} , \\
a_S &= \frac{\rho v_2}{y_n - y_s} + \frac{\alpha}{(y_P - y_S)(y_n - y_s)} , \\
a_P &= \frac{\rho v_1}{x_e - x_w} + \frac{\alpha (x_E - x_W)}{(x_P - x_W)(x_E - x_P)(x_e - x_w)} + \\
&\quad \frac{\rho v_2}{y_n - y_s} \qquad\qquad b_P = f_P .
\end{aligned}$$

$$+ \frac{\alpha(y_N - y_S)}{(y_P - y_S)(y_N - y_P)(y_n - y_s)},$$

If the grid is equidistant in each spatial direction (with grid spacings Δx and Δy), the coefficients become:

$$a_E = \frac{\alpha}{\Delta x^2}, \quad a_W = \frac{\rho v_1}{\Delta x} + \frac{\alpha}{\Delta x^2}, \quad a_N = \frac{\alpha}{\Delta y^2}, \quad a_S = \frac{\rho v_2}{\Delta y} + \frac{\alpha}{\Delta y^2},$$

$$a_P = \frac{\rho v_1}{\Delta x} + \frac{2\alpha}{\Delta x^2} + \frac{\rho v_2}{\Delta y} + \frac{2\alpha}{\Delta y^2}, \quad b_P = f_P .$$

In this particular case (4.18) coincides with a discretization that would result from a corresponding finite-difference method (for general grids this normallyis not the case).

It can be seen that – independent from the grid employed – one has forthe coefficients in (4.18) the relation

$$a_P = a_E + a_W + a_N + a_S .$$

This is characteristic for finite-volume discretizations and expresses the con- servativity of the method. We will return to this important property inSect. 8.1.4.

Equation (4.18) is valid in this form for all CVs, which are not locatedat the boundary of the problem domain. For boundary CVs the approxima-tion (4.18) includes nodal values outside the problem domain, such that they require a special treatment depending on the given type of boundary condi- tion.

4.7 Treatment of Boundary Conditions

We consider the three boundary condition types that most frequently oc-cur for the considered type of problems (see Chap. 2): a prescibed variable value, a prescibed flux, and a symmetry boundary. For an explanation of the implementation of such conditions into a finite-volume method, we consider as an example a Cartesian CV at the west boundary (see Fig. 4.16) for the transport equation (4.3). Correspondingly modified approaches for the non- Cartesian case or for other types of equations can be formulated analogously (for this see also Sect. 10.4).

Let us start with the case of a prescribed boundary value $\varphi_w = \varphi^o$. For the convective flux at the boundary one has the approximation:

$$F_w^C \approx \dot{m}_w \varphi_w = \dot{m}_w \varphi^o .$$

With this the approximation of F_w^C is known (the mass flux $\dot{m}_w$ at the bound- ary is also known) and can simply be introduced in the balance equation (4.6). This results in an additional contribution to the source term b_P.

The diffusive flux through the boundary is determined with the same ap- proach as in the interior of the domain (see (4.18)). Analogously to (4.9) the derivative at the boundary can be approximated as follows:

$$\left(\frac{\partial \varphi}{\partial x}\right)_w \approx \frac{\varphi_P - \varphi_w}{x_P - x_w} = \frac{\varphi_P - \varphi}{x_P - x_w}. \qquad (4.19)$$

This corresponds to a forward difference formula of 1st order. Of course, it is also possible to apply more elaborate formulas of higher order. However, since the distance between the boundary point w and the point P is smaller than

the distance between two inner points (half as much for an equidistant grid, see Fig. 4.16), a lower order approximation at the boundary usually does not influence the overall accuracy that much.

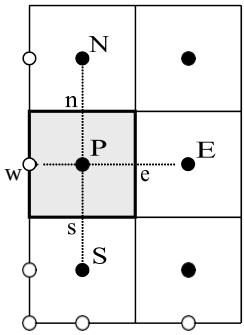

Fig. 4.16. Cartesian boundary CV at west boundary with notations

In summary, one has for the considered boundary CV a relation of the form (4.18) with the modified coefficients:

$$a_W = 0,$$

$$a_P = \frac{\rho v_1}{x_e - x_w} + \frac{\alpha(x_E - x_w)}{(x_P - x_w)(x_E - x_P)(x_e - x_w)} +$$

$$\frac{\rho v_2}{y_n - y_s} + \frac{\alpha(y_N - y_S)}{(y_P - y_S)(y_N - y_P)(y_n - y_s)},$$

$$b_P = f_P \quad \frac{\rho v_1}{x_e - x_w} + \frac{\alpha}{(x_P - x_w)(x_e - x_w)} \quad \varphi^o.$$

+

All other coefficients are computed as for a CV in the interior of the problem domain.

Let us now consider the case where the flux $F_w = F^o$ is prescribed at the west boundary. The flux through the CV face is obtained by dividing F^o through the length of the face $x_e x_w$. The resulting value is introduced in (4.6) as total flux and the modified coefficients for the boundary CV become:

$$a_W = 0,$$

$$a_P = \frac{\rho v_1}{x_e - x_w} + \frac{\alpha}{(x_E - x_P)(x_e - x_w)} +$$

$$\frac{\rho v_2}{y_n - y_s} \qquad b_P = f_P +$$

$$+ \frac{\alpha(y_N - y_S)}{(y_P - y_S)(y_N - y_P)(y_n - y_s)}, \quad \frac{\cdot}{x_e - x_w}$$

F^o

All other coefficients remain unchanged.

Sometimes it is possible to exploit symmetries of a problem in order todownsize the problem domain to save computing time or get a higher accuracy

(with a finer grid) with the same computational effort. In such cases one hasto consider symmetry planes or symmetry lines at the corresponding problem boundary. In this case one has the boundary condition:

$$\frac{\partial \varphi}{\partial x_i} n_i = 0 . \tag{4.20}$$

From this condition it follows that the diffusive flux through the symmetry boundary is zero (see (4.18)). Since also the normal component of the velocity vector has to be zero at a symmetry boundary (i.e., $v_i n_i = 0$), the mass flux and, therefore, the convective flux through the boundary is zero. Thus, in the balance equation (4.6) the total flux through the corresponding CV face canbe set to zero. For the boundary CV in Fig. 4.16 this results in the following modified coefficients:

$$a_W = 0 ,$$
$$a_P = \frac{\rho v_1}{} + \frac{\alpha}{} +$$
$$\frac{\rho v_2}{\dfrac{x_e - x_w}{y_n - y_s}} + \frac{\alpha (y_N - y_S)}{\dfrac{(x_E - x_P)(x_e - x_w)}{(y_P - y_S)(y_N - y_P)(y_n - y_s)}} .$$

If required, the (unknown) variable value at the boundary can be determined by a finite-difference approximation of the boundary condition (4.20). In the considered case, for instance, with a forward difference formula (cp. (4.19)) one simply obtains $\varphi_w = \varphi_P$.

As with all other discretization techniques, the algebraic system of equa- tions resulting from a finite-volume discretization has a unique solution onlyif the boundary conditions at all boundaries of the problem domain are taken into account (e.g., as outlined above). Otherwise there would be more un- knowns than equations.

4.8 Algebraic System of Equations

As exemplarily outlined in Sect. 4.6 for the general scalar transport equation,a finite-volume discretization for each CV results in an algebraic equation ofthe form:

$$a_P \varphi_P - \sum_c a_c \varphi_c = b_P ,$$

where the index c runs over all neighboring points that are involved in the approximation as a result of the discretization scheme employed. Globally, i.e., for all control volumes V_i ($i = 1, \ldots, N$) of the problem domain, this gives a linear system of N equations

$$a^i \varphi^i - \sum_{c} a^i \varphi^i = b^i \quad \text{for all} \quad i = 1, \ldots, N \tag{4.21}$$

for the N unknown nodal values φ^i in the CV centers.

After introducing a corresponding numbering of the CVs (or nodal values), in the case of a Cartesian grid the system (4.21) has a fully analogous structure that also would result from a finite-difference approximation. To illustrate this, we consider first the one-dimensional case. Let the problem domain be the interval $[0, L]$, which we divide into N not necessarily equidistant CVs (subintervals) (see Fig 4.17).

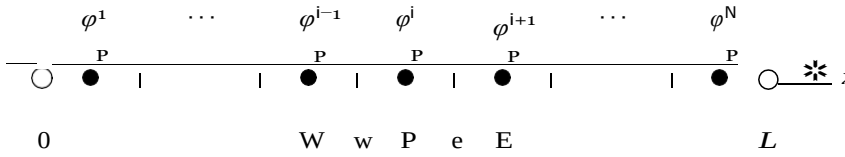

Fig. 4.17. Arrangement of CVs and nodes for 1-D transport problem

Using the second-order central differencing scheme, the discrete equations have the form:

$$a_P^i \varphi_P^i - a_E^i \varphi_E^i - a_W^i \varphi_W^i = b^i \,. \tag{4.22}$$

With the usual lexicographical numbering of the nodal values as given in Fig. 4.17 one has:

$$\varphi_W^i = \varphi_P^{i-1} \quad \text{for all} \quad i = 2, \ldots, N \,,$$
$$\varphi_E^i = \varphi_P^{i+1} \quad \text{for all} \quad i = 1, \ldots, N-1 \,.$$

Thus, the result is a linear system of equations which can be represented in matrix form as follows:

$$\begin{bmatrix} a_P^1 & -a_E^1 & & & \\ -a_W^2 & a_P^2 & -a_E^2 & & 0 \\ & \ddots & \ddots & \ddots & \\ & & -a_W^i & a_P^i & -a_E^i \end{bmatrix} \begin{bmatrix} \varphi_P^1 \\ \vdots \\ \varphi_P^{i-1} \\ \varphi_P^i \\ \varphi_P^{i+1} \\ \vdots \end{bmatrix} = \begin{bmatrix} b_P^1 \\ b_P^2 \\ \vdots \\ b_P^i \\ \vdots \end{bmatrix}.$$

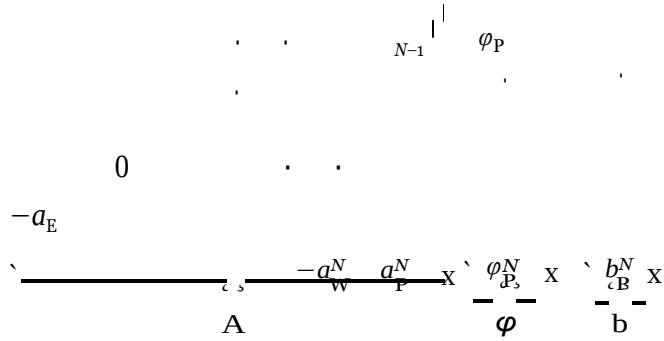

When using a QUICK discretization or a central differencing scheme of 4th order, there are also coefficients for the farther points EE and WW (see Fig. 4.18):

$$a_P\varphi_P - a_{EE}\varphi_{EE} - a_E\varphi_E - a_W\varphi_W - a_{WW}\varphi_{WW} = b_P\,, \qquad (4.23)$$

i.e., in the corresponding coefficient matrix A two additional non-zero diago-nals appear:

$$A = \begin{bmatrix} a_P^1 & -a_E^1 & -a_{EE}^1 & & & & \\ -a_W^2 & a_P^2 & -a_E^2 & -a_{EE}^2 & & 0 & \\ -a^3 & -a^3 & a^3 & -a^3 & -a^3_{WW} & & \\ & \ddots & \ddots & \ddots & \ddots & \ddots & \\ & & -a_{WW}^i & -a_W^i & a_P^i & -a_E^i & -a_{EE}^i \\ & & & \ddots & \ddots & \ddots & \ddots \\ & & & & & & -a_{EE}^{N-2} \\ & & & & & & \\ & & 0 & -a & & & -a_{EE}^{N-1} \\ & & & & -a_{WW}^N & -a_W^N & a_P^N \end{bmatrix}$$

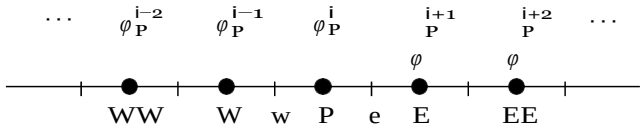

Fig. 4.18. CV dependencies with higher order scheme for 1-D transport problem

For the two- and three-dimensional cases fully analogous considerations can be made for the assembly of the discrete equation systems. For a two- dimensional rectangular domain with $N \times M$ CVs (see Fig. 4.19), we have, for instance, in the case of the discretization given in Sect. 4.6 equations of the form

$$a_P^{i,j}\varphi_P^{i,j} - a_E^{i,j}\varphi_E^{i,j} - a_W^{i,j}\varphi_W^{i,j} - a_S^{i,j}\varphi_S^{i,j} - a_N^{i,j}\varphi_N^{i,j} = b_P^{i,j}$$

for $i = 1, \ldots, N$ and $j = 1, \ldots, M$. In the case of a lexicographical columnwise numbering of the nodal values (index j is counted up

$$
\mathbf{A} = \begin{bmatrix}
a_P & -a_N & \cdots & 0 & \cdots & -a_E^{1,1} & & & \\
-a_{1,2} & \ddots & \ddots & & \ddots & & 0 & & \\
 & \ddots & \ddots & \ddots & \ddots & \ddots & & & \\
 & & \ddots & \ddots & \ddots & & & & \\
 & 0 & & \ddots & \ddots & \ddots & & & \\
 & & & & & & & -a_{N-1,M} & \\
 & & & & & & & & \ddots \\
 & & & & & & & & -a_E \\
 & & & & & & & & \ddots \\
 & & & & & & & & 0 \\
 & & & & & & & & \ddots \\
 & & & & & & & & -a_{N,M-1} \\
 & & & & & & & & \ddots \\
 & & & & & & & & -a_N \\
 & & & & & & & & a_P
\end{bmatrix}
$$

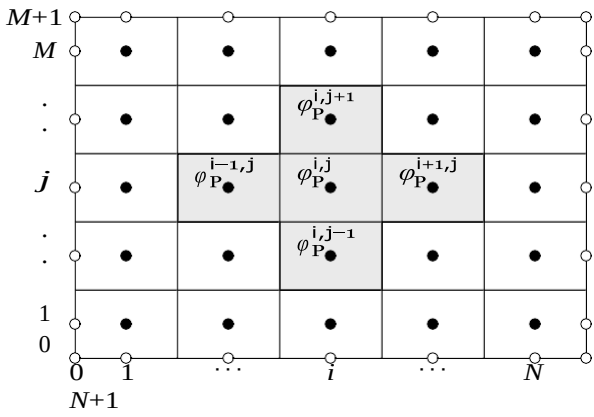

Fig. 4.19. Arrangement of CVs and nodes for 2-D transport problem

As outlined in Sect. 4.5, due to the discretization of the diffusive fluxes, in the non-Cartesian case additional coefficients can arise, whereby the number of non-zero diagonals in the system matrix increases. Using the discretization exemplarily given in Sect. 4.5, for instance, one would have additional depen- dencies with the points NE, NW, SE, and SW, which are required to

4.9 Numerical Example

As a concrete, simple (two-dimensional) example for the application of the FVM, we consider the computation of the heat transfer in a trapezoidal plate (density ρ, heat conductivity κ) with a constant heat source q all over the

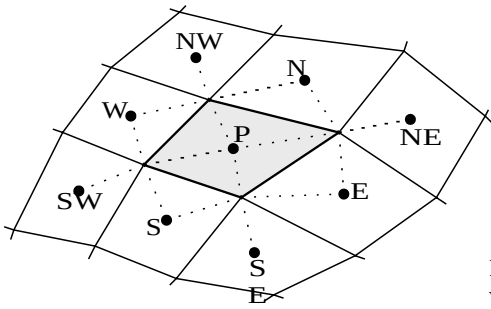

Fig. 4.20. Interpolation of vertice values for non-Cartesian CV

plate. At three sides the temperature T is prescribed and at the fourth side the heat flux is given (equal to zero). The problem data are summarized in Fig. 4.21. The problem is described by the heat conduction equation

$$-\kappa \frac{\partial^2 T}{\partial x^2} - \kappa \frac{\partial^2 T}{\partial y^2} = \rho q \tag{4.24}$$

with the boundary conditions as indicated in Fig. 4.21 (cp. Sect. 2.3.2). For the discretization we employ a grid with only two CVs as illustrated in Fig. 4.22. The required coordinates for the distinguished points for both CVs are indi-cated in Table 4.2.

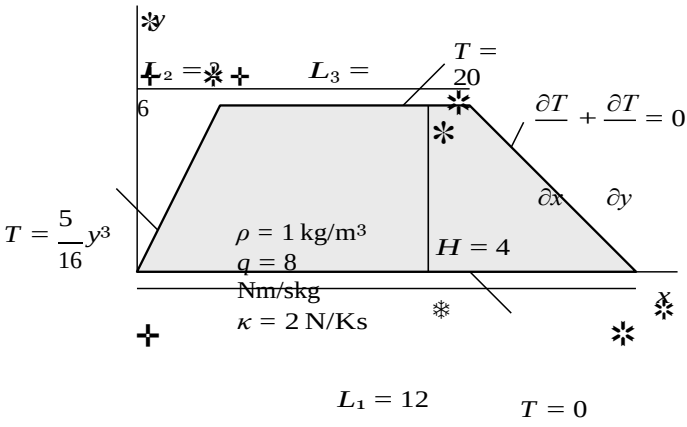

Fig. 4.21. Configuration of trapezoidal plate heat conduction example (temperature in K, length in m)

The integration of (4.24) over a control volume V and the application of the Gauß integral theorem gives:

$$\sum_c F_c = -\kappa \sum_c \int_{S_c} \left(\frac{\partial T}{\partial x} n_1 + \frac{\partial T}{\partial y} n_2 \right) \mathrm{d}S_c = \int_V q \, \mathrm{d}V \,,$$

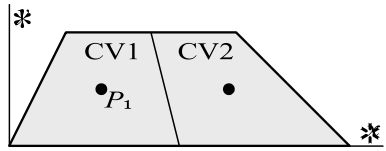

Fig. 4.22. CV definition for trapezoidal plate

Table 4.2. Coordinates of distinguished points for discretized trapezoidal plate

	CV1		CV2	
Point	*x*	*y*	*x*	*y*
P	13/4	2	31/4	2
e	11/2	2	10	2
w	1	2	11/2	2
n	7/2	4	13/2	4
s	3	0	9	0
nw	2	4	5	4
ne	5	4	8	4
se	6	0	12	0
sw	0	0	6	0
Volume	18		18	

where the summation has to be carried out over c = s, n, w, e. For the ap- proximation of the integrals we employ the midpoint rule and the derivatives at CV faces are approximated by second-order central differences. Thus, the approximations of the fluxes for CV1 is:

$$F_e = -\kappa \int_{S_e} \left(\frac{4}{\sqrt{17}} \frac{\partial T}{\partial x} + \frac{1}{\sqrt{17}} \frac{\partial T}{\partial y} \right) dS_e \approx$$

$$\approx D_e (T_E - T_P) + N_e (T_{ne} - T_{se}) = -\frac{17}{9} (T_E - T_P) - 10,$$

$$F_w = -\kappa \int_{S_w} \left(-\frac{2}{\sqrt{5}} \frac{\partial T}{\partial x} + \frac{1}{\sqrt{5}} \frac{\partial T}{\partial y} \right) dS_w =$$

$$= -\kappa \int_{S_w} \left(-\frac{2}{\sqrt{5}} \frac{120}{16} x^2 + \frac{1}{\sqrt{5}} \frac{15}{16} y^2 \right) dS_w = 60,$$

$$\frac{\partial T}{\partial}$$

$$F_{\mathrm{s}} = -\kappa \int_{S_{\mathrm{s}}} \frac{\partial T}{\partial y}\,\mathrm{d}S_{\mathrm{s}} \approx -\kappa \left(\frac{\partial T}{\partial y}\right)_{\mathrm{s}} (x_{\mathrm{se}} - x_{\mathrm{sw}}) \approx$$

$$\approx -\kappa \frac{T_{\mathrm{P}} - T_{\mathrm{S}}}{y_{\mathrm{P}} - y_{\mathrm{S}}} (x_{\mathrm{se}} - x_{\mathrm{sw}}) = 6T_{\mathrm{P}} ,$$

$$F_n = -\kappa \int_{S_n} \frac{\partial T}{\partial y}\, dS_n \approx -\kappa \left.\frac{\partial T}{\partial y}\right|_n (x_{ne} - x_{nw}) \approx$$

$$\approx -\kappa \frac{T_N - T_P}{y_N - y_P} (x_{ne} - x_{nw}) = 3T_P - 60\,.$$

The flux F_w has been computed exactly from the given boundary value func-tion. Similarly, one obtains for CV2:

$$F_e = 0\,, \quad F_w \approx \frac{17}{9}(T_P - T_W) + 10\,, \quad F_s \approx 6T_P\,, \quad F_n \approx 3T_P - 60\,.$$

For both CVs we have $\delta V = 18$, such that the following discrete balance equations result:

$$\frac{98}{9} T_P - \frac{17}{9} T_E = 154 \quad \text{and} \quad \frac{98}{9} T_P - \frac{17}{9} T_W = 194\,.$$

We have $T_P = T_1$ and $T_E = T_2$ for CV1, and $T_P = T_2$ and $T_W = T_1$ for CV2. This gives the linear system of equations

$$98T_1 - 17T_2 = 1386 \qquad \text{and} \qquad 98T_2 - 17T_1 = 1746$$

for the two unknown temperatures T_1 and T_2. Its solution gives $T_1 \approx 17,77$ and $T_2 \approx 20,90$.

Exercises for Chap. 4

Exercise 4.1. Determine the leading error terms for the one-dimensional midpoint and trapezoidal rules by Taylor series expansion and compare the results.

Exercise 4.2. Let the concentration of a pollutant $\varphi = \varphi(x)$ in a chimney be described by the differential equation

$$-3\varphi' - 2\varphi'' = x\cos(\pi x) \qquad \text{for} \quad 0 < x < 6$$

with the boundary conditions $\varphi'(0) = 1$ and $\varphi(6) = 2$. Compute the values φ_1 and φ_2 in the centers of the two control volumes CV1 =

finite-volume method for the two grids illustarted in Fig. 4.24. Compare the results with the analytic solution $T_a(x, y) = 20 - 2y + x\ y - xy$.

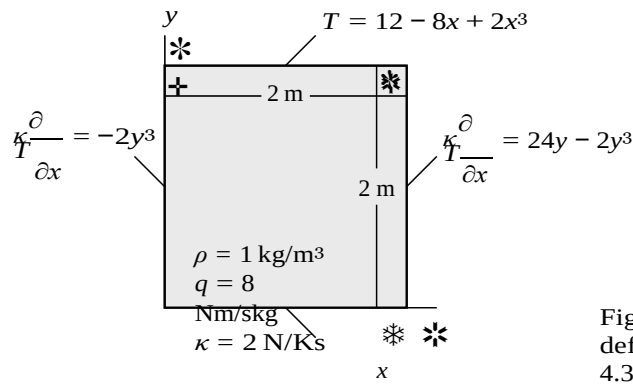

Fig. 4.23. Problem def-inition for Exercise 4.3

(temperatures in K)

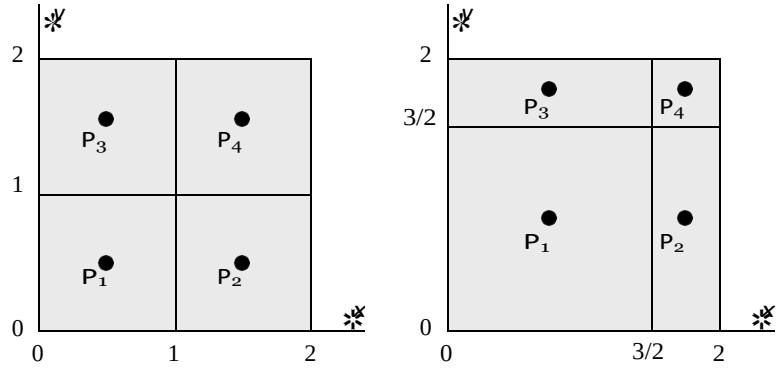

Fig. 4.24. Numerical grids for Exercise 4.3

Exercise 4.4. Formulate a finite-volume method of 2nd order for equidis- tant grids for the bar equation (2.38). Use this for computing the displace- ment of a bar of length L = 60 m with the boundary conditions (2.39) with $A(x) = 1 + x/60$, $u_o = 0$, and $k_L = 4$ N employing a discretization with three equidistant CVs.

Exercise 4.5. Formulate a finite-volume method of 4th order for the mem- brane equation (2.17) for an equidistant Cartesian grid.

Exercise 4.6. Consider the integral

$$I = \int \varphi \, dS$$

the length Δy of S_e) for the approximation

$$I \approx \varphi(3, \alpha)\Delta y$$

depending on the parameter$\in\alpha$ [1, 3]. (ii) Compute I for the function $\varphi(x, y) = x^3y^4$ directly (analytically) and with the approximation defined in (i) with $\alpha = 2$. Compare the two solutions.

Exercise 4.7. The velocity vector of a two-dimensional flow is given by

$$\mathrm{v} = (v_1(x, y), v_2(x, y)) = (x \cos \pi y, x^4 y) .$$

Let the flux through the surface S of the control volume $V = [1, 2]^2$ be defined

by

$$I = \int_S v_i n_i \, \mathrm{d}S .$$

(i) Approximate the integral with the Simpson rule. (ii) Transform the in- tegral with the Gauß integral theorem into a volume integral (over V) and approximate this with the midpoint rule.

UNIT IV

GRID GENERATION

STRUCTURED GRIDS

Structured grids can be considered as most 'natural' for flow problems as the flow is generally aligned with the solid bodies and we can imagine the grid lines to follow in some sense the streamlines, at least conceptually, when not possible realistically.

It has to be emphasized that structured grids will, compared to unstructured grids, often be more efficient from CFD point of view, in terms of accuracy, CPU time and memory requirement.

The reason behind the development of unstructured CFD codes is essentially connected to the time required to generate good quality block-structured grids on complex geometries. This task, with the best available software tools, can easily take weeks or months of engineering time and the associated engineering costs are considered as prohibitive industrially. Hence, the requirement for automatic grid generation tools has become essential for the further developmentof industrial CFD. This explains largely the preference given nowadays to unstructured CFD solvers, due to the availability of general-purpose automatic grid generation methods.

However, it remains also possible to generate automatic block-structured grids, when restricted to well-defined families of topologies. Examples are shown in the following.

The ideal mesh is a Cartesian distribution, where all the points are equidistant and where all the cells are perfect cubes, with $\Delta x=\Delta y=\Delta z$. This grid will be associated with the highest possible accuracy of the discretized formulas, where the finite volume method leads to the same formulas as finite differences. Hence, all evaluations of grid qualities will be done by comparing a selected cell to the ideal cubic cell.
When curved solid surfaces are present, they cannot be part of the Cartesian mesh lines and we have two options: either we keep the Cartesian structure of the grids or we move away from the ideal and introduce curvilinear grids in order to fit the grid lines to the solid surfaces. We call these types of grids '***body fitted***'. In the former case, we have to define a particular treatment to the cells cutting the solid surface. In the latter case, we have to generate grids that follow the solid surfaces, for instance by defining curvilinear coordinates (ξ , η , ζ) that would be constant along the lines of mesh points in the physical space and Cartesian in the mathematical space formed by these variables. Various topologies of the grid lines can be defined, and will be presented in this section.

The drawback of structured grids is a form of stiffness connected to the fact that adding a point locally implies adding lines of each family through that point, which will therefore affect the whole domain. In complex geometries, this can be very detrimental and render the grid generation process quite cumbersome. One way to ease these constraints is to define multi-block

grids, each block covering a subset of the computational domain with its own structured grid. This can be further generalized when the connectivity of the points at the block interfaces is relaxed by allowing ‘nonmatching’ lines at the inter-block boundaries. This provides maximum flexibility to block-structured grids.

Another way is to allow for overlapping grids, each grid being attached to a solid body, when multiple moving bodies are present, or to separate blocks. Both ways imply sophisticated treatment for the interpolation of the numerical flow variables between two independent grids, with the requirement to satisfy constraints of conservation and accuracy.

4.1.1 Cartesian Grids

As mentioned above, uniform Cartesian grids are the ideal solution from the point of view of accuracy and they should be applied whenever possible. It is a valid option when the solid walls are parallel to the Cartesian axes, or in absence of solid walls in free space.
Cartesian grids are often applied in aero-acoustic computations, where high order schemes are required for an accurate simulation of the propagation of acoustic pressure waves (see for instance the review paper by Tam (2004)).

4.1.2 Non-uniform Cartesian Grids

Variable mesh sizes

A first variant on the ideal Cartesian uniform grid is to allow for variable values of the mesh spacing, for instance in boundary layers where a strong clustering near solid walls is required. Figure 4.1.1 shows an example of a Cartesian grid applied to the flow simulation over and in a rectangular cavity.

Quadtree-Octree grid

A second variant consists of allowing for local refinements with ‘***hanging nodes***’, also called non-conformal grids, obtained by subdividing an initial Cartesian grid in sub-cells, either uniformly or non-isotropically, as shown in Figure 4.1.2. This leads to a ***quadtree*** structure in 2Dand an ***octree*** structure in 3D.
In presence of curved boundaries, Cartesian grids still remain an option, with the advantage that the grid generation process is trivial, while minimizing numerical errors. However, the treatment of the curved solid boundaries requires special attention.

Several options can be considered:

• *Method 1*: The Cartesian type grid on both sides of the surface is maintained and a numerical procedure is defined in the flow solver to handle the physical boundary conditions (Figure 4.1.3). This is called the ***immersed boundary method***

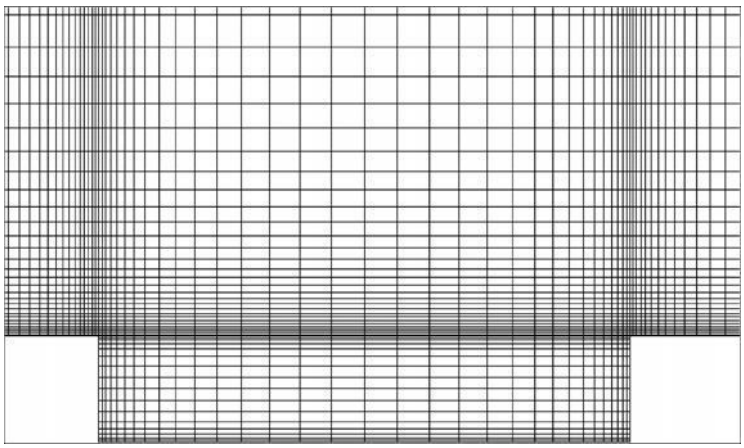

Figure 4.1.1 *Cartesian grid with non-uniform cell sizes for a cavity.*

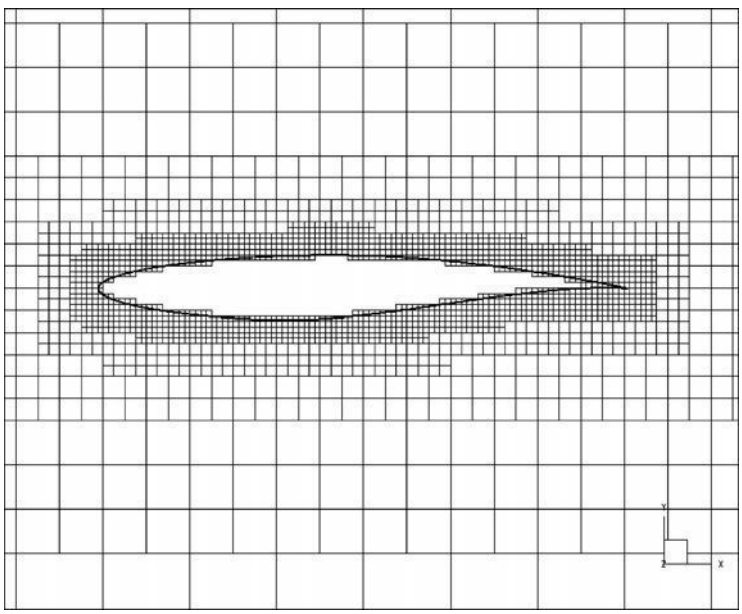

Figure 4.1.2 *Quadtree grid, with hanging nodes, around an airfoil, with staircase boundary approximation.*

- *Method 2*: The Cartesian cells outside the computational domain are removed, replacing hereby the solid boundaries by a ***staircase shape***; this is the case with Figure 4.1.2.
- *Method 3*: The intersection of the solid surface with the Cartesian cells is defined, leading to boundary cells of arbitrary shapes, called ***cut-cells***; see Figure 4.1.4, from Aftosmis et al. (2000). This requires the application of a finite volume discretization on the cut-cell faces.

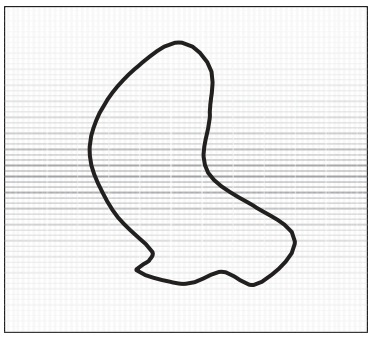

Figure 4.1.3 *Cartesian mesh around a solid boundary with Immersed Boundary Method.*

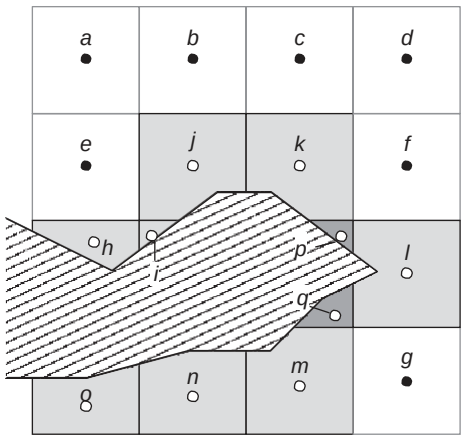

Figure 4.1.4 *Cut-cell configuration; from Aftosmis et al. (2000). AIAA copyright.*

4.1.3. Body-Fitted Structured Grids

In this approach, the grid is made curvilinear to adapt as far as possible to the geometries. It calls upon more sophisticated methods to generate the grids in order to satisfy requirements on smoothness and continuity of cell sizes. Depending on the orientation of the grid lines, various configurations can be selected, indicated by the letter to which they resemble the most. We refer in this context to grids of H-type, C-type, O-type, I-type and their various combinations.

H-mesh

The grid lines are curvilinear, approaching a set of horizontal and vertical lines in a pseudo-orthogonal configuration, with a topology that can be associated to the letter H (see Figure 4.1.5 for a representative example).

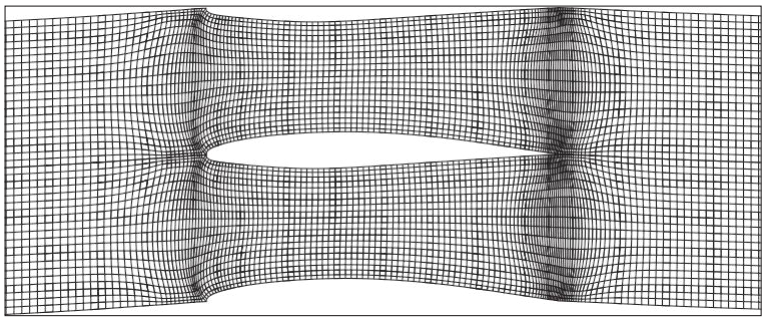

Figure 4.1.5 *Structured curvilinear body-fitted grid of the H-type.*

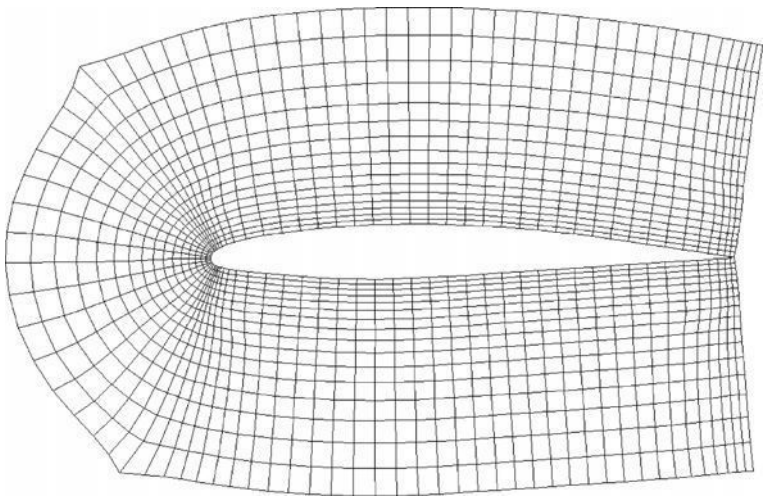

Figure 4.1.6 *Structured curvilinear body-fitted grid of the C-type.*

C-mesh
The grid lines are curvilinear, surrounding the geometry, with a topology that can be associated to the letter C, on one side (for instance around the leading edge of the airfoil), but remaining open at the other end of the computational domain. This can be adapted to concentrate grid lines in the wake region of an airfoil or wing (see Figure 4.1.6 for a representative example).

O-mesh
The grid lines are curvilinear, surrounding completely the geometry, with a topology that can be associated to the letter O. This option allows an accurate mesh point distribution around both leading and trailing edges of external aerodynamic configurations, such as wings and airfoil sections (see Figure 4.1.7 for a representative example).

I-mesh
In the particular case of highly staggered turbomachinery blade sections, the quality requirement of nearly orthogonal cells is better fulfilled with grid lines

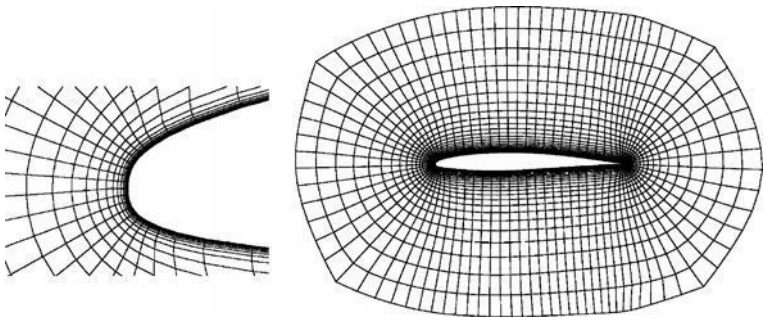

Figure 4.1.7 *Structured curvilinear body-fitted grid of the O-type.*

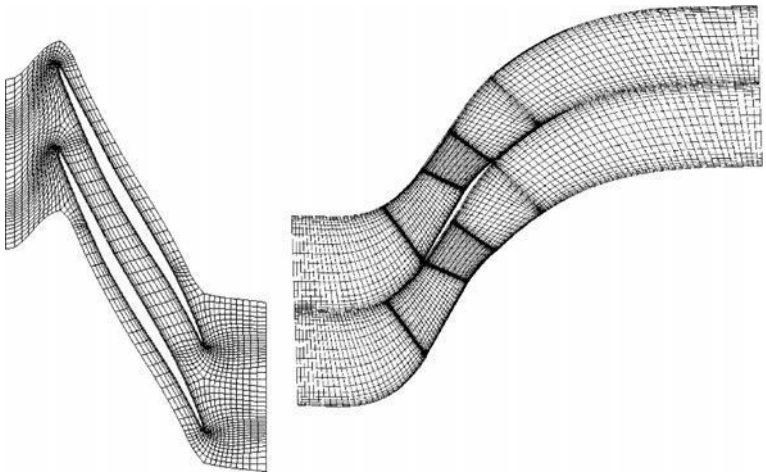

Figure 4.1.8 *Structured curvilinear body-fitted grid of the I-type, for turbomachinery blades. Courtesy Numeca Int.*

nearly orthogonal to the blade sections, leading to a I-type topology, as shown on Figure 4.1.8.

4.1.4 Multi-block Grids

In order to increase the flexibility, the range of application and the easiness of the meshing process of structured grids, combinations of basic topologies can offer significant advantages, in terms of achieving higher grid quality or adaptation to more complex topologies. In this strategy, different mesh topologies are applied in different regions of the computational domain, leading to ***multi-block*** configurations.

Matching and non-matching boundaries between blocks
Normally, we would attempt to satisfy the condition of full matching mesh lines between the blocks, whereby the mesh lines cross the block boundaries in a continuous

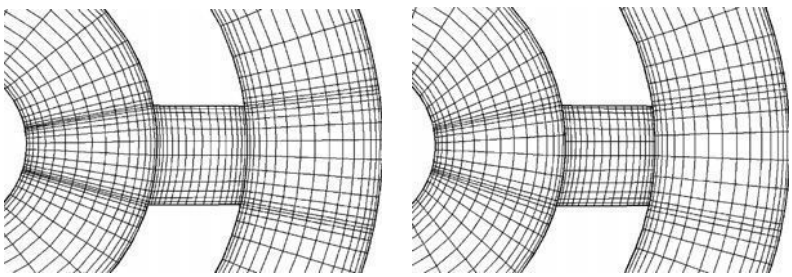

Figure 4.1.9 *Representation of (a) matching and (b) non-matching block boundary interfaces of a multi-block-structured grid, with a channel connecting two circular ducts.*

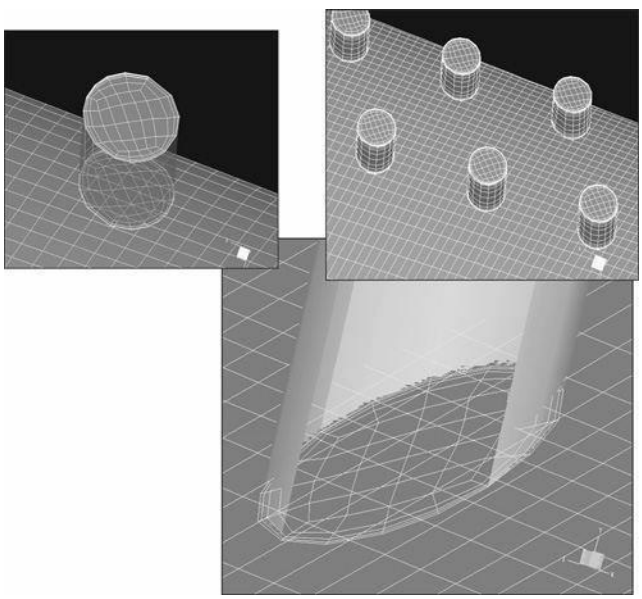

Figure 4.1.10 *Full non-matching block boundary interfaces of a multi-block-structured grid. Courtesy Numeca Int.*

way. However, in order to exploit maximally the potential of block-structured grids, the additional flexibility of allowing for ***non-matching block interfaces*** offers significant advantages. The price of this enhanced flexibility is the necessity for the flow solver to handle with sufficient accuracy the transfer of information through the non-matching interface, requiring sophisticated interpolation routines between two totally independent surface grids.

This is illustrated in Figure 4.1.9, where the choice between the two options is still available. This is not always the case and Figure 4.1.10 shows an example where

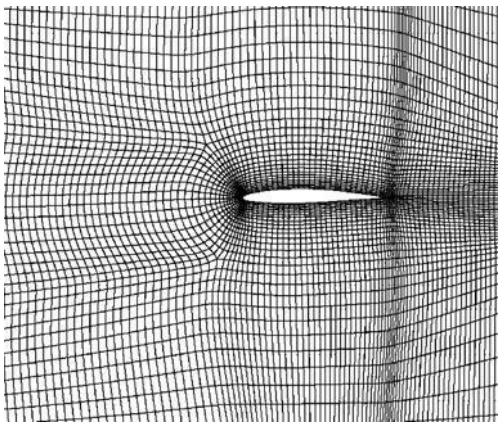

Figure 4.1.11 *Structured curvilinear body-fitted grid of the C–H type.*

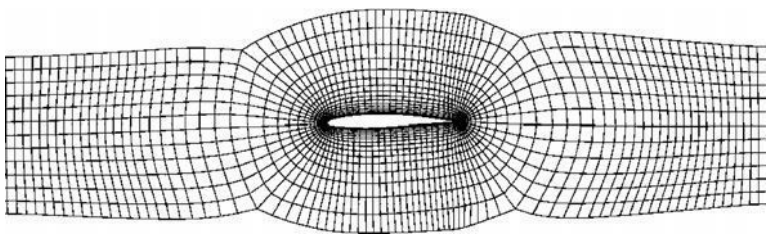

Figure 4.1.12 *Structured multi-block body-fitted grid of the H–O–H type.*

smaller exhaust pipes are connected on a larger duct. In this case, both components can be meshed optimally and freely connected in a non-matching mode.

C–H mesh

This combines a C-mesh around the body and an H-mesh in the upstream region as shown in Figure 4.1.11.

H–O–H mesh

In this configuration, an O-mesh is kept around the body, while H-topologies are defined in the upstream and downstream regions (see Figure 4.1.12).

'Butterfly' grids for internal flows

High quality structured grids with internal flow configurations, such as complex ducts, are difficult to ensure and a high level of flexibility is required. One of the options is obtained by the so-called '*butterfly*' topology shown in Figure 4.1.13, for a simple duct section.

It can also be applied to bulbs of a rotating axis, in order to avoid a singular mesh line on the axis of rotation, at zero radius. Figure 4.1.14 shows combinations of block-structured grids, obtained with the automatic grid generator Autogrid™ from Numeca Int. (http://www.numeca.be), applied to the pump inducer of the liquid hydrogen pump of the VULCAIN engine of the European ARIANE 5 rocket launcher.

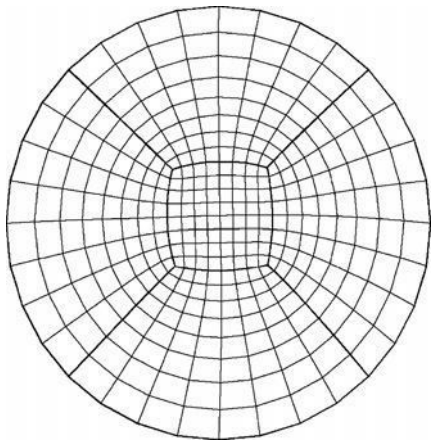

Figure 4.1.13 *Structured multi-block body-fitted grid of the 'butterfly' type.*

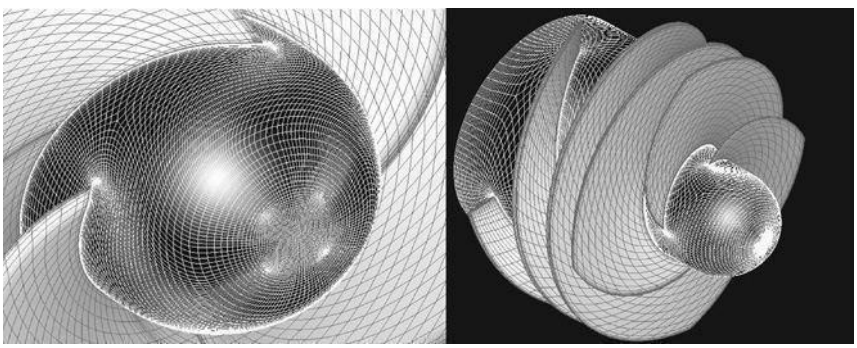

Figure 4.1.14 *Multi-block grid for the inducer of the hydrogen pump of the European ARIANE 5 rocket launcher. The figure on the left is a zoom on the 'butterfly' mesh on the bulb. Courtesy SNECMA and Numeca Int.*

O–H grids with matching and non-matching periodic boundaries

For internal turbomachinery flow simulations, a high degree of mesh flexibility is required and various combinations can be considered to enhance the quality of the grids. For instance, a combination O–H, associated with either matching (a) or non-matching (b) periodic boundaries for a turbine blade row are shown on Figure 4.1.15.

Figures 4.1.14 and 4.1.17 show two industrial examples, respectively, of an industrial heat exchanger combining matching and non-matching multi-block interfaces.

Overset grids

Another alternative to flexible block-structured grid generation is the technique of ***overset grids***, also called '***chimera***' technique, where independent generated grids around a fixed or moving body are made to overlap with a background fixed grid. This technique is largely applied with several bodies in relative motion where a mesh is

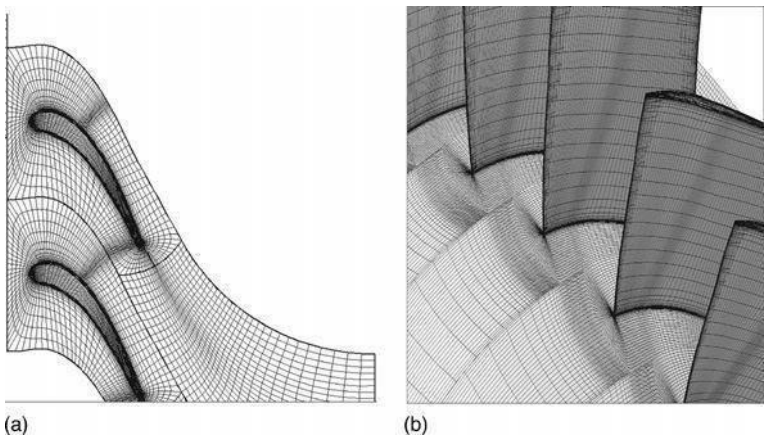

Figure 4.1.15 *Structured curvilinear body-fitted grid of the O–H type: (a) matching periodic boundaries and (b) non-matching periodic boundaries. Courtesy Numeca Int.*

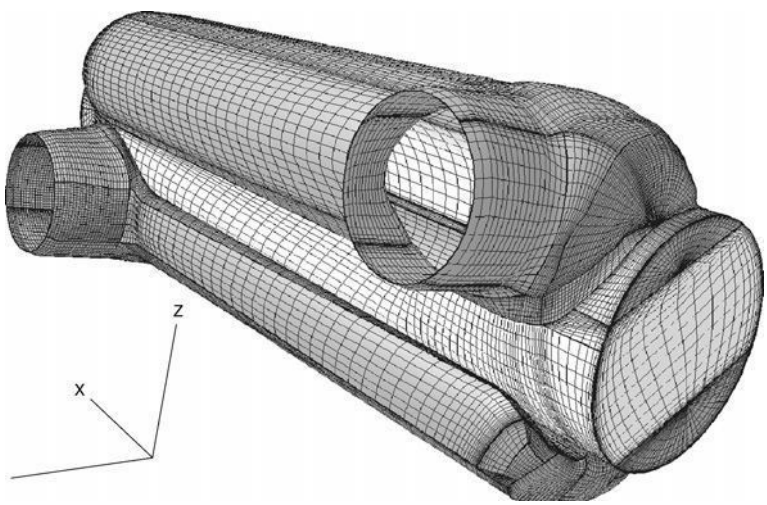

Figure 4.1.16 *Structured multi-block grid of an industrial heat exchanger combining matching and non-matching multi-block interfaces. Courtesy Atlas Copco and Numeca Int.*

attached to each body. The drawback is related to the necessity for an accurate interpolation between three-dimensional overlapping grids. This is extremely challenging, particularly if conservative interpolations are required.

Note that the overset principle can equally be applied with unstructured grids, although it was developed initially for structured grids (Steger et al., 1983; Benek et al., 1985).

Figure 4.1.18 shows overlapping grids around moving parts of a flying structure, with a zoom on a section of the overlapping region.

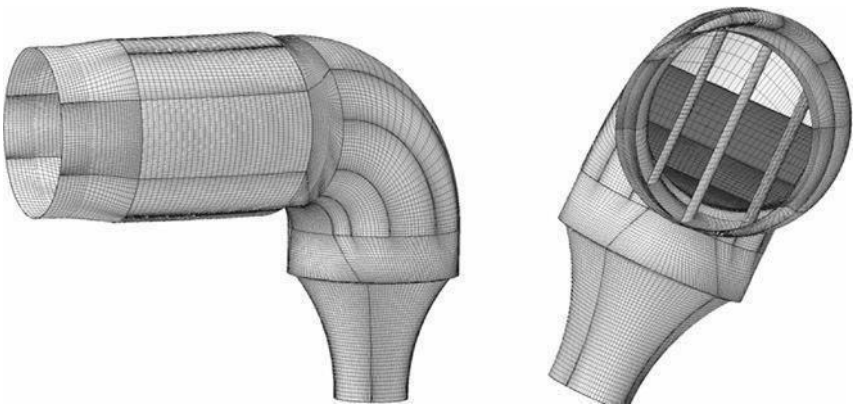

Figure 4.1.17 *Structured multi-block grid of an industrial inlet ducting with guide vanes, combining matching and non-matching multi-block interfaces. Courtesy Atlas Copco and Numeca Int.*

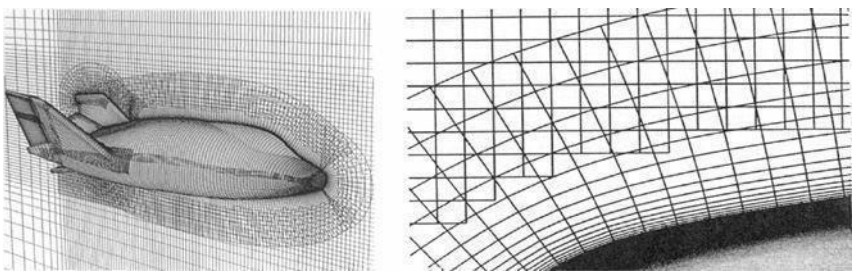

Figure 4.1.18 *Overlapping grids around moving parts of a flying structure, with a zoom on a section of the overlapping region.*

4.2 UNSTRUCTURED GRIDS

Unstructured grids have progressively become the dominating approach to industrial CFD, due to the impossibility to generate automatically block-structured grids on arbitrary geometries. It is indeed nearly impossible, for topology-connected reasons, to envisage an automatic block-structured grid generator without an a priori knowledge of the involved topologies. However, this is possible with unstructured grids and therefore unstructured flow solvers for the Navier–Stokes equations have gained wide acceptance.

Although on a same regular distribution of points, an unstructured grid, formed for instance by triangles in 2D, will tend to have a lower accuracy than the corresponding structured grid, as will be shown in Section 4.4, this trend has arisen because of the industrial requirements for automatic grid generation tools.

One of the advantages of unstructured grids is the possibility to perform local refinements in a certain region, without affecting the grid point distribution outside that region. This opens the way for flexible ***grid adaptation*** by local refinement or local coarsening, based on some criteria associated either to some flow gradients or

to some error estimation. Grid adaptation is based on the addition or removal of mesh points in order to increase the accuracy in regions of strong flow variations and by removing points in regions where the solutions has already reached an acceptable accuracy. This process has as objective to optimize the number of grid points for a certain level of accuracy.

The space domain can be discretized by subdivision of the continuum into elements of arbitrary shape and size. Since any polygonal structure with rectilinear or curved sides can finally be reduced to triangular and quadrilateral elements, they form the basis for the most current space subdivision in 2D space. Cells with an arbitrary number of faces can also be considered, resulting from a dual grid construction, or from an agglomeration process of groups of cells into coarser cells, as required by multigrid methods. The only restriction is that the elements may not overlap and have to cover the complete computational domain.

Most of the unstructured grid generators applied in practice are focused on the generation of basic cell shapes formed by:

4.2.4 triangle/tetrahedra elements;

4.2.5 hybrid elements involving combinations of tetrahedra, pyramids and prisms, the latter being concentrated near the solid surfaces;

4.2.6 quadrilaterals and hexahedra.

4.2.1 Triangle/Tetrahedra Cells

Various methods are available to generate triangular/tetrahedral grids around arbitrary bodies. Most of them require an initial surface triangulation, which has to be generated first, before launching the generation of the volume mesh. See for instance the books by George and Borouchaki (1998) and Frey and George (1999) for an overview.

The following examples are obtained with the system DELANDO developed by Jens-Dominik Müller (see http://www.cerfacs.fr/~muller/delaundo.html).

Figure 4.2.1 shows a two-dimensional unstructured grid with triangular cells, around an airfoil with flaps.

An example of a complex tetrahedral grid is shown on Figure 4.2.2, generated for the simulation of the electrochemical plating of a system of decorative cronium wheels.

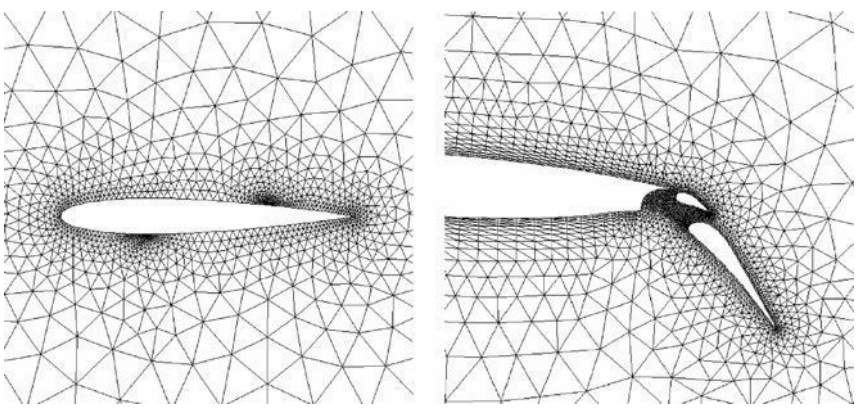

Figure 4.2.1 *Example of an unstructured triangular grid.*

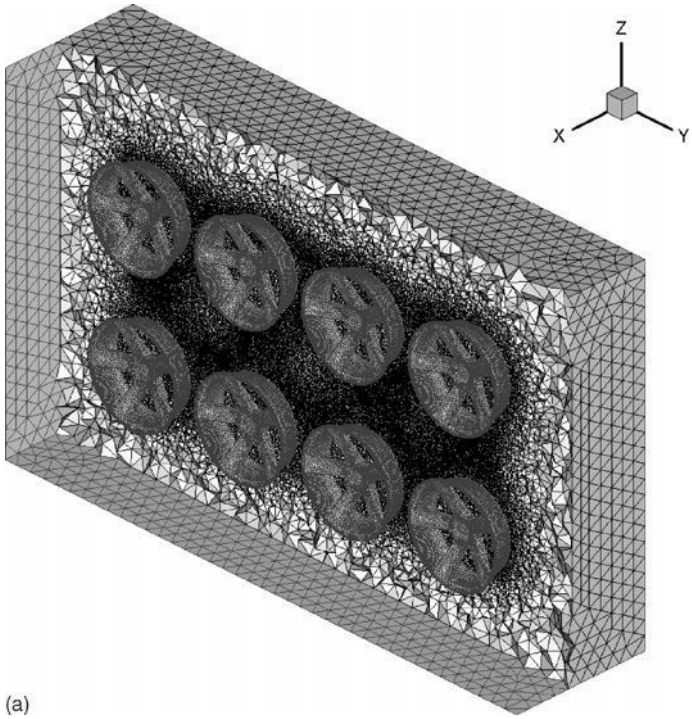

(a)

(b)

Figure 4.2.2 *Example of an unstructured tetrahedral grid for the simulation of electrochemical plating of a system of Decorative Cronium wheels. (a) Full view (b) Zoom on one of the wheels. Courtesy Von Karman Institute and Vrije Universiteit Brussel, Computational Electrochemistry Group.*

4.2.2 Hybrid Grids

The main difficulty with triangular/tetrahedral grids is connected to the boundary layer requirements of high Reynolds number flows, where the grid density in the normal direction has to be adapted to the boundary layer velocity profiles. As seen in Section 4.3, the ratio of mesh sizes should optimally be of the other $x/y \sim \sqrt{(\mathrm{Re})}$, where x and y are the representative mesh sizes in the streamwise and normal directions, respectively. This implies mesh aspect ratios x/y of the order of 1000, for typical industrial flows, which would lead to very poorly configured triangles with height to base ratios of that order and, consequently, a significant loss of accuracy.

To avoid this problem, hybrid grids have been developed, whereby layers of quadrilaterals or prisms are generated in the near-wall region, by a form of extrusion process out of the triangulated surface grid. This is shown on Figure 4.2.3, for a 2D case, from the same reference as the previous figure http://www.cerfacs.fr/~muller/hip.html.

A three-dimensional example of a hybrid grid for a gas-turbine stator with rows of film cooling holes in the leading edge region is shown on Figure 4.2.4. The grids are obtained with the CENTAUR™ grid generator from Centaursoft (http://www.centaursoft.com), showing different views of the hybrid grid. The top figure shows the 3D view and the other figures show a 2D section with a close-up view of the leading edge region.

4.2.3 Quadrilateral/Hexahedra Cells

It is known from numerous simulations (see also Section 4.4) that hexahedra offer significant advantages compared to tetrahedral cells, in terms of memory requirements and accuracy. For tetrahedral grids, the ratio of the number of cells to the number of vertices is close to 6, not taking into account the boundaries. (for a two-dimensional triangulation this ratio is of the order of 3); while this ratio remains close to one for hexahedral cells.

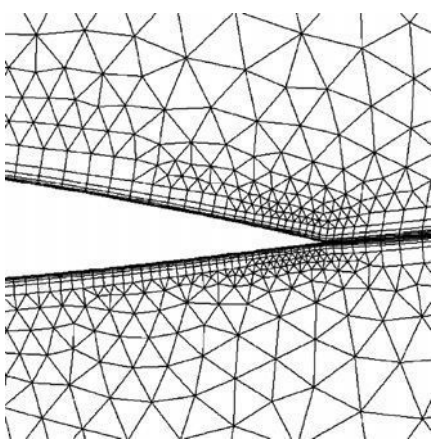

Figure 4.2.3 *Example of an unstructured hybrid grid showing the regular quadrilateral type structure near the solid walls.*

Automatic generation of unstructured hexahedra is quite challenging and some examples from the HEXPRESS™ generator from Numeca Int. (http://www.numeca.be) are shown in the following figures. In this approach, the surface mesh is obtained from the volume mesh, through a projection step of a Cartesian/octree volume mesh, whereby the initial generation of a surface mesh is not required. Figure 4.2.5 shows a 2D quadrilateral grid around an airfoil, while Figure 4.2.6 shows a 3D unstructured hexahedral grid of a valve system, with cuts displaying the internal cells.

Similarly, Figure 4.2.7 shows the hexahedral mesh for a complex dusting system, with appropriate cuts to visualize the internal volume cells.

4.2.4 Arbitrary Shaped Elements

The most general unstructured grid configuration is obtained with cells having an arbitrary number of faces. They can be defined either by considering the ***dual mesh*** of a base grid formed by simple shapes, or by an ***agglomeration process*** of cells.

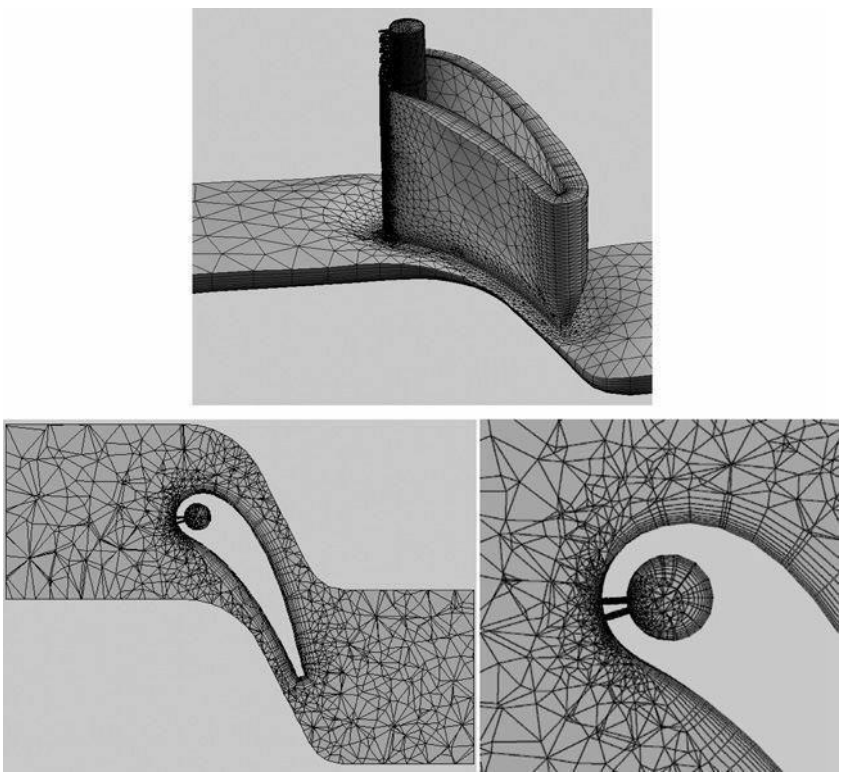

Figure 4.2.4 *Three-dimensional hybrid grid of a turbine blade with film cooling configuration, with a 2D section and a close-up view of the leading edge region. From http://www.centaursoft.com.*

UNIT V

CFD TECHNIQUES

Lax-Wendroff technique

MacCormack's technique

Relaxation technique

Alternating-Direction-Implicit (ADI) Technique

Pressure correction technique

Numerical procedure- SIMPLE algorithm

Boundary conditions for the pressure correction method

LAX WENDROFF TECHNIQUE

The Lax-Wendroff technique is an explicit, finite-difference method particularly suited to marching solutions. The idea of numerical solutions obtained by marching in steps of time or space is associated with the solution of hyperbolic and parabolic partial differential equations. A good example of a flow-field problem governed by hyperbolic equations is the time-marching solution of an inviscid flow using the unsteady Euler equations. The behavior of such a time- marching solution is discussed in the present section by considering an unsteady two dimensional inviscid flow. The governing Euler equations are given below

time t. Then the density at the same grid point (i, j) at time $t + \Delta t$, denoted by $\rho_{i,j}^{t+\Delta t}$, is given by the Taylor series

$$\rho_{i,j}^{t+\Delta t} = \rho_{i,j}^{t} + \left(\frac{\partial \rho}{\partial t}\right)_{i,j}^{t} \Delta t + \left(\frac{\partial^2 \rho}{\partial t^2}\right)_{i,j}^{t} \frac{(\Delta t)^2}{2} + \cdots \tag{6.5}$$

When employing Eq. (6.5), we assume that the flow field at time t is known, and Eq. (6.5) gives the new flow field at time $t + \Delta t$. In Eq. (6.5), $\rho_{i,j}^{t}$ is known from the

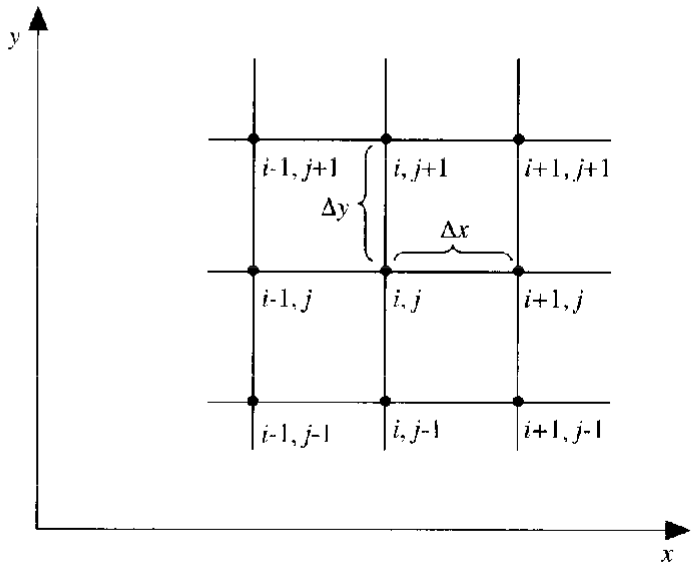

FIG. 6.1
Rectangular grid segment.

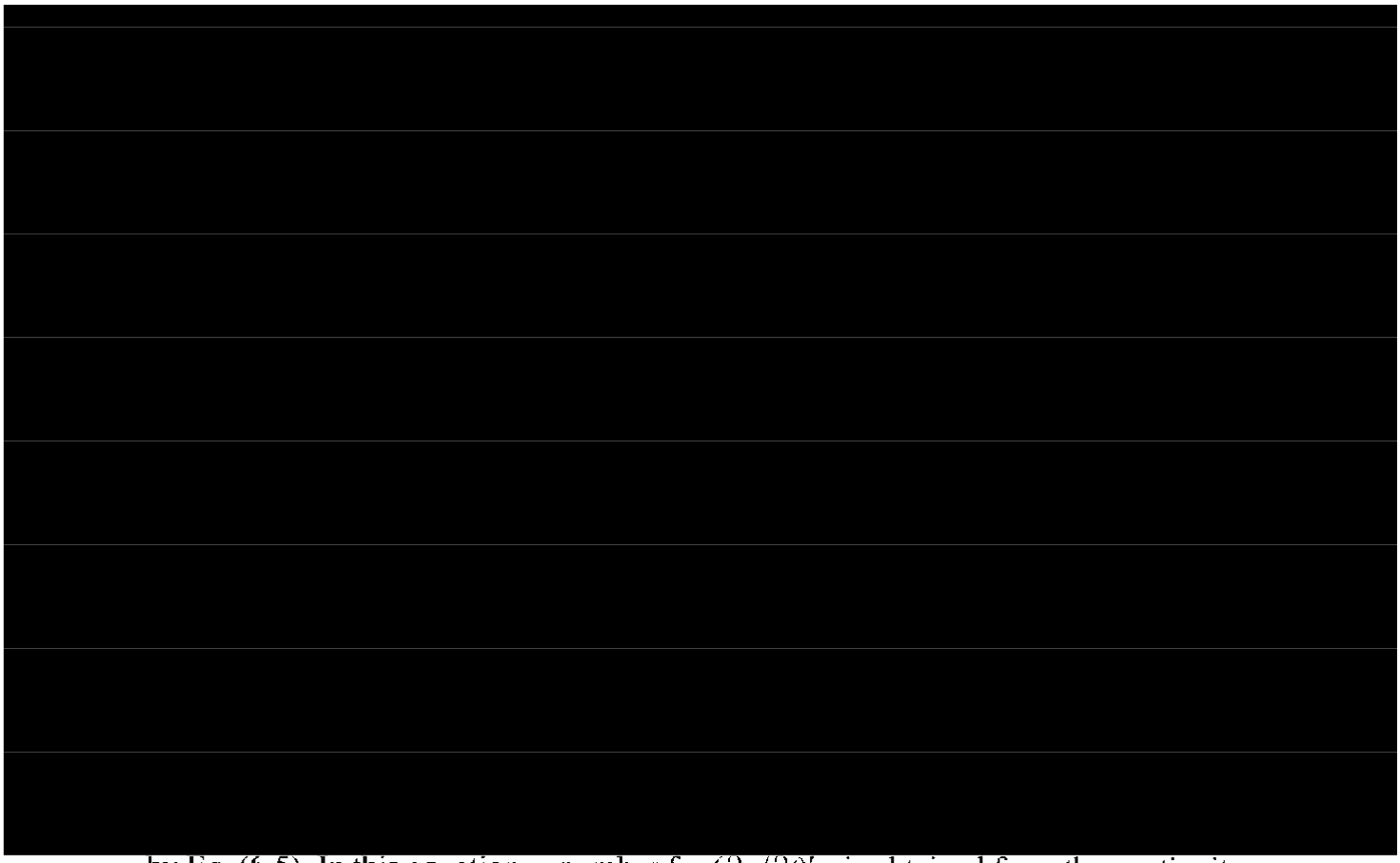

by Eq. (6.5). In this equation, a number for $(\partial\rho/\partial t)^t_{i,j}$ is obtained from the continuity equation, Eq. (6.1), where the spatial derivatives are given by second-order central differences. That is, from Eq. (6.1),

$$\left(\frac{\partial\rho}{\partial t}\right)^t_{i,j} = -\left(\rho^t_{i,j}\frac{u^t_{i+1,j}-u^t_{i-1,j}}{2\Delta x} + u^t_{i,j}\frac{\rho^t_{i+1,j}-\rho^t_{i-1,j}}{2\Delta x} + \rho^t_{i,j}\frac{v^t_{i,j+1}-v^t_{i,j-1}}{2\Delta y} + v^t_{i,j}\frac{\rho^t_{i,j+1}-\rho^t_{i,j-1}}{2\Delta y}\right) \tag{6.9}$$

In Eq. (6.9), all quantities on the right-hand side are known because the flow field at time t is known. Hence, Eq. (6.9) provides a number for $(\partial\rho/\partial t)^t_{i,j}$, which is inserted into Eq. (6.5). This takes care of the second term on the right side of Eq. (6.5). The third term, $(\partial^2\rho/\partial t^2)^t_{i,j}$, is obtained in a similar fashion but requires more effort. Specifically, differentiate Eq. (6.1) with respect to time.

$$\frac{\partial^2\rho}{\partial t^2} = -\rho\frac{\partial^2 u}{\partial x\,\partial t} + \frac{\partial u}{\partial x}\frac{\partial\rho}{\partial t} + u\frac{\partial^2\rho}{\partial x\,\partial t} + \frac{\partial\rho}{\partial x}\frac{\partial u}{\partial t} + \rho\frac{\partial^2 v}{\partial y\,\partial t} + \frac{\partial v}{\partial y}\frac{\partial\rho}{\partial t} + v\frac{\partial^2\rho}{\partial y\,\partial t} + \frac{\partial\rho}{\partial y}\frac{\partial v}{\partial t} \tag{6.10}$$

The mixed second derivatives in Eq. (6.10), such as $\partial^2 u/(\partial x\,\partial t)$, are obtained by differentiating Eqs. (6.1) to (6.4) with respect to the proper spatial variable. For example, $\partial^2 u/(\partial x\,\partial t)$ is obtained by differentiating Eq. (6.2) with respect to x.

[redacted]

appears in Eq. (6.10). Continuing with the evaluation of Eq. (6.10), a number for $\partial^2\rho/(\partial x\ \partial t)$ is found by differentiating Eq. (6.1) with respect to x and replacing all derivatives on the right side with second-order central differences, analogous to the form of Eq. (6.12). To conserve space, we will not write out the full result here. Continuing further with Eq. (6.10), a number for $\partial^2 v/(\partial y\ \partial t)$ is found by differentiating Eq. (6.3) with respect to y and replacing all derivatives on the right side with second-order central differences. The last mixed derivative in Eq. (6.10), $\partial^2\rho/(\partial y\ \partial t)$, is found by differentiating Eq. (6.1) with respect to y and replacing all derivatives on the right side with second-order central differences. The only remaining derivatives on the right side of Eq. (6.10) are the first spatial derivatives, namely, $\partial u/\partial x$, $\partial v/\partial y$, $\partial\rho/\partial x$, and $\partial\rho/\partial y$, replaced by second-order central differences

$$\left(\frac{\partial u}{\partial x}\right)_{i,j}^{t} = \frac{u_{i+1,j} - u_{i-1,j}}{2\Delta x}$$

and so forth, as well as the first time derivatives $\partial\rho/\partial t$, $\partial u/\partial t$, and $\partial v/\partial t$. A number for $\partial\rho/\partial t$ has already been obtained from Eq. (6.9). Numbers for $\partial u/\partial t$ and $\partial v/\partial t$ are obtained in like fashion by inserting second-order central differences into the right-hand side of Eqs. (6.2) and (6.3), respectively. With all this, we finally obtain a number for $\partial^2\rho/\partial t^2$ from Eq. (6.10). In turn, this is substituted into Eq. (6.5). Since $\partial\rho/\partial t$ was obtained earlier from Eq. (6.9), we now have known values at time t for all three terms on the right side of Eq. (6.5), namely, $\rho_{i,j}^{t}$, $(\partial\rho/\partial t)_{i,j}^{t}$, and $(\partial^2\rho/\partial t^2)_{i,j}^{t}$. This allows the calculation of density at time $t + \Delta t$, namely, $\rho_{i,j}^{t+\Delta t}$, obtained from Eq. (6.5).

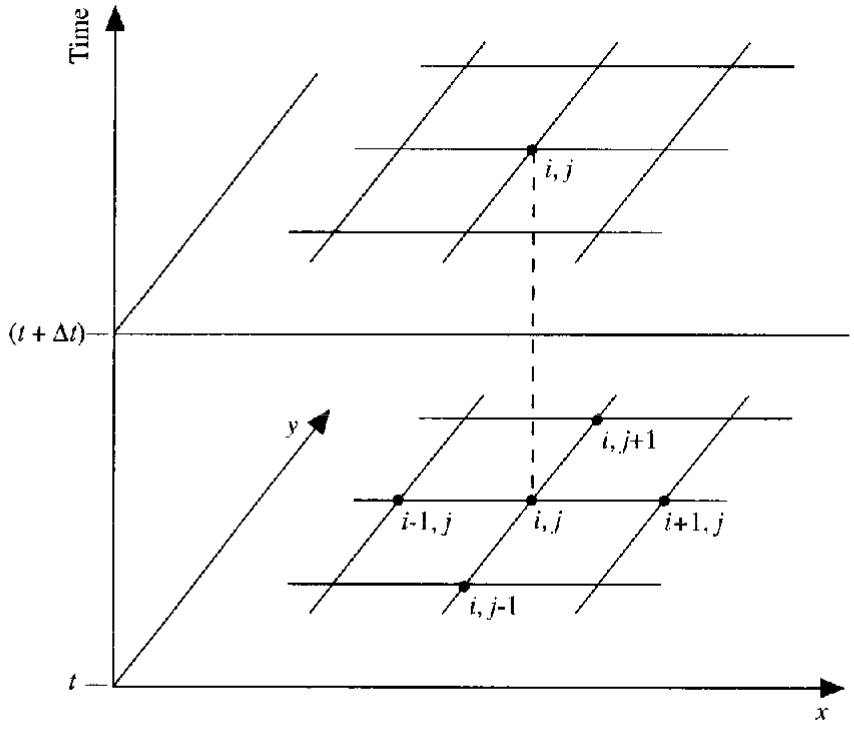

FIG. 6.2
A schematic of the grid for time marching.

[redacted]

is obtained from

$$\rho_{i,j}^{t+\Delta t} = \rho_{i,j}^{t} + \left(\frac{\partial \rho}{\partial t}\right)_{\text{av}} \Delta t \tag{6.13}$$

where $(\partial\rho/\partial t)_{\text{av}}$ is a representative mean value of $\partial\rho/\partial t$ between times t and $t + \Delta t$. Compare Eq. (6.13) with its counterpart for the Lax-Wendroff method, Eq. (6.5). In Eq. (6.5), the time derivatives are evaluated at time t, and the carrying of the second derivative $(\partial^2\rho/\partial t^2)_{i,j}^{t}$ is necessary to obtain second-order accuracy. In contrast, in Eq. (6.13), the value of $(\partial\rho/\partial t)_{\text{av}}$ is calculated so as to preserve second-order accuracy *without* the need to calculate values of the second time derivative $(\partial^2\rho/\partial t^2)_{i,j}^{t}$, which is the term which involves a lot of algebra. With MacCormack's technique, this algebra is circumvented.

Similar relations are written for the other flow-field variables.

$$u_{i,j}^{t+\Delta t} = u_{i,j}^{t} + \left(\frac{\partial u}{\partial t}\right)_{\text{av}} \Delta t \tag{6.14}$$

$$v_{i,j}^{t+\Delta t} = v_{i,j}^{t} + \left(\frac{\partial v}{\partial t}\right)_{\text{av}} \Delta t \tag{6.15}$$

$$e_{i,j}^{t+\Delta t} = e_{i,j}^{t} + \left(\frac{\partial e}{\partial t}\right)_{\text{av}} \Delta t \tag{6.16}$$

Let us illustrate by using the calculation of density as an example. Return to Eq. (6.13). The average time derivative, $(\partial\rho/\partial t)_{\text{av}}$, is obtained from a predictor-corrector philosophy as follows.

$$(\bar{v})_{i,j}^{t+\Delta t} = v_{i,j}^{t} + \left(\frac{\partial v}{\partial t}\right)_{i,j}^{t} \Delta t \tag{6.20}$$

$$(\bar{e})_{i,j}^{t+\Delta t} = e_{i,j}^{t} + \left(\frac{\partial e}{\partial t}\right)_{i,j}^{t} \Delta t \tag{6.20a}$$

In Eqs. (6.19) to (6.20a), numbers for the time derivatives on the right-hand side are obtained from Eqs. (6.2) to (6.4), respectively, with *forward* differences used for the spatial derivatives, similar to those shown in Eq. (6.17) for the continuity equation.

Corrector step. In the corrector step, we first obtain a *predicted* value of the *time derivative* at time $t + \Delta t$, $(\overline{\partial\rho/\partial t})_{i,j}^{t+\Delta t}$, by substituting the *predicted* values of ρ, u, and v into the right side of the continuity equation, replacing the spatial derivatives with *rearward* differences.

$$\left(\overline{\frac{\partial\rho}{\partial t}}\right)_{i,j}^{t-\Delta t} = -\left[(\bar{\rho})_{i,j}^{t+\Delta t}\frac{(\bar{u})_{i,j}^{t+\Delta t} - (\bar{u})_{i-1,j}^{t+\Delta t}}{\Delta x} + (\bar{u})_{i,j}^{t+\Delta t}\frac{(\bar{\rho})_{i,j}^{t-\Delta t} - (\bar{\rho})_{i-1,j}^{t+\Delta t}}{\Delta x} + (\bar{\rho})_{i,j}^{t+\Delta t}\frac{(\bar{v})_{i,j}^{t+\Delta t} - (\bar{v})_{i,j-1}^{t+\Delta t}}{\Delta y} + (\bar{v})_{i,j}^{t+\Delta t}\frac{(\bar{\rho})_{i,j}^{t-\Delta t} - (\bar{\rho})_{i,j-1}^{t+\Delta t}}{\Delta y}\right] \tag{6.21}$$

[redacted]

MacCormack's technique as described above, because a two-step predictor-corrector sequence is used with forward differences on the predictor and with rearward differences on the corrector, is a second-order-accurate method. Therefore, it has the same accuracy as the Lax–Wendroff method described in Sec. 6.2. However, the MacCormack method is much easier to apply, because there is no need to evaluate the second time derivatives as was the case for the Lax-Wendroff method. To see this more clearly, recall Eqs. (6.10) and (6.11), which are required for the Lax-Wendroff method. These equations represent a large number of additional calculations. Moreover, for a more complex fluid dynamic problem such as the flow of a viscous fluid, the differentiation of the continuity, momentum, and energy equations to obtain the second derivatives, first with respect to time, and then the mixed derivatives with respect to time and space, can be very tedious and provides an extra source for human error. MacCormack's method does *not* require such second derivatives and hence does *not* deal with equations such as (6.10) and (6.11).

In MacCormack's technique, the use of forward differences on the predictor and rearward differences on the corrector is not sacrosanct; the same order of accuracy is obtained by using rearward diffences on the predictor and forward differences on the corrector. Indeed, a time-marching solution can be carried out by alternating between these two sequences at every other time step, if you so choose.

GUIDEPOST

If you are anxious to start a computer project using MacCormack's technique, you can follow this guidepost now and return to Chap. 6 at a later time.

2.8.1. Written in the form for steady flow, these equations have a mathematical behavior which is partially elliptic. The Lax-Wendroff and MacCormack techniques are not appropriate for the solution of elliptic partial differential equations. However, the *unsteady* Navier-Stokes equations have a mixed parabolic and elliptic behavior, and therefore the Lax-Wendroff and MacCormack techniques are suitable. Indeed, the MacCormack technique has been used extensively for solutions of the unsteady Navier-Stokes equations by means of time-marching solutions. The idea is the same as discussed in Sec. 6.3; the Navier-Stokes equations are written with the time derivatives on the left side and spatial derivatives on the right side of the equations. The spatial derivatives are replaced in turn by forward and rearward differences on the predictor and corrector steps, respectively.* The approach is exactly the same as discussed in Sec. 6.3; the only difference is the larger number of spatial derivatives that are present in the Navier-Stokes equations compared to the Euler equations.

6.4.2 Conservation Form

For simplicity, we will continue to use the Euler equations in our discussion. The conservation form of the Euler equations suitable for CFD calculations was

* This statement is true for the convective terms. However, it has been the author's experience, as well as that of many others, that the *viscous* terms should be *centrally differenced* on both the predictor and corrector steps.

two-dimensional flow shown in Fig. 6.3. The general flow direction is from left to right in the xy plane. For simplicity, assume the flow is inviscid; hence the governing flow equations are the Euler equations. In the generic, conservation form, this system of equations is given by Eq. (2.110), reduced to a two-dimensional form as

$$\frac{\partial F}{\partial x} = J - \frac{\partial G}{\partial y} \tag{6.24}$$

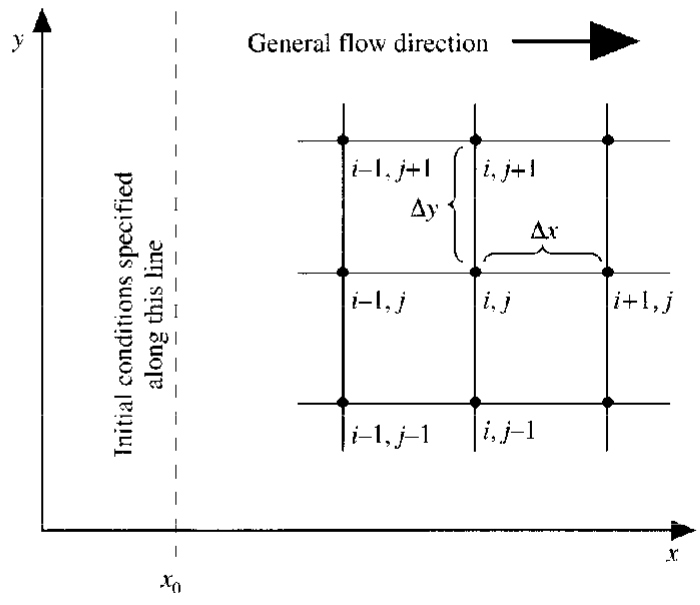

FIG. 6.3
A schematic of the grid for space marching.

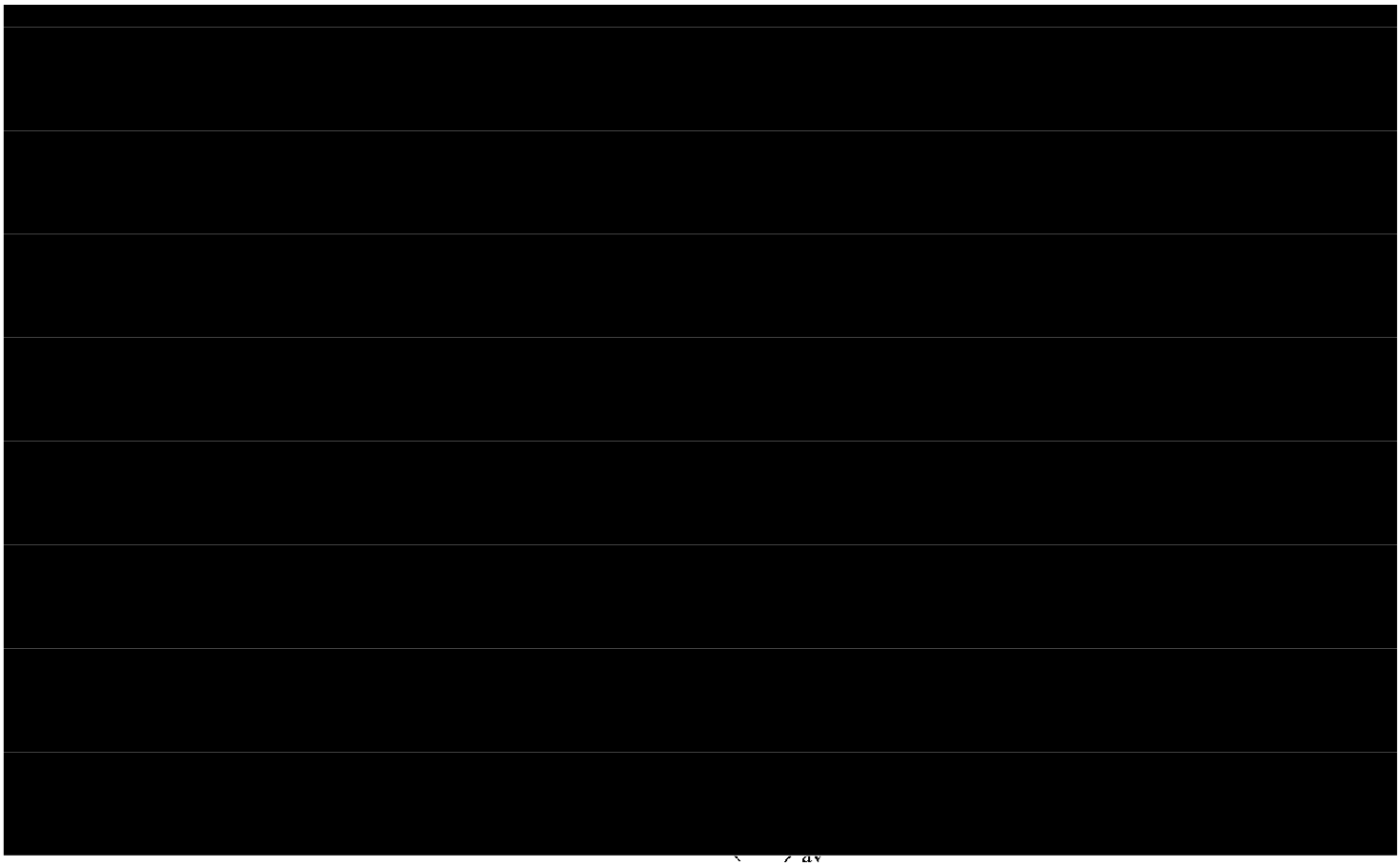

Note that, in keeping with our previous notation, the index for the marching variable, in this case i, is used as a superscript. In Eq. (6.25), $(\partial F/\partial x)_{\text{av}}$ is a representative average value of the x derivative of F evaluated between x and $x + \Delta x$. It is found from Eq. (6.24) by means of a predictor-corrector approach, as follows.

Predictor step. In Eq. (6.24), replace the y derivative with a forward difference:

$$\left(\frac{\partial F}{\partial x}\right)_j^i = J_j^i - \frac{G_{j+1}^i - G_j^i}{\Delta y} \tag{6.26}$$

In Eq. (6.26), all terms on the right side are known numbers, because the flow is known along the vertical line through point (i, j). Calculate a predicted value for F at point $(i + 1, j)$ from a Taylor series:

$$\bar{F}_j^{i+1} = F_j^i + \left(\frac{\partial F}{\partial x}\right)_j^i \Delta x \tag{6.27}$$

where, as in Sec. 6.3, the barred quantity represents a predicted quantity. Keep in mind that the shorthand vector notation shown in Eqs. (6.26) and (6.27) represents these operations on the individual continuity, momentum, and energy equations, where the elements of F and G are given by Eqs. (2.106) and (2.107), respectively. That is, F_j^{i+1} represents the *predicted* values of its individual elements, given for

In Eq. (6.29), the values of $\bar{G}_j^{i+1}$ and $\bar{G}_{j-1}^{i+1}$ are constructed from the predicted primitive variables which had been decoded earlier in the predictor step. The average value, $(\partial F/\partial x)_{\text{av}}$, is now formed as an arithmetic mean

$$\left(\frac{\partial F}{\partial x}\right)_{\text{av}} = \frac{1}{2}\left[\underbrace{\left(\frac{\partial F}{\partial x}\right)_j^i}_{\substack{\text{From Eq.}\\(6.26)}} + \underbrace{\left(\overline{\frac{\partial F}{\partial x}}\right)_j^{i+1}}_{\substack{\text{From Eq.}\\(6.29)}}\right] \tag{6.30}$$

In turn, the final, corrected value of $F_{i+1,j}$ is obtained from Eq. (6.25), repeated below:

$$F_j^{i+1} = F_j^i + \left(\frac{\partial F}{\partial x}\right)_{\text{av}} \Delta x \tag{6.25}$$

Clearly, this spatial, downstream marching solution using MacCormack's technique is a direct analog of the time-marching solution discussed in Sec. 6.3, with the marching variable x playing the role of the earlier marching variable t.

There are two noteworthy differences associated with the downstream marching approach compared to the time-marching approach. The first has already been mentioned; it is associated with the need to decode the primitive variables from the flux variables. This decoding is simple when a time-marching solution of the conservation form of the equations is employed, as reflected in Eqs. (2.100) to (2.104), but it is more elaborate when a spatial-marching solution of the con-

Therefore, the relaxation technique is frequently applied to the solution of low-speed subsonic flow. Relaxation techniques can be either explicit or implicit. See Ref. 13 for an in-depth discussion of various relaxation techniques as applied to CFD problems. In the present section, we will describe an explicit relaxation technique, sometimes called a *point-iterative* method.

For purposes of illustration, let us consider an inviscid, incompressible, two-dimensional irrotational flow. For such a flow, the governing flow equations reduce to a single partial differential equation, namely, Laplace's equation, in terms of the scalar velocity potential Φ, where Φ is defined such that $\mathbf{V} = \nabla\Phi$. We will not provide the details here but rather make the assumption that you have some familiarity with such matters. If not, or if you simply need a review of the derivation, see, for example, Sec. 3.7 of Ref. 8. We will simply state here that the governing equation is

$$\frac{\partial^2\Phi}{\partial x^2} + \frac{\partial^2\Phi}{\partial y^2} = 0 \tag{6.31}$$

We wish to solve Eq. (6.31) numerically on the grid shown in Fig. 6.4. Replace the partial derivatives in Eq. (6.31) with second-order, central second differences, given by Eqs. (4.12) and (4.13).

$$\frac{\Phi_{i+1,j} - 2\Phi_{i,j} + \Phi_{i-1,j}}{(\Delta x)^2} + \frac{\Phi_{i,j+1} - 2\Phi_{i,j} + \Phi_{i,j-1}}{(\Delta y)^2} = 0 \tag{6.32}$$

Examining the grid in Fig. 6.4, note that grid points 1 through 20 constitute the

stipulated over the *entire* boundary enclosing the domain in order for the solution of an elliptic equation to be well-posed. In terms of the grid shown in Fig. 6.4, this means that Φ_1 through Φ_{20} are known values, equal to the given boundary conditions at points 1 through 20. The values of Φ at all other grid points—the internal grid points—are unknown. Equation (6.32), centered around grid point (i, j), contains five of these unknowns, namely, $\Phi_{i-1,j}$, $\Phi_{i,j}$, $\Phi_{i+1,j}$, $\Phi_{i,j+1}$, $\Phi_{i,j-1}$. In principle, Eq. (6.32) can be written around each of the internal grid points (there are 15 such points in Fig. 6.4), leading to a system of 15 linear algebraic equations with a total of 15 unknowns. There are several direct methods for solving these simultaneous equations. One is the standard Cramer's rule; however, the number of calculations required for the implementation of Cramer's rule is very large, due to the need to evaluate determinants of the size 15×15 for the present example. For any real calculation, hundreds or even thousands of grid points may be employed. Clearly, the use of Cramer's rule is out of the question for such applications. Another, and much more reasonable, direct solution is gaussian elimination (see, for example, Ref. 13). However, the simplest approach is to use a relaxation technique, as described below.

The relaxation technique is an iterative method, wherein values of four of the quantities in Eq. (6.32) are assumed to be the *known* values at iteration step n and only one of the quantities is treated as an unknown at iteration step $n + 1$. In Eq. (6.32), let us choose $\Phi_{i,j}$ as that unknown. Solving Eq. (6.32) for $\Phi_{i,j}$, we have

$$\Phi_{i,j}^{n+1} = \frac{(\Delta x)^2(\Delta y)^2}{2(\Delta y)^2 + 2(\Delta x)^2}\left[\frac{\Phi_{i+1,j}^n + \Phi_{i-1,j}^n}{(\Delta x)^2} + \frac{\Phi_{i,j+1}^n + \Phi_{i,j-1}^n}{(\Delta y)^2}\right] \tag{6.33}$$

[redacted]

(6.34), we move on to grid point 22, where an application of Eq. (6.33) yields

$$\Phi_{22}^{n+1} = \frac{(\Delta x)^2(\Delta y)^2}{2(\Delta y)^2 + 2(\Delta x)^2}\left[\frac{\Phi_{23}^{n} + \Phi_{21}^{n+1}}{(\Delta x)^2} + \frac{\Phi_{25}^{n} + \Phi_{3}}{(\Delta y)^2}\right] \tag{6.35}$$

In Eq. (6.35), Φ_{22}^{n+1} is the unknown; Φ_{23}^{n} and Φ_{25}^{n} are known from the previous iteration, Φ_3 is known from the stipulated boundary condition, and Φ_{21}^{n+1} is known from Eq. (6.34), which was the immediately preceding calculation. In this fashion, the unknown Φ's at iteration $n + 1$ are progressively calculated along a given horizontal line, sweeping from left to right. (This approach is called the *Gauss-Seidel method.*) There is nothing magic about this sweeping direction. During the progressive solution of Eq. (6.33), we could just as well set up sequences that sweep from right to left, from top to bottom, or from bottom to top.

The above procedure is repeated for a number of iterations; *convergence* is achieved when $\Phi_{i,j}^{n+1} - \Phi_{i,j}^{n}$ becomes less than some prescribed value at all grid points. The degree to which you wish convergence to be achieved is up to you; the more iterations you take, the greater will be the accuracy.

Frequently, the convergence to a solution sometimes can be enhanced by a technique called *successive overrelaxation.* This is an extrapolation procedure based on the following idea. We interpret Eq. (6.33) as yielding an intermediate value of $\Phi_{i,j}$, denoted by $\overline{\Phi_{i,j}^{n+1}}$, where

$$\overline{\Phi_{i,j}^{n+1}} = \frac{(\Delta x)^2(\Delta y)^2}{2(\Delta y)^2 + 2(\Delta x)^2}\left[\frac{\Phi_{i-1,j}^{n} + \Phi_{i-1,j}^{n+1}}{(\Delta x)^2} + \frac{\Phi_{i,j+1}^{n} + \Phi_{i,j-1}^{n+1}}{(\Delta y)^2}\right] \tag{6.36}$$

DISSIPATION AND DISPERSION; ARTIFICIAL VISCOSITY

Many aspects of life are never quite what they appear to be at first impression—CFD is no different. For example, in the present chapter we have discussed several techniques for the numerical solution of the governing flow equations. We have approached these discussions, as well as those in previous chapters, from the point of view that numerical solutions of the Euler or Navier-Stokes equations are being obtained within an accuracy determined by the truncation and round-off errors. The focus has been on the fact that we are solving some *specific partial differential equations* but that the numerical solutions are always somewhat in error.

There is a different perspective that we can take on this matter, one with a shade of difference compared to our previous discussions. For simplicity, let us consider a model equation, namely, the one-dimensional wave equation given by

$$\frac{\partial u}{\partial t} + a\frac{\partial u}{\partial x} = 0 \tag{6.38}$$

with $a > 0$. We consider (6.38) to be the *specific* partial differential equation that we want to solve numerically. Let us choose to discretize this equation by using a first-order forward difference in time and a first-order rearward difference in space. Then Eq. (6.38) is represented by the following difference equation:

$$\frac{u_i^{t+\Delta t} - u_i^t}{\Delta t} + a\frac{u_i^t - u_{i-1}^t}{\Delta x} = 0 \tag{6.39}$$

Rearranging Eq. (6.42), we obtain

$$\left(\frac{\partial u}{\partial t}\right)_i^t + a\left(\frac{\partial u}{\partial x}\right)_i^t = -\left(\frac{\partial^2 u}{\partial t^2}\right)_i^t \frac{\Delta t}{2} - \left(\frac{\partial^3 u}{\partial t^3}\right)_i^t \frac{(\Delta t)^2}{6} + \left(\frac{\partial^2 u}{\partial x^2}\right)_i^t \frac{a\,\Delta x}{2} - \left(\frac{\partial^3 u}{\partial x^3}\right)_i^t \frac{a(\Delta x)^2}{6} + \cdots \quad (6.43)$$

Pause for a moment and examine Eq. (6.43). The left-hand side is exactly the left-hand side of the original partial differential equation given by Eq. (6.38); the right-hand side of Eq. (6.43) is the truncation error associated with the difference equation given by Eq. (6.39). Clearly, this truncation error is $O(\Delta t, \Delta x)$. Let us now replace the time derivatives on the right-hand side of Eq. (6.43) with x derivatives as follows. First, differentiate Eq. (6.43) with respect to t. (We will drop the subscript i and superscript t, since we know that all derivatives are being evaluated at point i and at time t.)

$$\frac{\partial^2 u}{\partial t^2} + a\frac{\partial^2 u}{\partial x\,\partial t} = -\frac{\partial^3 u}{\partial t^3}\frac{\Delta t}{2} - \frac{\partial^4 u}{\partial t^4}\frac{(\Delta t)^2}{6} + \frac{\partial^3 u}{\partial x^2\,\partial t}\frac{a\,\Delta x}{2} - \frac{\partial^4 u}{\partial x^3\,\partial t}\frac{a(\Delta x)^2}{6} + \cdots \quad (6.44)$$

[redacted]

$$2\left[\frac{\partial^3 u}{\partial x^2\,\partial t} \quad \frac{\partial^3 u}{\partial x^3} \quad \right] \tag{6.47}$$

Equation (6.47) provides the expression for $\partial^2 u/\partial t^2$ which is to be substituted for the first term on the right-hand side of Eq. (6.43). Before carrying out this substitution, however, let us treat the second term on the right-hand side of Eq. (6.43), namely, the third time derivative. We do this by differentiating Eq. (6.47) with respect to time, yielding

$$\frac{\partial^3 u}{\partial t^3} = a^2 \frac{\partial^3 u}{\partial x^2\,\partial t} + \mathrm{O}(\Delta t,\, \Delta x) \tag{6.48}$$

Differentiating Eq. (6.45) with respect to x and multiplying by a, we have

$$a^2 \frac{\partial^3 u}{\partial x^2\,\partial t} + a^3 \frac{\partial^3 u}{\partial x^3} = \mathrm{O}(\Delta t,\, \Delta x) \tag{6.49}$$

Adding Eqs. (6.48) and (6.49), we have

$$\frac{\partial^3 u}{\partial t^3} = -a^3 \frac{\partial^3 u}{\partial x^3} + \mathrm{O}(\Delta t,\, \Delta x) \tag{6.50}$$

Equation (6.50) provides an expression for the third time derivative to be inserted into both Eqs. (6.47) and (6.43). Returning to Eq. (6.47), we see two mixed derivatives with respect to t and x that must be treated. Differentiating Eq. (6.47) with respect to x, we have

$$\frac{\partial^3 u}{\partial t^3\,\partial x} = a^2 \frac{\partial^3 u}{\partial x^3} + \mathrm{O}(\Delta t,\, \Delta x) \tag{6.51}$$

$$+O[(\Delta t)^3, (\Delta t)^2(\Delta x), (\Delta t)(\Delta x)^2, (\Delta x)^3] \quad (6.55)$$

A rearrangement of Eq. (6.55), along with the definition of v as $v = a\,\Delta t/\Delta x$, yields

$$\boxed{\frac{\partial u}{\partial t} + a\frac{\partial u}{\partial x} = \frac{a\,\Delta x}{2}(1 - v)\frac{\partial^2 u}{\partial x^2} + \frac{a(\Delta x)^2}{6}(3v - 2v^2 - 1)\frac{\partial^3 u}{\partial x^3} + O[(\Delta t)^3, (\Delta t)^2(\Delta x), (\Delta t)(\Delta x)^2, (\Delta x)^3]} \quad (6.56)$$

Note that Eq. (6.56) is a *partial differential equation* in its own right, containing the terms $\partial u/\partial t$, $\partial u/\partial x$, $\partial^2 u/\partial x^2$, $\partial^3 u/\partial x^3$, etc. Finally, with Eq. (6.56) in mind, we are ready to emphasize the different perspective mentioned at the beginning of this long paragraph. Previously, we viewed an exact solution (no round-off error) of the difference equation, Eq. (6.39), as constituting a numerical solution of the *original* partial differential equation given by Eq. (6.38) but with an error given by the truncation error. However, there is another way of looking at this matter. In reality, the exact solution (no round-off error) of the difference equation, Eq. (6.39), constitutes an *exact solution* (no truncation error) of a *different* partial differential equation, namely, Eq. (6.56). Eq. (6.56) is called the *modified equation*. To repeat, when the difference equation, Eq. (6.39), is used to obtain a numerical solution of the original partial differential equation, Eq. (6.38), in reality this difference equation is solving quite a different partial differential equation—it is solving Eq. (6.56) instead of Eq. (6.38).

The derivation and display of the modified equation, as obtained above, is of more importance than just establishing a different perspective on the meaning of the

we start at time zero with an exact discontinuous wave as sketched in Fig. 6.5, then during the course of the solution the effect of numerical dissipation will be to spread out this wave in much the same way that real physical viscosity would spread the wave. Of course, the reason why the wave will spread in our numerical solution has nothing to do with physical viscosity; rather, it has everything to do with the fact that the exact numerical solution of the difference equation, Eq. (6.39), is a solution of Eq. (6.56) instead of the original partial differential equation given by Eq. (6.38), and Eq. (6.56) has some terms on the right-hand side that play the role of

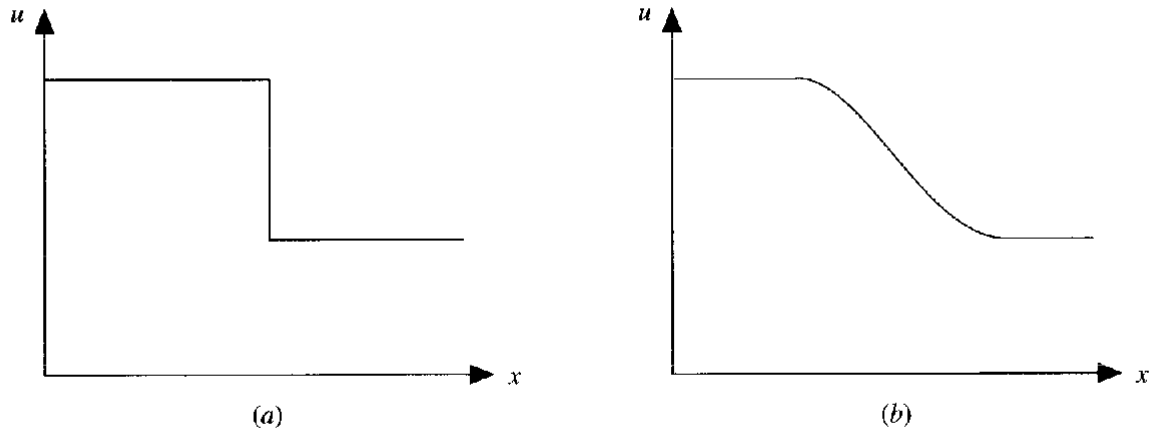

FIG. 6.5
Effect of numerical dissipation. (*a*) Initial wave at time $t = 0$. (*b*) Shape of the wave at some time $t > 0$ from the numerical solution as affected by numerical dissipation.

the solution does not have enough artificial viscosity implicitly in the algorithm, and the solution will go unstable unless more artificial viscosity is added *explicitly* to the calculation. This raises one of the most perplexing aspects of CFD. As you intentionally add more artificial viscosity to a numerical solution, you are increasing the probability of making the solution more inaccurate. On the other hand, by adding this artificial viscosity, you are at least able to obtain a stable solution, whereas without it, in some cases no solution would be attainable. (Flow problems with very strong gradients, such as shock waves, wherein such shock waves are

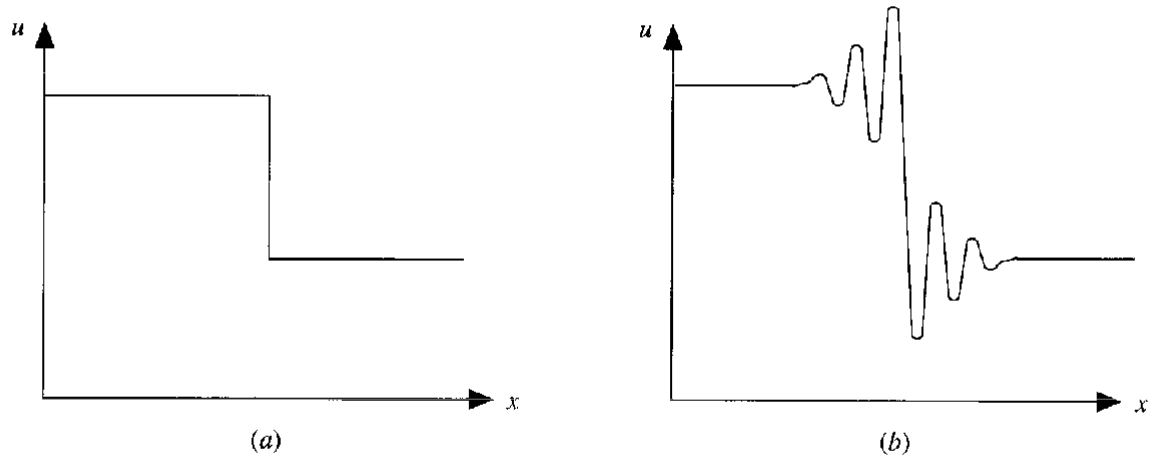

FIG. 6.6
Effect of numerical dispersion. (*a*) Initial wave at $t = 0$. (*b*) Shape of the wave at some time $t > 0$ from the numerical solution as affected by numerical dispersion.

time-marching solution, a small amount of artificial viscosity can be added in the following form:

$$S^t_{i,j} = \frac{C_x|p^t_{i+1,j} - 2p^t_{i,j} + p^t_{i-1,j}|}{p^t_{i+1,j} + 2p^t_{i,j} + p^t_{i-1,j}}(U^t_{i+1,j} - 2U^t_{i,j} + U^t_{i-1,j}) + \frac{C_y|p^t_{i,j+1} - 2p^t_{i,j} + p^t_{i,j-1}|}{p^t_{i,j+1} + 2p^t_{i,j} + p^t_{i,j-1}}(U^t_{i,j+1} - 2U^t_{i,j} + U^t_{i,j-1}) \quad (6.58)$$

Equation (6.58) is a fourth-order numerical dissipation expression; it is designed to "tweak" the calculations by a magnitude equivalent to a fourth-order term in the truncation error; i.e., it is equivalent to adding an extra fourth-order term to the right-hand side of the modified equations for the system of difference equations which are being solved. The fourth-order nature of Eq. (6.58) can be seen in the numerators, which are products of two second-order central difference expressions for second derivatives. In Eq. (6.58), C_x and C_y are two arbitrarily specified parameters; typical values of C_x and C_y range from 0.01 to 0.3. The choice is up to you and is usually determined after some experimentation with different values, assessing their effect on the particular calculation. In Eq. (6.58), U denotes the individual elements of the solutions vector, taken separately. To see this more clearly, assume that we are using MacCormack's technique. On the predictor step, $S^t_{i,j}$ is evaluated based on the known quantities at time t; on the corrector step, the

[redacted]

Note: There is nothing sacrosanct about the form for artificial viscosity expressed by Eqs. (6.58) and (6.59). It happens to be an empirically based expression which is given here just for the sake of discussion.

To what extent does the addition of artificial viscosity affect the accuracy of a problem? There is no pat answer to this question; it depends in a large part on the nature of the flow problem itself. However, some feel for the extent to which artificial viscosity can impact the solution of a flow problem can be obtained from Ref. 44; there, a series of numerical experiments are reported wherein the value of artificial viscosity was progressively varied and the resulting effects on the flow-field variables were examined. Some of the results are reviewed here so that you can obtain some of this feel. The flow problem is that of the supersonic viscous flow over a rearward-facing step, as shown in Fig. 6.7*a*. The finite-difference grid used for this study is shown in Fig. 6.7*b*. The flow field is calculated by means of a time-marching numerical solution of the Navier-Stokes equations using the MacCormack technique described in Sec. 6.3. The expression for artificial viscosity is given by Eqs. (6.58) and (6.59), and various calculations are made with values of C_x and C_y ranging from 0 to 0.3. The calculations are made for a freestream Mach number of 4.08 and a Reynolds number (based on step height) of 849. The step height is 0.51 cm, and the calculations are made for a surface which extends 12.5 cm upstream of the step and 2.04 cm downstream of the step. A calorically perfect gas with the ratio of specific heats equal to 1.31 is used (this is to partially simulate the "effective gamma" for partially dissociated air in a supersonic combustion ramjet environment). Figure 6.8 shows the computed pressure contours for the flow, using MacCormack's technique. Here, four different contour pictures are shown, one each

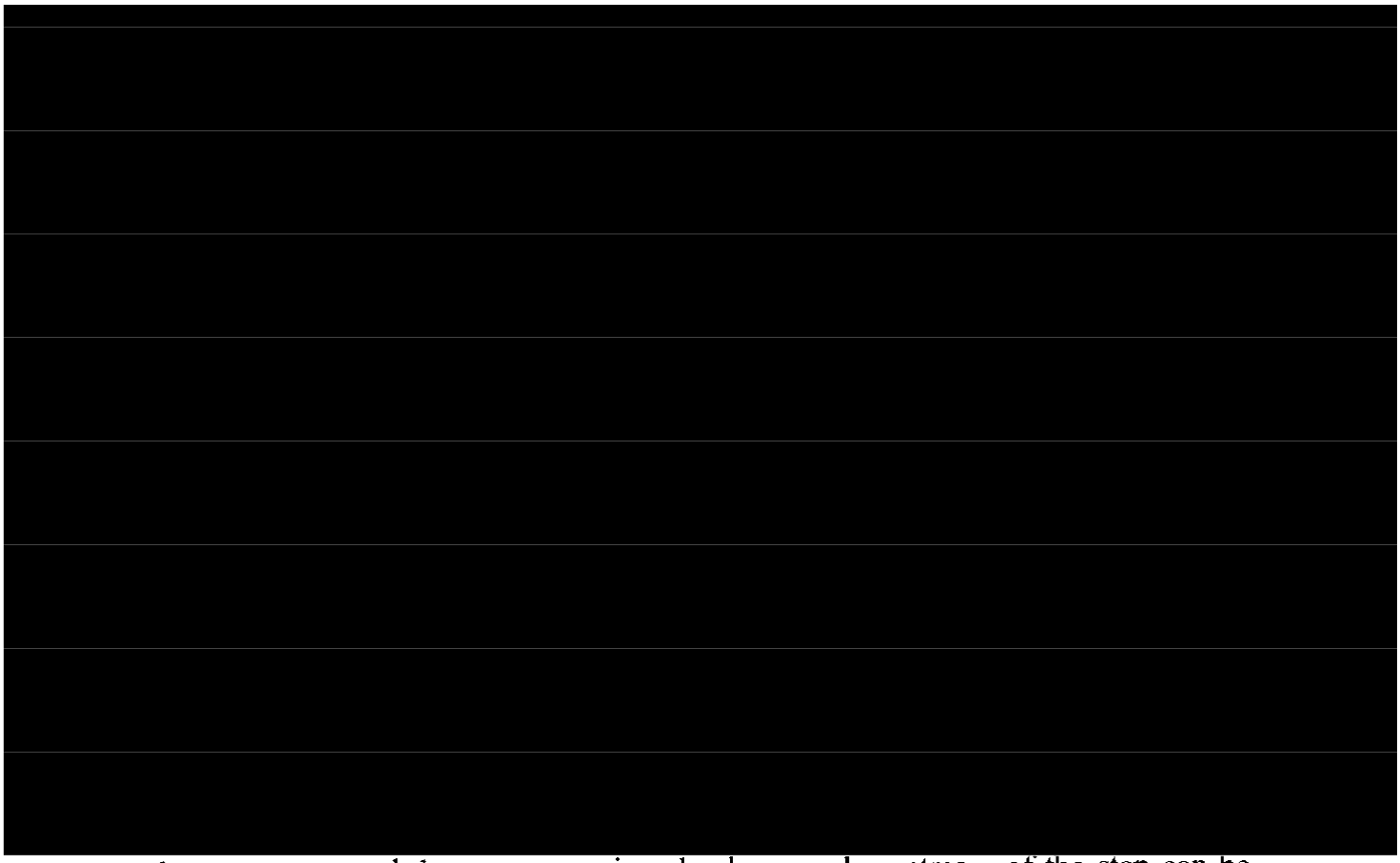

the top corner and the recompression shock wave downstream of the step can be seen in all frames. However, careful examination of Fig. 6.8 shows that as C_x and C_y are progressively increased (the magnitude of the artificial viscosity is increased), the quantitative and qualitative aspects of the flow are perturbed. In Fig. 6.8*a*, where zero artificial viscosity is used, the recompression shock wave is fairly sharp and distinct, but there are wiggles ahead of and behind the shock. It is not easy to obtain a stable, converged solution in this case; the calculations are sensitive, and some "nursing" of the program is required. As the magnitude of the artificial viscosity is progressively increased, as shown in Fig. 6.8*b* to *d*, the solution behaves in a more stable fashion, but the structures of the resulting steady-state flows are somewhat different. This can be seen by comparing Fig. 6.8*a* and *d*; in Fig. 6.8*d* with heavy artificial viscosity, the recompression shock has been smoothed by the increased numerical dissipation. In contrast to Fig. 6.8*a*, we see no wiggles in Fig. 6.8*d*, and the shock wave is much more diffuse, while at the same time its location has translated upward. In Fig. 6.7*a*, three different axial locations are denoted by the numbers 1, 2, and 3. The velocity profiles (velocity versus vertical location y) for these three locations are shown in Fig. 6.9*a* to *c*. In each figure, the profiles are given for four different values of the artificial viscosity. Note that the velocity profiles are affected by artificial viscosity. Finally, the wall pressure distribution—the variation of pressure on the wall versus x location measured along the surface—is given in Fig. 6.10. Here, $x = 1$ cm is the location of the step, and the pressure distributions shown are those downstream of the step. The pressure at $x = 1$ cm is essentially the base pressure, i.e., the pressure on the vertical step itself. Four different curves are shown in Fig. 6.10, each one corresponding to a different value

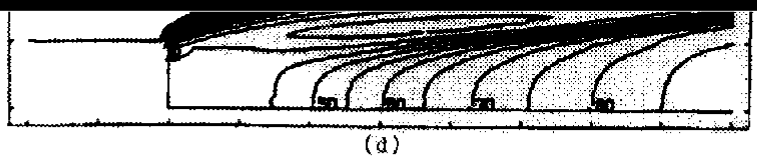

FIG. 6.8
Numerical experiment on the effects of artificial viscosity. Pressure contours calculated with values of the dissipation factors C_x and C_y ranging from 0 to 0.3. The freestream conditions are $M_\infty = 4.08$, $T_\infty = 1046$ K, ratio of specific heats $\gamma = 1.31$, and Reynolds number = 849 (based on a step height of 0.51 cm). The wall temperature $T_W = 0.2957T_\infty$.

of artificial viscosity. Although the pressure distribution farther downstream of the step is relatively insensitive to the amount of artificial viscosity, the base pressure itself is quite sensitive to the artificial viscosity.

Note: The impact of artificial viscosity on the qualitative aspects of a flow solution is like that of the physical viscosity μ. By increasing the artificial viscosity, shock waves are thickened and smoothed, just like an increased physical coefficient of viscosity would cause. The details of separated flow regions are affected by artificial viscosity, just like an increase in physical viscosity would cause. By adding artificial viscosity, we are changing the overall entropy level of the flow field, just as physical viscosity would cause. Finally, by increasing the artificial viscosity in a numerical solution, we are in effect reducing the effective Reynolds number of the flow, just as an increase in μ would cause.

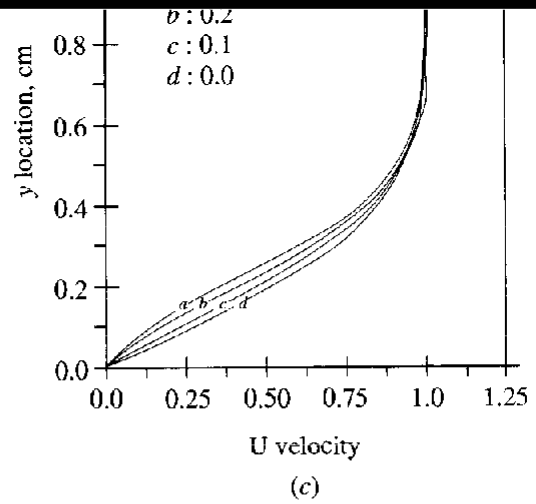

FIG. 6.9
Numerical experiment on the effects of artificial viscosity. Velocity profiles at the three locations marked in Fig. 6.7*a*. Same freestream conditions as listed in Fig. 6.8. The velocity given here is the nondimensional value referenced to freestream velocity.

The purpose of this section has been to introduce you to the concepts of numerical dissipation and the use of artificial viscosity for the stabilization and smoothing of some numerical solutions. Many applications in CFD do not require the addition of artificial viscosity. On the other hand, artificial viscosity, both implicit in an algorithm and explicitly added as needed, is a fact of life in many other CFD solutions. Such matters still remain a highly empirical aspect of CFD

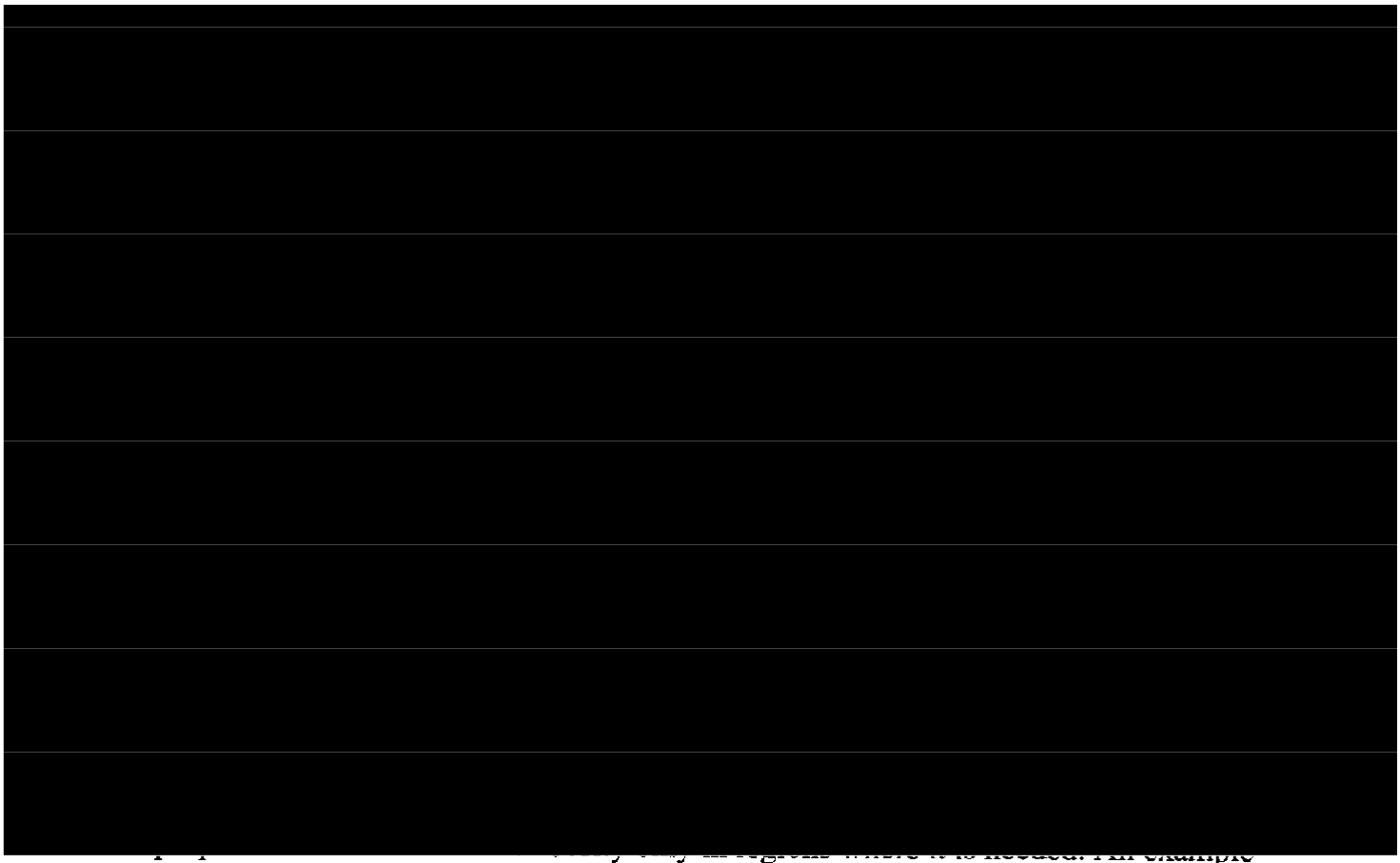

is the TVD (total-variation-diminishing) concept. Such aspects are discussed in Chap. 11. As you proceed further with your studies of CFD in the future, you will most likely reap the benefits of such mathematical advancements.

6.7 THE ALTERNATING-DIRECTION-IMPLICIT (ADI) TECHNIQUE

Let us return to the consideration of implicit solutions as exemplified by the Crank-Nicolson technique, introduced in Sec. 4.4. In this section, an example of a marching solution is given; Eq. (3.28) is used as a model equation with t as the marching variable. There exists only one other independent variable in the equation, namely, x. As long as we are dealing with linear equations, the implicit solutions using the Crank-Nicolson scheme are directly obtained from the use of Thomas' algorithm (see App. A). This is the case in Sec. 4.4, where a finite-difference representation of Eq. (3.28) is given in the tridiagonal form by Eq. (4.42). This tridiagonal form is readily solved by the use of Thomas' algorithm.

Note that the difference equation is linear. In Sec. 4.4, the original partial differential equation, Eq. (3.28), is linear, hence leading to a linear difference equation. In cases governed by nonlinear partial differential equations, a more general idea for obtaining linear difference equations is discussed in Sec. 11.3.1. When solving an inherently nonlinear problem by means of an implicit scheme, the matter of linearizing the difference equations is of utmost importance so that Thomas' algorithm (or some equivalent) can be used to expedite the calculations.

by Eq. (4.40). However, unlike Eq. (4.40) which reduces to the tridiagonal form given by Eq. (4.42), Eq. (6.63) contains *five* unknowns, namely, $T_{i-1,j}^{n+1}$, $T_{i,j}^{n+1}$, $T_{i-1,j}^{n+1}$, $T_{i,j+1}^{n+1}$, and $T_{i,j-1}^{n+1}$, where the last two unknowns prevent a tridiagonal form. Hence, Thomas' algorithm can not be used. Although matrix methods exist which can solve Eq. (6.63), the computer time is much longer than that for a tridiagonal system. As a result, there is a distinct advantage in developing a scheme that will allow Eq. (6.62) to be solved by means of tridiagonal forms only. Such a scheme, namely, the alternating-direction-implicit (ADI) scheme, is the main subject of this section.

Recall that Eq. (6.62) is being solved by means of a marching technique; that is, $T(t + \Delta t)$ is being obtained in some fashion from the known values of $T(t)$. Let us achieve the solution of $T(t + \Delta t)$ in a *two-step process*, where intermediate values of T are found at an intermediate time, $t + \Delta t/2$, as follows. In the first step over a time interval $\Delta t/2$, replace the spatial derivatives in Eq. (6.62) with central differences, where only the x derivative is treated implicitly. That is, from Eq. (6.62),

$$\frac{T_{i,j}^{n+1/2} - T_{i,j}^{n}}{\Delta t/2} = \alpha \frac{T_{i+1,j}^{n+1/2} - 2T_{i,j}^{n+1/2} + T_{i-1,j}^{n+1/2}}{(\Delta x)^2} + \alpha \frac{T_{i,j+1}^{n} - 2T_{i,j}^{n} + T_{i,j-1}^{n}}{(\Delta y)^2} \tag{6.64}$$

Equation (6.64) reduces to the tridiagonal form

$$AT_{i-1,j}^{n+1/2} - BT_{i,j}^{n+1/2} + AT_{i+1,j}^{n+1/2} = K_i \tag{6.65}$$

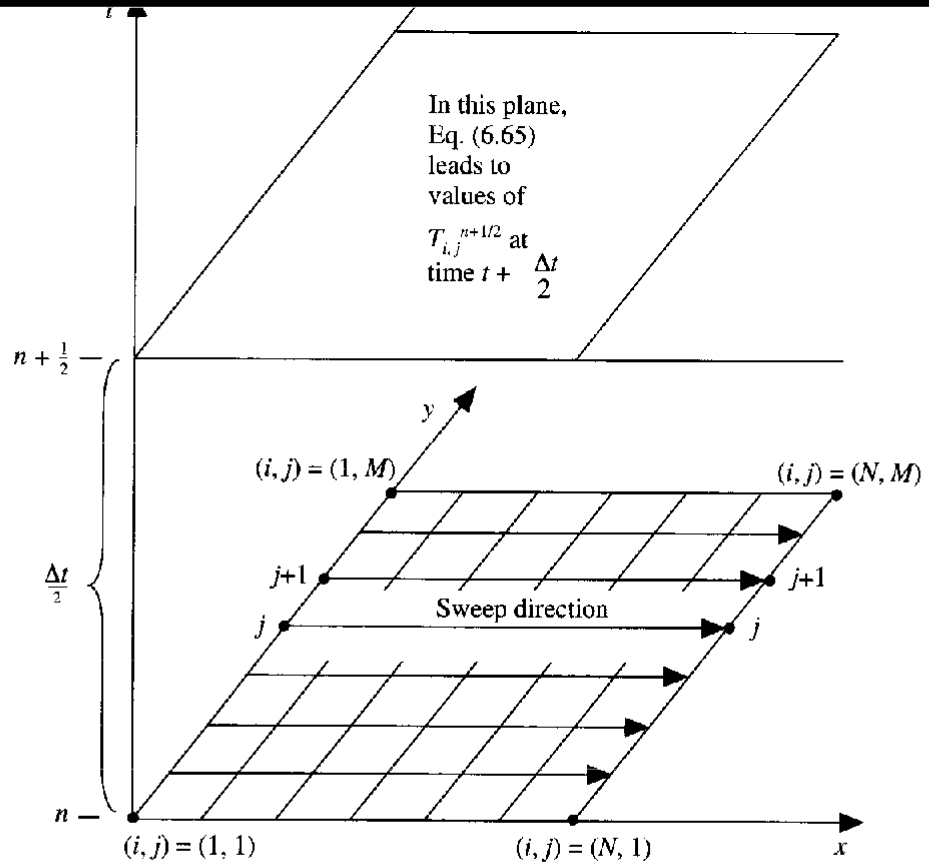

FIG. 6.11
First step in the ADI process. Sweeping in the x direction to obtain T at time $t + \Delta t/2$.

$$L_j = -T_{i,j}^{n+1/2} - \frac{\alpha\,\Delta t}{2(\Delta x)^2}\left(T_{i+1,j}^{n+1/2} - 2T_{i,j}^{n+1/2} + T_{i-1,j}^{n+1/2}\right)$$

Note that $T^{n+1/2}$ is known at all grid points from the first step. Equation (6.67) yields a solution for $T_{i,j}^{n+1}$ for all j, keeping i fixed, using Thomas' algorithm. That is, examining Fig. 6.12, at a fixed value of i, we sweep in the y direction, using Eq. (6.67) to solve for $T_{i,j}^{n+1}$ for all values of j, where j goes from 1 to M. This sweep utilizes Thomas's algorithm once. This calculation is then repeated at the next column of grid points designated by $i - 1$. That is, replace i in Eq. (6.67) by $i + 1$ and solve for $T_{i+1,j}^{n}$ for all values of j from 1 to M, using Thomas's algorithm. This process is repeated N times; i.e., there are N sweeps in the y direction, resulting in Thomas' algorithm being used N times. This sweeping in the y direction is shown schematically in Fig. 6.12. At the end of this step, the values of T at time $t + \Delta t$ are known at all grid points (i, j); that is, $T_{i,j}^{n+1}$ is known at all (i, j).

At the end of this two-step process, the dependent variable T has been marched a value Δt in the direction of t. Although there are two independent spatial variables x and y in addition to the marching variable t, this marching scheme involves only tridiagonal forms, and the solution has been achieved by the repeated application of Thomas' algorithm. Because the scheme involves two steps, one in which the difference equation is implicit in x and the other in which the difference equation is implicit in y, the source of the name of the scheme—*alternating-direction-implicit*—is obvious.

The ADI scheme is second-order-accurate in t, x, and y; that is, the truncation error is of $O[(\Delta t)^2, (\Delta x)^2, (\Delta y)^2]$. See Refs. 13 to 17 for details.

FIG. 6.12
Second step in the ADI process. Sweeping in the y direction to obtain T at time $t + \Delta t$.

This scheme has found application in many fluid flow problems. In the form described above, it is particularly useful for the solution of problems described by parabolic partial differential equations. Also, the scheme described above is a special form of a *general class* of schemes involving a splitting of two or more directions in an implicit solution of the governing flow equations so as to obtain tridiagonal forms. Hence, ADI can represent a general descriptor of a whole class of schemes, one of which has been described in this section. Another popular version of an ADI scheme is called *approximate factorization*; this is a more advanced topic which is discussed in Sec. 11.3.2.

6.8 THE PRESSURE CORRECTION TECHNIQUE: APPLICATION TO INCOMPRESSIBLE VISCOUS FLOW

A numerical technique for the solution of inviscid, incompressible flow was discussed in Sec. 6.5, namely, the relaxation technique. Inviscid, incompressible flow is governed by elliptic partial differential equations, and the relaxation technique, which is essentially an *iterative* process, is a classical numerical method for solving elliptic problems. In contrast, *viscous*, incompressible flow is governed

compressible form simply by setting density equal to a constant. That is, with ρ = constant, Eq. (2.29) becomes

$$\nabla \cdot \mathbf{V} = 0 \tag{6.68}$$

With the further assumption that μ is constant throughout the flow, Eqs. (2.50*a*) to (2.50*c*) combined with Eqs. (2.57*a*) to (2.57*f*) become

$$\rho \frac{Du}{Dt} = -\frac{\partial p}{\partial x} + 2\mu \frac{\partial^2 u}{\partial x^2} + \mu \frac{\partial}{\partial y}\left(\frac{\partial v}{\partial x} + \frac{\partial u}{\partial y}\right) + \mu \frac{\partial}{\partial z}\left(\frac{\partial u}{\partial z} + \frac{\partial w}{\partial x}\right) + \rho f_x \tag{6.69}$$

$$\rho \frac{Dv}{Dt} = -\frac{\partial p}{\partial y} + \mu \frac{\partial}{\partial x}\left(\frac{\partial v}{\partial x} + \frac{\partial u}{\partial y}\right) + 2\mu \frac{\partial^2 v}{\partial y^2} + \mu \frac{\partial}{\partial z}\left(\frac{\partial w}{\partial y} + \frac{\partial v}{\partial z}\right) + \rho f_y \tag{6.70}$$

$$\rho \frac{Dw}{Dt} = -\frac{\partial p}{\partial z} - \mu \frac{\partial}{\partial x}\left(\frac{\partial u}{\partial z} + \frac{\partial w}{\partial x}\right) + \mu \frac{\partial}{\partial y}\left(\frac{\partial w}{\partial y} + \frac{\partial v}{\partial z}\right) + 2\mu \frac{\partial^2 w}{\partial z^2} + \rho f_z \tag{6.71}$$

Note that in writing Eqs. (6.69) to (6.71), the terms in Eqs. (2.57*a*) to (2.57*f*) explicitly involving $\nabla \cdot \mathbf{V}$ have been set to zero due to Eq. (6.68). The fact that $\nabla \cdot \mathbf{V} = 0$ for incompressible flow allows a further reduction of Eqs. (6.69) to (6.71), as follows.

$$\nabla \cdot \mathbf{V} = \frac{\partial u}{\partial x} + \frac{\partial v}{\partial y} + \frac{\partial w}{\partial z} = 0 \tag{6.72}$$

Rearranging Eq. (6.72), we have

$$\rho \frac{Du}{Dt} = -\frac{\partial p}{\partial x} + \mu\left(\frac{\partial^2 u}{\partial x^2} + \frac{\partial^2 u}{\partial y^2} + \frac{\partial^2 u}{\partial z^2}\right) + \rho f_x$$

or

$$\rho \frac{Du}{Dt} = -\frac{\partial p}{\partial x} + \mu \nabla^2 u + \rho f_x \tag{6.76}$$

where $\nabla^2 u$ is the laplacian of the x component of velocity, u. Equations (6.70) and (6.71) can be treated in a similar fashion. The resulting system of equations is the *incompressible Navier-Stokes equations*, summarized below.

Continuity :	$\nabla \cdot \mathbf{V} = 0$	(6.77)
x momentum :	$\rho \frac{Du}{Dt} = -\frac{\partial p}{\partial x} + \mu \nabla^2 u + \rho f_x$	(6.78)
y momentum :	$\rho \frac{Dv}{Dt} = -\frac{\partial p}{\partial y} + \mu \nabla^2 v + \rho f_y$	(6.79)
z momentum :	$\rho \frac{Dw}{Dt} = -\frac{\partial p}{\partial z} + \mu \nabla^2 w + \rho f_z$	(6.80)

Note that Eqs. (6.77) to (6.80) are self-contained; they are four equations for the four dependent variables u, v, w, and p. Through the assumptions of ρ = constant and μ = constant, the energy equation has been completely decoupled from the analysis. The implication here is that the continuity and momentum equations are all that are necessary to solve for the velocity and pressure fields in an incompressible flow, and that *if* a given problem involves heat transfer, and hence temperature

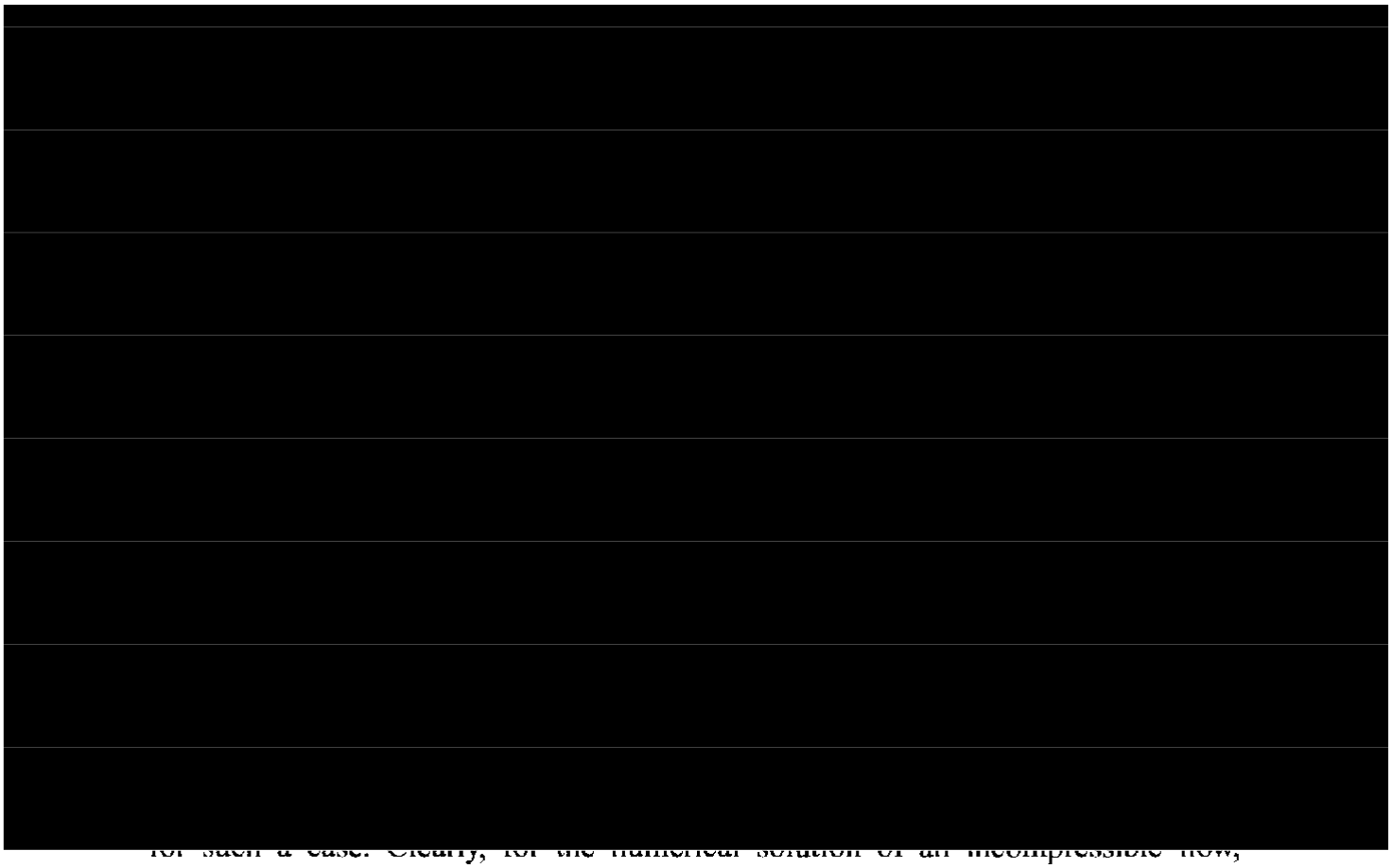

for such a case. Clearly, for the numerical solution of an incompressible flow, something else must be done. This phenomenon is further reinforced by the observation that a compressible-flow CFD solution technique, when applied to a flow field where the Mach number is progressively reduced toward zero, takes progressively more time steps to converge; it is the author's experience that a compressible-flow code run for a flow which is everywhere at a local Mach number of about 0.2 or less takes a prohibitive amount of time to converge, and indeed has a tendency to be unstable at such a low Mach number.

For such reasons, in CFD, solution techniques for the incompressible Navier-Stokes equations are usually different from those used for the solution of the compressible Navier-Stokes equations. The pressure correction method, to be described shortly, transcends this difficulty; it has been used with reasonable success for compressible flow but with even more success for incompressible flow. It is an accepted and widely used technique for incompressible, viscous, CFD applications. Therefore, we focus on this method in the present section.

6.8.2 Some Comments on Central Differencing of the Incompressible Navier-Stokes Equations: The Need for a Staggered Grid

The incompressible continuity equation is given by Eq. (6.77), which in two dimensions is

$$\frac{\partial u}{\partial x} + \frac{\partial v}{\partial y} = 0 \tag{6.82}$$

$$\frac{\partial p}{\partial x} = \frac{p_{i+1,j} - p_{i-1,j}}{2\Delta x} \tag{6.84a}$$

$$\frac{\partial p}{\partial y} = \frac{p_{i,j+1} - p_{i,j-1}}{2\Delta y} \tag{6.84b}$$

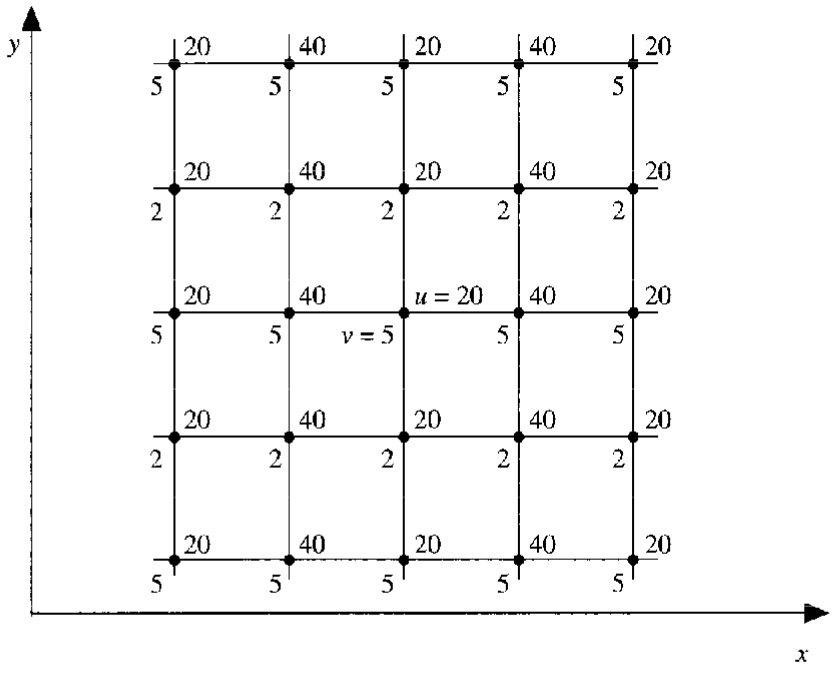

FIG. 6.13
Discrete checkerboard velocity distribution at each grid point; the number at the upper right is u and that at the lower left is v.

For the checkerboard pressure distribution illustrated in Fig. 6.14, Eqs. (6.84*a*) and (6.84*b*) give zero pressure gradients in the x and y directions, respectively. Clearly, the pressure field discretized in Fig. 6.14 would not be felt by the Navier-Stokes equations; rather, the numerical solution would effectively see only a uniform pressure in x and y.

In short, when central differences are used for the incompressible Navier-Stokes equations, the resulting difference equations are of a form that, when presented with the nonsensical velocity and pressure distributions shown in Figs. 6.13 and 6.14, will tend to perpetuate these distributions. Admittedly, some early central difference algorithms for incompressible viscous flow ignored this problem, and successful solutions were still obtained, presumably because of special treatment of the boundary conditions or by some other fortuitous aspect of the numerical procedure. However, given the weakness of the central difference formulation described above, we should justifiably feel uncomfortable, and we should look for some "fix" before embarking on the solution of a given problem.

Two such fixes are suggested. If upwind differences are used instead of central differences, the problem immediately goes away. A discussion of upwind differences is given in Sec. 11.4. However, another fix is to maintain central differencing but *stagger* the grid, as described below.

A staggered grid is illustrated in Fig. 6.15. Here, the pressures are calculated at the solid grid points, labeled $(i-1, j)$, (i, j), $(i+1, j)$, $(i, j+1)$, $(i, j-1)$, etc., and the velocities are calculated at the open grid points, labeled $(i-\frac{1}{2}, j)$, $(i+\frac{1}{2}, j)$, $(i, j+\frac{1}{2})$, $(i, j-\frac{1}{2})$, etc. Specifically, u is calculated at points $(i-\frac{1}{2}, j)$, $(i+\frac{1}{2}, j)$,

etc., and v is calculated at different points $(i, j + \frac{1}{2})$, $(i, j - \frac{1}{2})$, etc. The key feature here is that pressures and velocities are calculated at *different* grid points. In Fig. 6.15, the open grid points are shown equidistant between the solid grid points, but this is not a necessity. An advantage of this staggered grid is, for example, that when $u_{i+1/2,\,j}$ is calculated, a central difference for $\partial p/\partial x$ yields $(p_{i+1,\,j} - p_{i,\,j})/\Delta x$; that is, the pressure gradient is based on *adjacent* pressure points, which eliminates the possibility of a checkerboard pressure pattern as sketched in Fig. 6.14. Also, a central difference expression for the continuity equation, Eq. (6.82), centered around point (i, j) becomes

$$\frac{u_{i+1/2,\,j} - u_{i-1/2,\,j}}{\Delta x} + \frac{v_{i,\,j+1/2} - v_{i,\,j-1/2}}{\Delta y} = 0 \tag{6.85}$$

Because Eq. (6.85) is based on *adjacent* velocity points, the possibility of a checkerboard velocity pattern as sketched in Fig. 6.13 is eliminated.

6.8.3 The Philosophy of the Pressure Correction Method

The pressure correction technique is basically an iterative approach, where some innovative physical reasoning is used to construct the next iteration from the results of the previous iteration. The thought process is as follows:

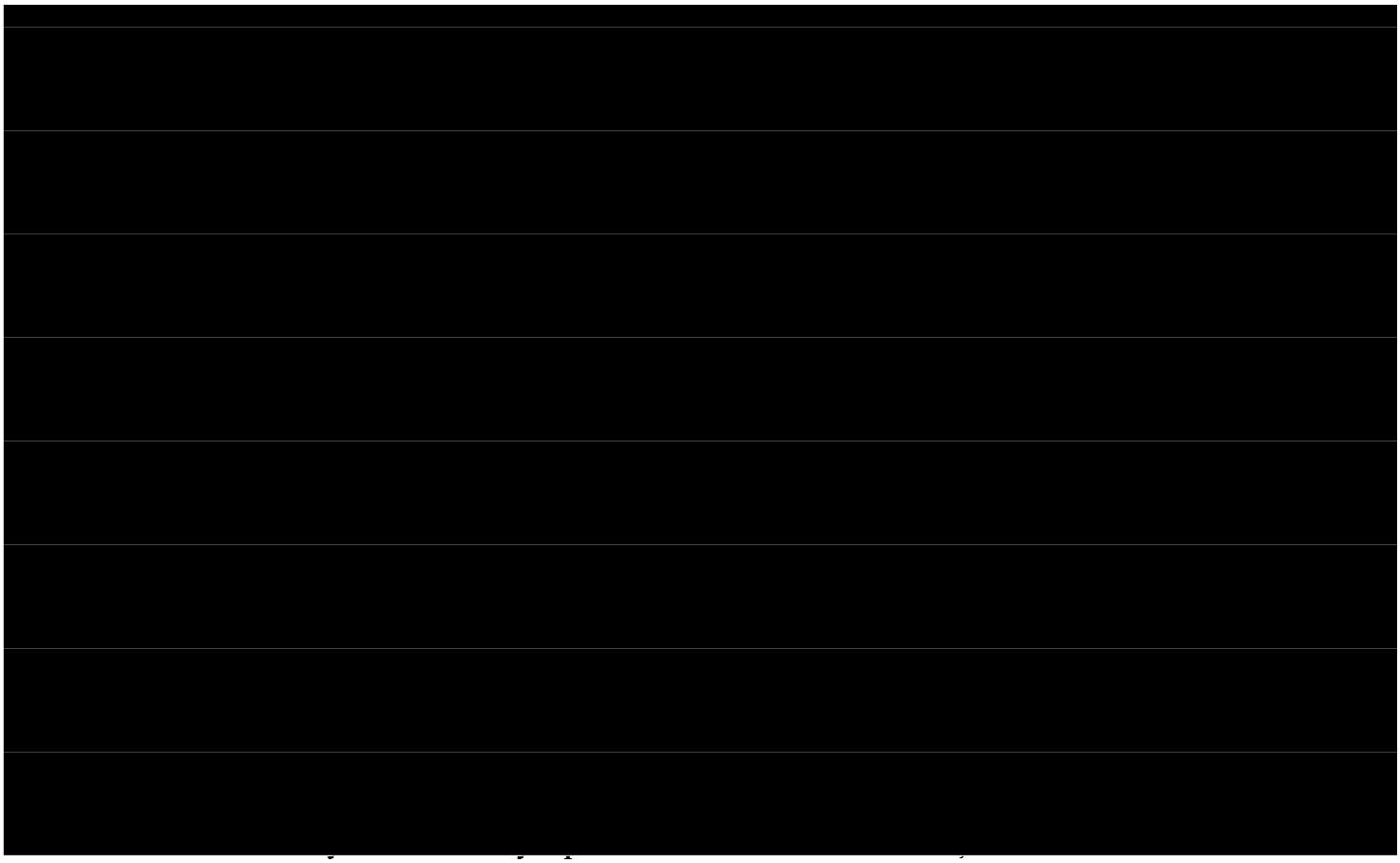

is at hand.

6.8.4 The Pressure Correction Formula

The pressure correction p' was introduced in Eq. (6.86). The calculation of the value of p' is the subject of this subsection. For simplicity, we will consider a two-dimensional flow; the additional terms associated with the third dimension are treated in a like manner. Also, we will neglect body forces.

The x- and y-momentum equations for an incompressible viscous flow are given by Eqs. (6.78) and (6.79), respectively. These equations are in nonconservation form. In conservation form, they are (see Sec. 2.8)

$$\frac{\partial(\rho u)}{\partial t}+\frac{\partial(\rho u^2)}{\partial x}+\frac{\partial(\rho uv)}{\partial y}=-\frac{\partial p}{\partial x}+\mu\left(\frac{\partial^2 u}{\partial x^2}+\frac{\partial^2 u}{\partial y^2}\right) \tag{6.88}$$

and

$$\frac{\partial(\rho v)}{\partial t}+\frac{\partial(\rho vu)}{\partial x}+\frac{\partial(\rho v^2)}{\partial y}=-\frac{\partial p}{\partial y}+\mu\left(\frac{\partial^2 y}{\partial x^2}+\frac{\partial^2 v}{\partial y^2}\right) \tag{6.89}$$

As discussed in Chap. 2, the conservation form follows directly from the model of an infinitely small volume fixed in space. Because of this model, a finite-difference form of Eqs. (6.88) and (6.89) will be somewhat akin to the discretized equations obtained from a finite-volume approach. The original formulation of the pressure correction method by Patankar and Spalding (Refs. 67 and 68) involved a finite-

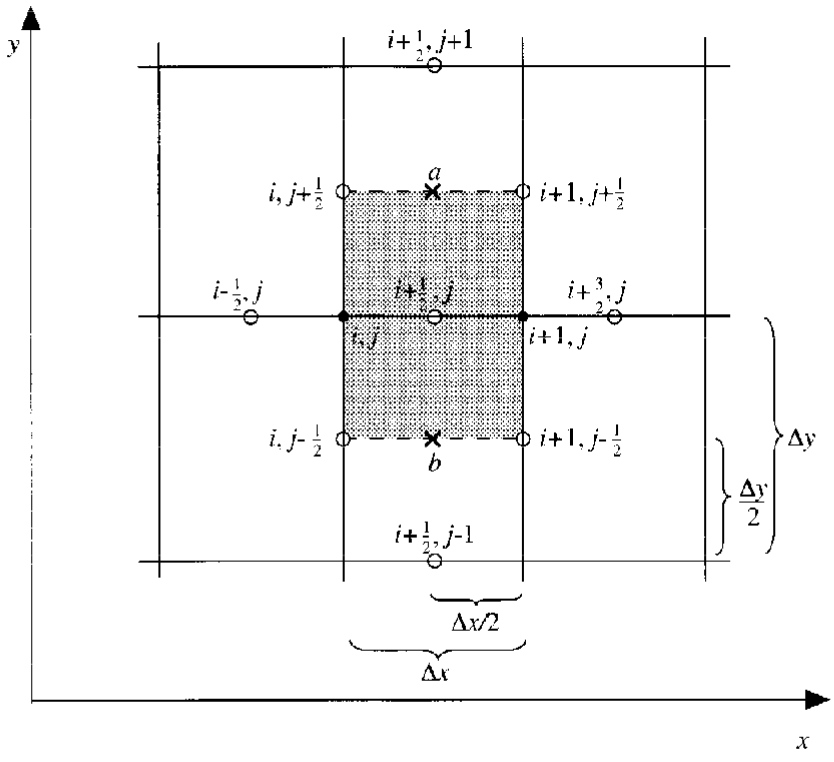

FIG. 6.16
Computational module for the x-momentum equation. The filled-in area is an effective control volume.

$$A = -\left[\frac{(\rho u^2)_{i+3/2,j} - (\rho u^2)_{i-1/2,j}}{2\Delta x} + \frac{(\rho uv)_{i+1/2,j+1} - (\rho uv)_{i-1/2,j-1}}{2\Delta y}\right]$$
$$+ \mu\left[\frac{u^n_{i+3/2,j} - 2u^n_{i+1/2,j} + u^n_{i-1/2,j}}{(\Delta x)^2} + \frac{u^n_{i-1/2,j+1} - 2u^n_{i+1/2,j} + u_{i+1/2,j-1}}{(\Delta y)^2}\right]$$

Equation (6.92) is a difference equation representing the x-momentum equation. Note that $\bar{v}$ and v in Eqs. (6.91) and (6.92) are those values defined by Eqs. (6.90*a* and *b*), i.e., $\bar{v}$ and v use different grid points than those for u.

In like manner, a difference equation for the y-momentum equation is obtained. Here, we will difference Eq. (6.89) centered around point $(i, j + \frac{1}{2})$ as shown in Fig. 6.17. We define average values of u at the points c and d on the left and right sides of the shaded cell in Fig. 6.17 as follows:

$$\textit{At point } c: \qquad u = \tfrac{1}{2}(u_{i-1/2,j} + u_{i-1/2,j+1})$$
$$\textit{At point } d: \qquad \bar{u} = \tfrac{1}{2}(u_{i+1/2,j} + u_{i+1/2,j+1})$$

Using a forward difference in time and central differences in space, Eq. (6.89) becomes

$$\boxed{(\rho v)^{n+1}_{i,j+1/2} = (\rho v)^n_{i,j-1/2} + B\,\Delta t - \frac{\Delta t}{\Delta x}(p^n_{i,j+1} - p^n_{i,j})} \qquad (6.93)$$

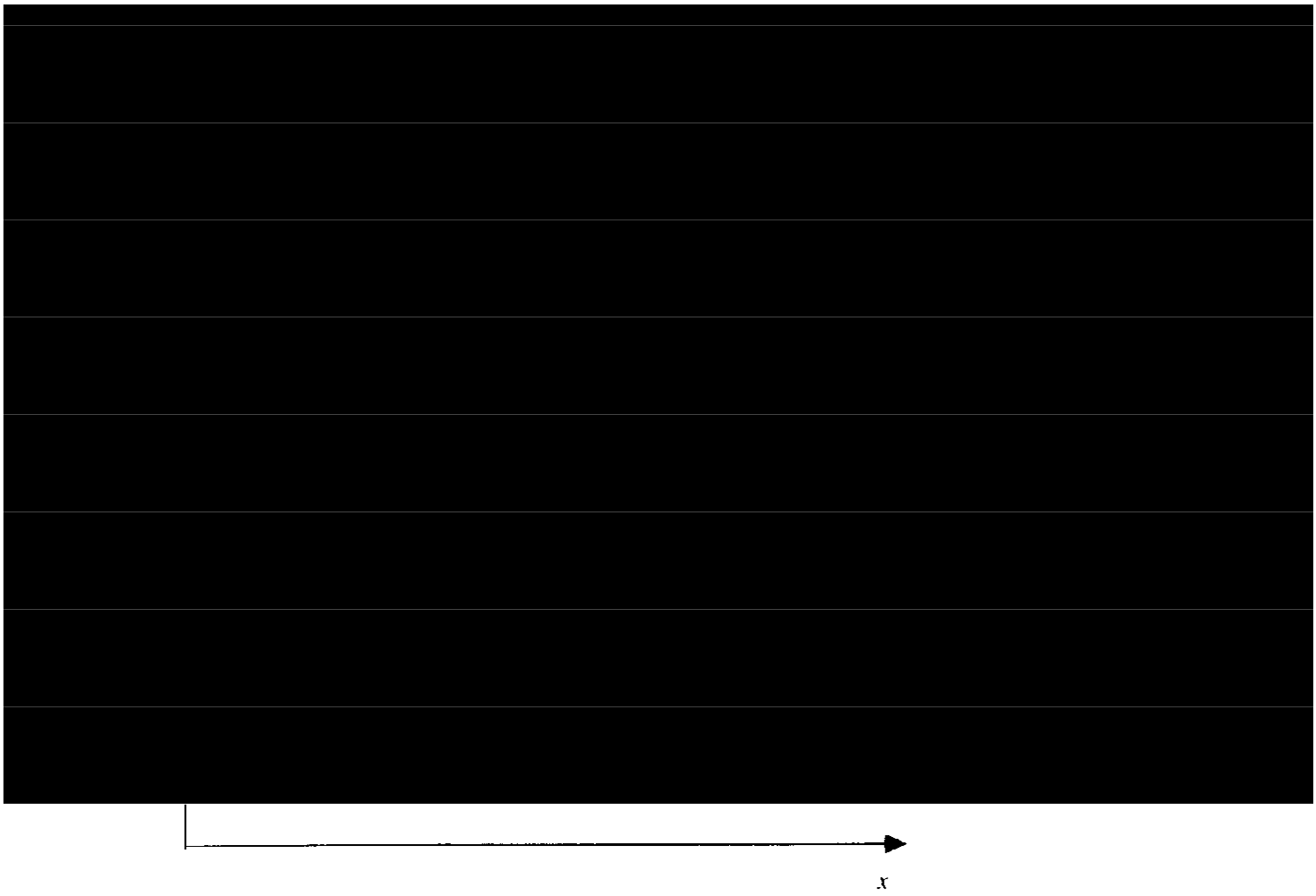

FIG. 6.17
Computational module for the y-momentum equation. The filled-in area is an effective control volume.

where

$$B = -\left[\frac{(\rho v\bar{u})^n_{i+1,j+1/2} - (\rho vu)^n_{i-1,j+1/2}}{2\Delta x} + \frac{(\rho v^2)^n_{i,j+3/2} - (\rho v^2)_{i,j-1/2}}{2\Delta y}\right]$$

$$+ \mu\left[\frac{v^n_{i+1,j+1/2} - 2v^n_{i,j+1/2} + v_{i-1,j+1/2}}{(\Delta x)^2} + \frac{v^n_{i,j+3/2} - 2v^n_{i,j-1/2} + v^n_{i,j-1/2}}{(\Delta x)^2}\right]$$

Note that u and $\bar{u}$ in Eq. (6.93) are those values defined by the average values at points c and d, i.e., u and $\bar{u}$ use different grid points than those for v.

As outlined in Sec. 6.8.3, at the beginning of each new iteration, $p = p^*$. For this situation, Eqs. (6.92) and (6.93) become, respectively,

$$(\rho u^*)^{n+1}_{i+1/2,j} = (\rho u^*)^n_{i+1/2,j} + A^*\,\Delta t - \frac{\Delta t}{\Delta x}(p^*_{i+1,j} - p^*_{i,j}) \qquad (6.94)$$

$$(\rho v')_{i,j+1/2} = (\rho v)_{i,j+1/2} - (\rho v^*)_{i,j+1/2}$$

$$(\rho v')^n_{i,j-1/2} = (\rho v)^n_{i,j+1/2} - (\rho v^*)^n_{i,j+1/2}$$

$$B' = B - B^*$$

$$p'_{i,j+1} = p_{i,j+1} - p^*_{i,j+1}$$

$$p'_{i,j} = p_{i,j} - p^*_{i,j}$$

Eqs. (6.96) and (6.97) are the x- and y-momentum equations expressed in terms of the pressure and velocity corrections p', u', and v' defined by Eqs. (6.86), (6.87a), and (6.87b), respectively.

We are now in a position to obtain a formula for the pressure correction p' by insisting that the velocity field must satisfy the continuity equation. However, we are reminded that the pressure correction method is an iterative approach, and therefore there is no inherent reason why the formula designed to predict p' from one iteration to the next be physically correct; rather, we are concerned with only two aspects: (1) the formula for p' must yield the values that ultimately lead to the proper, converged solution, and (2) in the limit of the converged solution, the formula for p' must reduce to the physically correct continuity equation. That is, we are allowed to construct a formula for p' which is simply a *numerical artifice* designed to expedite the convergence of the velocity field to a solution that satisfies the continuity equation. When this convergence is achieved, $p' \to 0$, and the formula for p' reduces to the physically correct continuity equation.

With the above aspects in mind, let us proceed to obtain the pressure correction formula. Following Patankar (Ref. 68), let us arbitrarily set A', B',

$$(\rho v')_{i,j+1/2}^{n+1} = (\rho v)_{i,j+1/2}^{n+1} - (\rho v^*)_{i,j+1/2}^{n+1}$$

we can write Eq. (6.99) as

$$(\rho v)_{i,j+1/2}^{n+1} = (\rho v^*)_{i,j+1/2}^{n+1} - \frac{\Delta t}{\Delta y}(p'_{i,j+1} - p'_{i,j})^n \tag{6.101}$$

Returning to the continuity equation

$$\frac{\partial(\rho u)}{\partial x} + \frac{\partial(\rho v)}{\partial y} = 0$$

and writing the corresponding central difference equations centered around point (i, j), we have

$$\frac{(\rho u)_{i+1/2,j} - (\rho u)_{i-1/2,j}}{\Delta x} + \frac{(\rho v)_{i,j-1/2} - (\rho v)_{i,j\ \ 1/2}}{\Delta y} = 0 \tag{6.102}$$

Substituting Eqs. (6.100) and (6.101) into (6.102) and dropping the superscripts,

$$d = \frac{1}{\Delta x}\left[(\rho u^*)_{i+1/2,j} - (\rho u^*)_{i-1/2,j}\right] + \frac{1}{\Delta y}\left[(\rho v^*)_{i,j+1/2} - (\rho v^*)_{i,j-1/2}\right]$$

Equation (6.104) is the *pressure correction formula*. It has an elliptic behavior, consistent with the fact that a pressure disturbance will propagate everywhere throughout an incompressible flow. Thus, Eq. (6.104) can be solved for p' by means of a numerical relaxation technique, such as described in Sec. 6.5.

Note that d in Eq. (6.104) is the central difference formulation of the left-hand side of the continuity equation expressed in terms of u^* and v^*. During the course of the iterative process, u^* and v^* define a velocity field that does *not* satisfy the continuity equation; hence in Eq. (6.104), $d \neq 0$ for all but the last iteration. In this sense, d is a *mass source* term. By definition, in the last iteration, the velocity field has converged to a field that satisfies the continuity equation, and hence, theoretically, $d = 0$ for this last iteration. In this sense, although a mathematical artifice was used to obtain Eq. (6.104), in the last iterative step we can construe Eq. (6.104) as being a proper physical statement of the conservation of mass.

It is interesting to note that the pressure correction formula, Eq. (6.104), is a central difference formulation of the *Poisson equation* in terms of the pressure correction p'.

$$\frac{\partial^2 p'}{\partial x^2} + \frac{\partial^2 p'}{\partial y^2} = Q \tag{6.105}$$

If the second partial derivatives in Eq. (6.105) are replaced by central differences and if $Q = d/(\Delta t\ \Delta x)$, then Eq. (6.104) is obtained. (This short derivation is left as

[redacted]

Instead, because of the above artifice, Eq. (6.104) contains pressure corrections at only four grid points, and hence it is termed as only *semi-implicit* by Patankar (Ref. 68).

The step-by-step procedure for the SIMPLE algorithm is as follows:

1. Keeping in mind the staggered grid as sketched in Fig. 6.15, guess values of $(p^*)^n$ at all the "pressure" grid points (the filled points in Fig. 6.15). Also, arbitrarily set values of $(\rho u^*)^n$ and $(\rho v^*)^n$ at the proper "velocity" grid points (the open points in Fig. 6.15). Here, we are considering the grid points internal to the flow field; the treatment of points on the boundaries will be discussed later.
2. Solve for $(\rho u^*)^{n+1}$ from Eq. (6.94) and $(\rho v^*)^{n+1}$ from Eq. (6.95) at all appropriate internal grid points.
3. Substitute these values of $(\rho u^*)^{n+1}$ and $(\rho v^*)^{n+1}$ into Eq. (6.104), and solve for p' at all interior grid points. (This solution can be carried out by a relaxation procedure such as described in Sec. 6.5.)
4. Calculate p^{n+1} at all internal grid points from Eq. (6.86), i.e.,

$$p^{n+1} = (p^*)^n + p'$$

5. The values of p^{n+1} obtained in step 4 are used to solve the momentum equations again. For this, we designate p^{n+1} obtained above as the *new* values of $(p^*)^n$ to be inserted into Eqs. (6.94) and (6.95). With this interpretation, return to step 2 and repeat steps 2 to 5 until convergence is achieved. A reasonable criterion to use for a measure of convergence is when the mass source term d approaches zero.

relaxation in such cases; i.e., instead of using Eq. (6.86) in step 4, use the equation

$$p^{n+1} = (p^*)^n + \alpha_p p' \tag{6.106}$$

where α_p is an underrelaxation factor; a value of about 0.8 is suggested. It may also be helpful in some cases to underrelax the values of u^* and v^* obtained from Eqs. (6.94) and (6.95).

6.8.6 Boundary Conditions for the Pressure Correction Method

How are boundary conditions specified consistent with the philosophy of the pressure correction method? This question is addressed here. For geometric simplicity, consider the constant-area duct sketched in Fig. 6.18; a staggered grid is distributed inside the duct. For an incompressible viscous flow, the physical problem is uniquely specified if:

1. *At the inflow boundary*, p and v are specified and u is allowed to float. If p is specified, then p' is zero at the inflow boundary. Hence, in Fig. 6.18,

$$p'_1 = p'_3 = p'_5 = p'_7 = 0$$

   v_2, v_4, v_6 are specified and held fixed.
2. *At the outflow boundary*, p is specified and u and v are allowed to float. Hence

$$p'_8 = p'_{10} = p'_{12} = p'_{14} = 0$$

[redacted]

at the wall is zero.

$$u_{15} = u_{17} = u_{19} = u_{21} = u_{22} = u_{24} = u_{26} = u_{28} = 0$$

For the numerical solution, we need one more boundary condition at the wall. Since Eq. (6.104) has elliptic behavior and is solved by a relaxation technique, a boundary condition associated with p' must be specified over the *complete* boundary containing the computational domain. From items 1 and 2 above, we have $p' = 0$ at the inflow and outflow boundaries. A condition associated with p' at the walls can be derived as follows. Evaluate the y-momentum equation at the wall, where $u = v = 0$. With these velocity values inserted into Eq. (6.79), we have at the wall (neglecting body forces)

$$\left(\frac{\partial p}{\partial y}\right)_w = \mu\left(\frac{\partial^2 v}{\partial x^2} + \frac{\partial^2 v}{\partial y^2}\right)_w \tag{6.107}$$

Since $v_w = 0$, then in Eq. (6.107), $(\partial^2 v/\partial x)_w = 0$. Also, in the near vicinity of the wall, v is small; hence, in Eq. (6.107) we can reasonably assume that $(\partial^2 v/\partial y)_w$ is small. Thus, from Eq. (6.107) we can comfortably state the approximate (but reasonable) pressure boundary condition at the wall to be given by

$$\left(\frac{\partial p}{\partial y}\right)_w = 0 \tag{6.108}$$

Discretizing Eq. (6.108), we have (refering to Fig. 6.18)

$$p_1 = p_3 \qquad p_{16} = p_{29} \qquad p_5 = p_7 \qquad \text{etc.}$$